EFFECT OF DESICCATION CRACKS ON EARTH EMBANKMENTS

A Thesis

by

SIDDHARTH KHANDELWAL

Submitted to the Office of Graduate Studies of
Texas A&M University
in partial fulfillment of the requirements for the degree of

MASTER OF SCIENCE

May 2011

Major Subject: Civil Engineering

Effect of Desiccation Cracks on Earth Embankments

EFFECT OF DESICCATION CRACKS ON EARTH EMBANKMENTS

A Thesis

by

SIDDHARTH KHANDELWAL

Submitted to the Office of Graduate Studies of
Texas A&M University
in partial fulfillment of the requirements for the degree of

MASTER OF SCIENCE

Approved by:

Co-Chairs of Committee,	Marcelo Sanchez
	Zenon Medina-Cetina
Committee Member,	Mark Everett
Head of Department,	John Niedzwecki

May 2011

Major Subject: Civil Engineering

ABSTRACT

Effect of Desiccation Cracks on Earth Embankments.

(May 2011)

Siddharth Khandelwal, B.Tech., Institute of Technology, Banaras Hindu University,

Varanasi, India

Co-Chairs of Advisory Committee: Dr. Marcelo Sanchez
Dr. Zenon Medina-Cetina

Levees are earth structures used for flood protection. Due to their easy availability and low permeability, clays are the most common material used for the construction of levees. Clays are susceptible to desiccation cracks when subjected to long dry spells during summers. There has been an increased interest in studying the occurrence of cracks in soil mass. In particular, many experimental investigations for soils have been undertaken to learn about the crack pattern in earth embankment. However, there is a dearth of work that focuses on the numerical modeling of desiccation cracks effects on levees. This study has been undertaken to analyze the effect of desiccation cracking on the hydraulic behavior of an earth embankment under flooding conditions. A numerical model was developed using the finite element package CODE_BRIGHT. The model was validated from the data obtained from a small scale embankment experiment under controlled environmental conditions. As the phenomenon of desiccation cracking is highly random, a simple random model was developed to capture the variability in crack geometry. The random crack geometry was then passed

on to the finite element mesh, so that a probabilistic analysis can be carried out using a Monte Carlo approach, for assessing the embankment's integrity. The results obtained from the analysis such as time to steady state saturation and steady state flow rate at the outward slope were very interesting to study and provided an insight on the effect of desiccation cracks on unsaturated earth embankments.

DEDICATION

In memory of my grandmother, the late Smt. Shanti Devi

ACKNOWLEDGEMENTS

I would like to take this opportunity to gratefully acknowledge the support of my advisor, Dr. Marcelo Sanchez for his sustained support, guidance and encouragement throughout the course of my graduate studies and for the enormous time he dedicated for my masters research. I would like to thank Dr. Zenon Medina-Cetina for providing his expert guidance and offering the cluster required to perform the rigorous calculations involved in the research, without which it would have been impossible to complete this research. I would also like to thank Dr. Mark Everett for kindly consenting to be a member of my committee and helping me revise this document. I would also like to acknowledge Dr. Marcin Zielinski for providing me the data required for the research.

I wish to thank the entire faculty of the Department of Civil Engineering at Texas A&M University for providing me with the tools and knowledge required for this work. I must also acknowledge the effort and time given by my friend, Ajay Shastri.

Finally, my deepest gratitude is due to my parents and my sister for their constant love and support.

TABLE OF CONTENTS

Page

LIST OF FIGURES

FIGURE Page

FIGURE Page

FIGURE Page

FIGURE Page

LIST OF TABLES

1. INTRODUCTION

1.1 Background

The phenomenon of cracking is present in most geotechnical structures and has been of particular interest to civil and mining engineers. Cracks pose a threat to the integrity of geotechnical structures such as slopes, embankments, dams, tunnels, pavements, foundations, etc. Allied branches such as geo-environment engineering, petroleum engineering and agricultural engineering have also shown deep interest on the influence of cracks on affluent discharge from a waste deposit, hydraulic fracturing due to high fluid pressure and nutrient flow through root zones, respectively. The present work is more relevant to geotechnical engineering.

A number of researchers for decades have been interested in the problem of instability caused to slopes and dams because of cracking (Cooling and Marsland, 1953; Nawari et al., 1997; Cho and lee, 2001; Aubeny and Lytton, 2004; Yang et al., 2004; Jimenez-Rodriguez et al., 2006; Yang and Zou, 2006; Low, 2007; Li et al., 2008, Shukla et al., 2009). Every year in the United States, slope failures cause damages of approximately $2 billion. Cracks adversely influence the stability of slopes by: 1) providing a preferential path to water flow, thereby inducing high pore water pressures and 2) cracks can form part of the slip surface providing little or no shear strength. Figure 1.1 shows a picture of failed flood protection levee. Therefore, a clear understanding of the effect of cracks is vital for safe and economical designs of levees, dams and slopes. The present

---

This thesis follows the style of *Geological and Geotechnical Engineering.*

work focuses on the effect of desiccation cracks on the hydraulic behavior of earth embankments.

Figure 1.1. Picture depicting total failure of a levee

1.2 Motivation

There has been an increased interest in the performance of levees in the past decade due to certain catastrophic failure events, for example, the havoc caused by hurricane Katrina on the flood embankments of New Orleans causing huge damage to life and property. Apart from that, the prediction of rising sea levels as a result of global warming has triggered a sense of great concern particularly in the regions that will be worst hit by

such an eventuality, for example the eastern parts of the Indian subcontinent and Pacific Islands.

Many countries will have to upgrade their flood protection system in order to counter the threats imposed by the global climatic changes. Therefore, it is imperative to improve our knowledge on all possible modes of failure of a flood embankment.

Traditional design of earth embankments is based on the hypothesis of intact fill, i.e., the presence and occurrence of cracks is disregarded. But under actual conditions, it is unavoidable to prevent cracks formation. Desiccation cracks are formed due to shrinkage of the soil mass as a result of evaporation of water during summer seasons. The phenomenon of desiccation cracking is presumed to increase in future due to global warming, when the range of the extreme temperatures will increase. The presence of cracks makes the soil slopes susceptible to water seepage, erosion, loss of shear strength and consequent failures. Every year millions of dollars are spent in the repair and maintenance of these slopes. For example, an expected cost of $ 960,000 was estimated by geotechnical engineers for slope maintenance and shallow slides in Indiana (Hopkins et al., 1988).

Therefore, understanding the mechanisms of desiccation cracking and the flow of water through these cracks and how these influence the stability of the soil slope is crucial in avoiding such failures. Researchers have identified the effect of water flow through the

cracks in the soil slopes (e.g., Lytton et al., 1987; Kuhn and Zornberg, 2006). However, in practice, the effect of cracks is not considered while designing embankments. There has been little focus on this problem because of the scarce information about some aspects related to desiccation cracks, as for example:

1. Absence of a reliable theory to explain the phenomenon of desiccation cracking, formation and propagation.
2. Difficulty in measuring the geometry of desiccation cracks.
3. Lack of numerical tools to simulate the effect of cracks in soil.
4. Limited understanding on the uncertainty-based determination of the embankment's integrity

The present work focuses on achieving a better understanding of the effect of desiccation cracks in an earth embankment. In particular, an effort has been made to numerically model the impact of water flow through desiccation cracks by adapting a finite element code.

1.3 Objective and scope

Researchers in the past have attempted to model flow of water through cracks (e.g., Liu et al., 2004; Li Jinhui, 2007; Zielinski et al., 2008). Desiccation cracking is a highly random process and in all the previous attempts to numerically model the effect of desiccation cracks on earth embankments, an equivalent hydraulic permeability was imposed on the fissured zone, instead of discretizing cracks into the soil mass. The main

objective of the present research was to numerically model the seepage of water through an unsaturated soil embankment subjected to randomly distributed desiccation cracks. The model was validated against the experimental data obtained from the sensors of a scaled embankment under controlled conditions. The scaled embankment was subjected to repeated cycles of wetting and drying and thus developing desiccation cracks. In order to capture the aleatory nature of the desiccation cracks a simple random model was developed. The crack geometry was then imposed on the finite element mesh to see the effect of various crack geometries on time to saturation and flow rate at the outward face of the slope. The numerical analysis was done with help of finite element package CODE_BRIGHT (DIT-UPC, 2011) which has a feature of using joint elements that can be used to simulate effect of individual cracks on the flow through a porous media.

Analyzing the effect of desiccation cracks on earth embankments under flooding conditions is a three-dimensional problem. But the earth embankments are very long as compared to the other two dimensions and also for a given embankment, the crack geometry is more or less regular. Thus the problem can be treated as a plain strain problem, reducing it to a two-dimensional problem. In real life, cracks open and close due to variation in moisture content and also depend on the stress conditions the soil is subjected to. In the present work, however, the geometry of the crack network was constant for a single realization of crack geometry and only the hydraulic effects of cracks on an embankment were analyzed.

1.4 Methodology

Broadly, four tasks were accomplished to meet the objectives as outlined in section 1.3. The tasks accomplished were as follows:

Task1: Field observations

A detailed literature review was completed to understand the pattern and geometry of desiccation cracks. Various researchers such as Cooling and Marsland (1953), Zein el Abedine and Robinson (1971), Dasog et al. (1988), Dyer et al. (2009) have collected data for the depth, aperture and spacing between the cracks for different kinds of soils under different environmental conditions.

Task 2 Modeling desiccation cracks in soil

In order to simulate the effect of cracks on the seepage of an unsaturated embankment, joint elements were used. The joint elements need to be assigned material properties to describe the flow through cracks. Several scaled numerical models were tested to verify the response of the proposed elements. The effect on the flow rate was observed for the different thicknesses of the joint element.

Task 3 Scaled embankment

Validation is an important part of any numerical analysis. An experiment was conducted at the University of Strathclyde, Glasgow to study the effect desiccation cracks on a scaled embankment constructed inside controlled environment chamber. The

embankment was subjected to repeated drying and wetting cycles thereby inducing desiccation cracks. Sensors were placed inside the embankment to measure moisture content and suction at different depths. Figure 1.2 shows the scaled embankment after a drying cycle. Superficial desiccation cracks induced because of drying can be easily seen along with the resistivity arrays that were used to find the depth of the cracks.

Figure 1.2. An image of the slope of the scaled embankment after a drying cycle

Based on the data collected in the experiment mentioned above, a numerical model was developed with cracks introduced via the joint elements. The numerical model closely matched the results obtained from the experiment.

Tas4: Monte –Carlo simulation for a full scale embankment with random cracks

The data collected in task1 was used to formulate the probability density functions (PDFs) for depth, aperture and spacing between the cracks. Guided by the PDFs, a random geometry of the cracks was generated. This geometry was then imposed on the finite element mesh. The crack geometry parameters namely depth, aperture and spacing

between the cracks were varied individually, in pairs and all at the same time. The effect of crack geometry was analyzed on time to saturation (Ts) and flow rate (Q). This allowed understanding the effect of desiccation cracks on an unsaturated soil embankment under flooding conditions. The cumulative density functions for Ts and flow rate Q at the outward slope were plotted for the different cases mentioned above.

1.5 Summary

The objective of the study was to explore the effect of desiccation cracks on seepage of an unsaturated soil embankment. Desiccation cracks are formed due to evaporation of water from the soil causing shrinkage of the soil. The shrinkage causes a change in the stress field inside the soil leading to desiccation cracks. In order to study the effect of desiccation cracks on seepage of an embankment, a numerical model was developed using finite element methods. In order to validate the model, experimental data from a small scale embankment was used. The model results closely matched the experimental results thus validating the numerical model. The geometry and location of cracks has a high degree of variability. To capture the random distribution of cracks a simple random model was developed. The randomly generated crack geometry was superimposed on the finite element mesh. Finally, the effect of crack depth, aperture and spacing on Ts and Q were found. Thus, a numerical model was developed which can be used as a tool by engineers to incorporate the effect of desiccation cracks while designing levees.

1.6 Layout of the thesis

Section 2 of the thesis comprises of notes on different kinds of discontinuities in soils with a special emphasis on desiccation cracks. A detailed literature review on the geometrical and morphological properties of the desiccation is presented in this section. In Section 3, a theoretical background to model flow in porous media is discussed. All the governing equations and concepts related to fluid flow in porous media are discussed in this section along with a joint element model to simulate the effect of flow through cracks in soil. Section 4 contains details about the scaled embankment experiment along with the numerical model developed to capture the experimental data from the various sensors. In section 5, the random model is presented and the numerical model to study the effects of random crack geometry on Ts and Q has been described. The results from the Monte Carlo simulations have also been discussed in this section. Finally, in section 6 summary and conclusions from the research done as well as proposed plan for future work have been presented.

2. OCCURRENCE OF CRACKS IN SOILS

2.1 Overview of the section

Different mechanics by which cracks appear in soils have been discussed in this section with a special emphasis on desiccation cracks. A detailed literature review has been done on the work published by the researchers in the past in order to understand the morphology and geometry of the desiccation cracks.

2.2 Mechanisms of crack formation

Though the prime interest of this section is to discuss about desiccation cracks, some major processes by which desiccation as well as other type of cracks are formed in an earth structure are discussed below:

1. Desiccation cracks or shrinkage cracks: Desiccation cracks are formed due to evaporation of water from the soil causing shrinkage of the soil. The shrinkage causes a change in the stress field inside the soil leading to desiccation cracks.
2. Hydraulic fracturing: These kinds of cracks are associated in porous media with high fluid pressure. When the fluid pressure exceeds the lateral or vertical pressure in the embankment or dam, hydraulic cracks are formed.
3. Cracking induced by lateral stress relief from differential settlement: This problem is common in slopes or dams constructed on compressible foundations where irregular profiles, buried channels and areas of different soil properties are present.

4. Cracking induced by earthquakes: The response of a slope or a dam to a strong earthquake produces tensile stresses and permanent displacements that cause soils to crack.
5. Freeze-thaw cracking: The cracks formed during a freezing process can close when thawing occurs, but it is noticed that after its first five freeze-thaw cycles the hydraulic conductivity increases to 10 to 100 times of its original value.
6. Synaeresis: Cracks occur in loose saturated natural clay beds due to the colloidal nature of clay particles. Synaeresis cracks are induced by the rapid settlement under gravity due to clay flocculation or grouping of particles. The settlement causes strange sinuous, spindle or polygonal shaped cracking patterns in subsurface.
7. Cracking due to subsidence: Excessive pumping of water may sometimes lead to large scale consolidation of the soil, causing subsidence in a very large area. The subsidence in turns leads to very long and deep cracks around the area of subsidence. Such cracks are very common in areas like Mexico City and Bogota.

2.3 Desiccation cracks in soil

Desiccation of soils usually involves a reduction in the moisture content of the soil induced by evaporation of water from the soil surface to the atmosphere. The phenomenon of desiccation cracking is very complex and involves strong hydro-mechanical coupling (Rodriguez, Sanchez, et al., 2007). For instance during the drying process the pores are progressively filled with air, inducing negative pore water

pressures (or suction). This results in surface tension that affects the mechanical behavior of the soil. Thus, evolution of desiccation cracks which is largely a hydraulic phenomenon has ramifications on the mechanical behavior of the soil as well. Apart from that, initial moisture content, compaction, temperature, drying and wetting cycles also affect desiccation cracking (Morris et al., 1992; Kim and Hwang, 2002; Zielinski, Sanchez et al., 2010)

2.3.1 Formation of desiccation cracks

In general, the criteria for crack initiation can be divided into two approaches: the stress criterion (Abu-Hejleh and Znidarcic, 1995; Konrad and Ayad, 1997) and the strain criterion (Meakin, 1987; Hornig et al., 1996; Kitsunezaki, 1999; Vogel et al., 2005). In the stress criterion, the crack is believed to initiate as soon as the tensile stress in the soil exceeds its tensile strength. Whereas, in the strain criterion the clay layer is represented through a network of Hookean springs which break when a critical strain is exceeded. Such models reproduce the phenomenologically observed experiments by simulating the redistribution of stresses in the neighborhood of the broken spring.

There is no a consensus on the mechanism of the onset of desiccation cracks. One of the more relevant works is the one done by Konrad and Ayad (1997). They proposed a model for prediction of depth and spacing of desiccation cracks. The model is based on the theory of linear elastic fracture mechanics (LEFM) and fictitious stress superposition concept. The main features of model are:

1. The crack initiation occurs when the minor principal stress (horizontal stress) equals the tensile strength of the soil.
2. The prediction of primary spacing between the cracks is based on two soil parameters: fracture toughness and tensile strength of the soil.
3. Crack propagation is analyzed using trapezoidal distribution of total stresses as governed by the material constitutive equations.

Figure 2.1 shows the various stages in the development of a crack as proposed by Konrad and Ayad (1997).

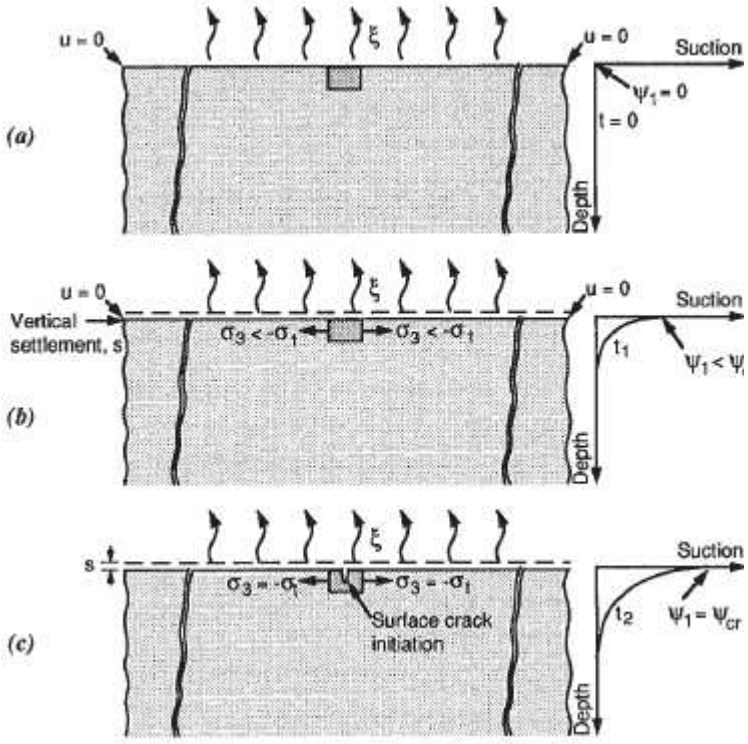

Figure2.1. Schematic illustration of stages in cracking (after Konrad and Ayad, 1997)

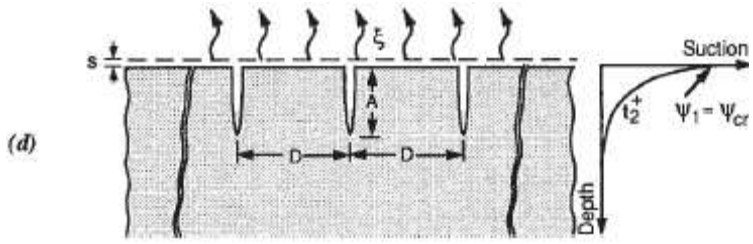

Figure 2.1. continued

A major drawback of this approach is that the LEFM theory is primarily applicable for fragile materials. However, at the onset of desiccation cracks the soil is almost saturated and thus cannot be treated as a fragile material.

2.3.2 Morphology of crack network

The desiccation cracks can either be V shaped or U shaped. Where clay tenacity (Kindle, 1917) is low and the desiccated layer is able to react independently of the underlying layer, the crack shape is generally parallel-sided. Where clay tenacity is high, the degree of desiccation (number of cracks per unit length) decreases downward and the resultant crack is usually V-shaped (Plumer and Gostin, 1981). In rare instances where prolonged desiccation occurs, cracks are known to penetrate as deep as 15 m (Fairbridge and Bourgeois, 1978).

If the curvature at the tip of the crack is V shaped, then the crack is prone to continue propagating as the area around the tip is very weak. On the other hand, a crack with a U shaped tip will not propagate quickly. This means that a V shaped cracks are likely to deepen over time, while a U shaped crack will stay the same unless desiccation occurs

again at the broad tip of the crack (Plummer and Gostin 1981). The shape of the crack may be a good indication of how deep into the soil mass it may penetrate.

Owing to the difficulty in observing the depth of the crack, more often surface crack patterns are observed. The observed patterns are generally in polygonal shapes (Konrad and Ayad, 1997; Dyer et al., 2009). The number of sides of the polygons generally lies between three and six. The size of polygons and the spacing of joints are determined primarily by the rate of evaporation. The polygons may be combined triangles, quadrangles, pentagons or hexagons because of the heterogeneous soil and boundary conditions. Some researchers have attempted to model the crack geometry mathematically. Horgan and Young (2000) developed a random model to capture the geometry of two-dimensional crack growth. Chertkov and Ravina (1998) developed a physically based probabilistic model of the crack network. The model described the distribution in terms of: (i) Number of cracks in a unit volume of soil, (ii) crack dimensions (depth, length and width), (iii) crack area at the soil surface, (iv) crack volume as a function of soil depth.

Apart from propagating in vertical direction, horizontal cracks joining the vertical cracks have been also been observed (Konrad and Ayad, 1997; Lakshmikantha, 2009 and Dyer et al., 2009). These subhorizontal cracks highly influence the hydraulic conductivity of the soil by increasing the interconnectivity between the cracks. Konrad and Ayad (1997) exposed an excavation to continuous evaporation for 35 days and observed subhorizontal

cracks at some depth below the surface. A schematic diagram explaining the mechanism of formation of subhorizantal cracks as described by Konrad and Ayad is shown in Figure 2.2.

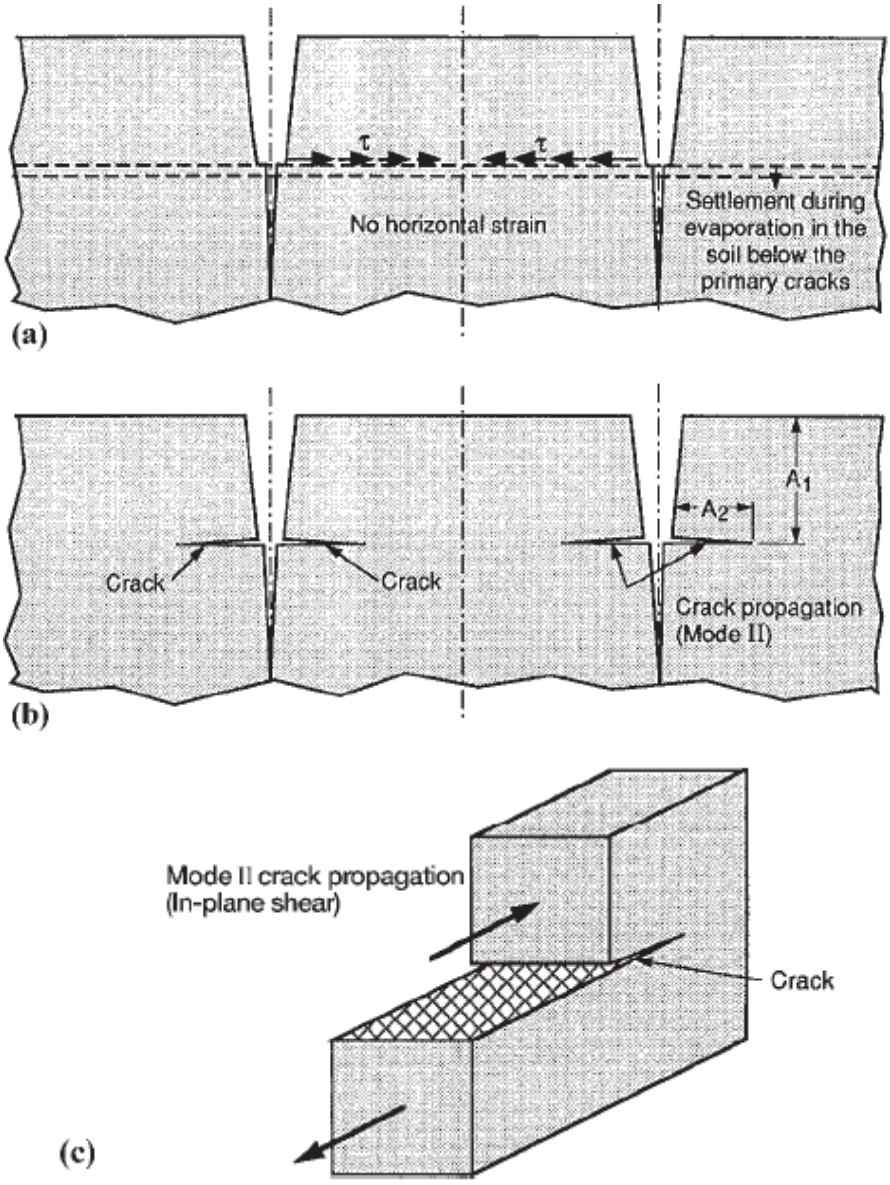

Figure 2.2. Schematic description of propagation of cracks in soil (after Konrad and Ayad, 1997)

Chertkov and Ravina (1999) developed a mathematical model to predict the mean width and volume of cracks as a function of soil depth. They assumed that the horizontal cracks appear as result of inhomogeneous soil subsidence caused by rapid drying and shrinkage of thin layers at the wall of vertical cracks.

2.4 Observations of desiccation crack geometry recorded in literature

It is very difficult to ascertain the geometry of a crack without disturbing the soil (and therefore changing the crack geometry). Various methods have been devised both direct and indirect to quantify the geometry of cracks. Some of them are mentioned below:

a) Needle-for crack depth (Zein el Abedine and Robinson, 1971):

Deep cracks were measured with a 150 cm long probe with a diameter of 3 mm, and shallow cracks were measured by a 50 cm long probe with a 1.5 mm diameter.

b) Wedge-for crack width (Zein el Abedine and Robinson, 1971)

A wedge with head angle 22.5 degrees was used to find the width of the crack.

c) Digital Photogrammetry (Jessell et al., 1995)

Pictures of the crack network were taken and then digitized to analyze the surface crack pattern.

d) Shadow profilometry-for aperture (Maerz et al., 1990)

Shadow cast were used to determine the roughness of a rock joint. The image of the shadow was video recorded and digitized so that more accurate estimates could be made about rock joint aperture and roughness.

e) Time domain reflectometer (Dyer et al., 2009)

Time domain reflectometer (TDR) sensors were inserted in the soil to measure its dielectric properties. As the cracks are usually filed with air, they can be detected by this method because of the poor conductivity of air.

f) Tomography- (L. Øygarden et al., 1997)

Soil cores were scanned using x-ray computed tomography (CT) to determine if macropores such as cracks, earthworm holes and root channels could be distinguished and characterized. It was found that macropores 1 mm and larger could be easily and quickly distinguished by the method.

2.4.1 Laboratory observations

Many laboratory experiments have been conducted to estimate the geometry of desiccation cracks or to find their effects on hydraulic behavior namely permeability. Some of the prominent ones are discussed below:

Hinsby et al. (1996) took a cylindrical sample of undisturbed till 0.5 m diameter and 0.5 m high from a depth of 2-2.5 m. The soil was massive clay (12 % clay, 31 % silt and 57 % sand and gravel) with various vertical fractures. Typical fracture spacing was approximately 5-10 cm and typical fracture length was 5-30 cm. Tracer fluid was injected into the soil to clearly see the density of the cracks and the permeability was measured. Finally, calculations were made to estimate the aperture using the cubic law as given by Snow (1969) using the permeability tests done on the sample.

Laboratory experiments were done by Nahlawi and Kodikara (2006), primarily to find the spacing between the cracks. The soil used was natural clay from Victoria, Australia. The specimens were prepared in long glass trays and the sides were greased (Figure 2.3). The depth of the soil sample was 5 mm, 8 mm and 11 mm. The cracks were parallel to each other as the ratio of length to width of the sample was large. The spacing between the soils was recorded and it was concluded that the crack spacing follows a lognormal distribution.

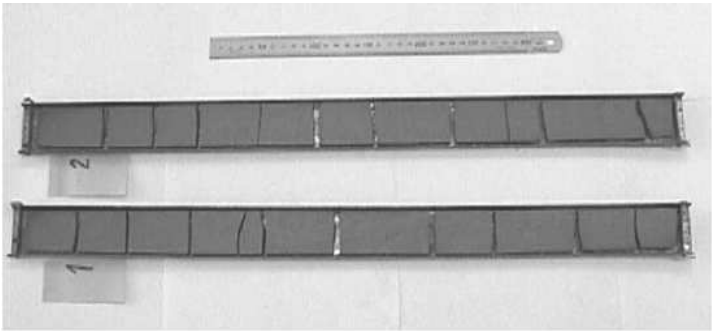

Figure 2.3. Soil samples in glass plates exhibiting desiccation cracks (after Nahlawi and Kodikara, 2006)

2.4.2 Field observations

Zein el Abedine and Robinson (1971) developed a method to find the dimensions of the cracks in the field. A wedge with head angle 22.5 degrees was used to find the width of the crack. The depth of cracks was measured using thin flexible graduated metal probes with pointed smooth noses. Deep cracks were measured with a 150 cm long probe of a diameter of 3 mm, and shallow cracks were measured by a 50 cm long probe with a 1.5 mm diameter. The field measurements were done on soils subjected to different

conditions such as irrigated, natural, delta, etc. In conclusion it was found that irrigation reduces cracking to about one thirds.

Dasog et al. (1988) did field experiments to understand the swell-shrink potential of soil in Saskatchewan. Six clayey soils representing the brown, dark brown, black, dark gray and gray zones were sampled. The method used for crack size measurement was same as that used by Zein el Abedine and Robinson (1971). A modified sampling method as well as a larger area was used to get better representation of the spatial variability of cracks.

Realizing the practical difficulty in finding the aperture of cracks in soil because of their expected small size, McKay et al. (1993) devised a set up to find the field hydraulic conductivity of the soil. The experiment was done on clay rich tills of Ontario which were fractured to depths of 4-6 m. The crack aperture was then back calculated using the hydraulic conductivity of the soil by cubic law. Statistical analysis of the crack aperture suggested that it follows lognormal distribution. The insitu setup to find hydraulic conductivity of the soil is shown schematically in Figure 2.4

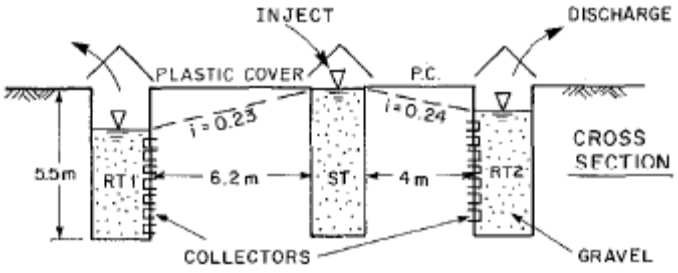

Figure 2.4. Field trench cell and collector system used by McKay et al. (1993)

Konrad and Ayad (1997) exposed marine clay to continuous evaporation for 35 hours. The base of the excavation was instrumented with thermistors, settlement plates and TDR probes. They observed the surface crack geometry was in the shape of polygons with the average crack spacing of 20 to 24 cm. After about 100 hours of evaporation, horizontal cracks started to appear. Further evaporation led to newly induced polygons with protuberance (Figure 2.5) at their bottom indicating that the depth of crack propagation was 4 to 6 cm.

Figure 2.5. Picture depicting polygonal cracking with protuberance (after Konrad and Ayad, 1997)

Li Jinhui (2007) in her PhD study investigated the crack development and characterized crack geometrical parameters under natural atmosphere conditions through field tests. A digital imaging method was used to investigate the cracks near the foot of a slope. The images were imported to AutoCAD and scaled to full size to find the crack length and

aperture (Figure 2.6). It was found that crack length and crack aperture both follow lognormal distribution.

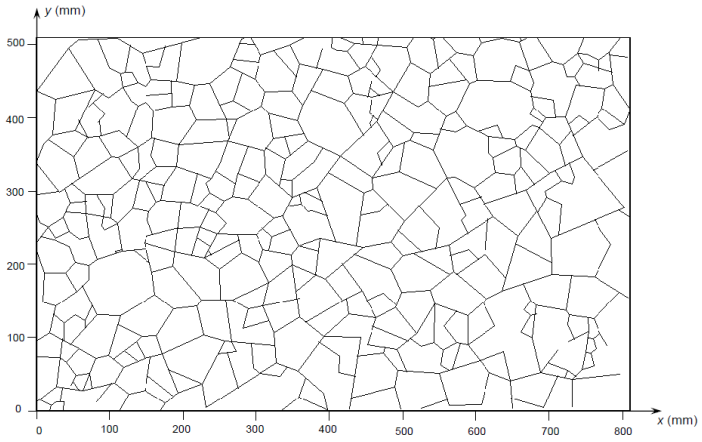

Figure 2.6. Crack geometry imported to AutoCAD (after Li Jinhui, 2007)

Dyer, Utili and Zielinski (2009) conducted field surveys on flood embankments made of alluvial clays in UK. Actual field data was gathered by making trenches in the embankment (Figure 2.7). They found that cracks extended to a depth of 60 cm. There were subhorizontal cracks as well running at a depth of 30 cm from the surface. Some of the trenches had no subhorizontal cracks but long deep vertical cracks running to a depth of 1.1 m were observed.

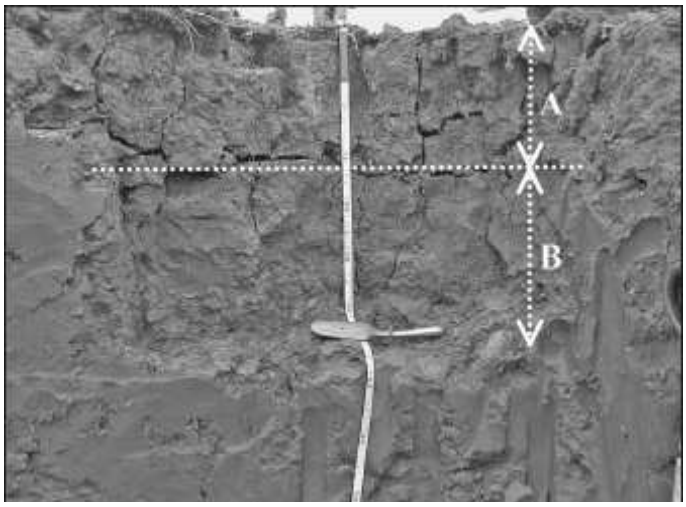

Figure 2.7. Trench dug in slopes showing vertical and subhorizontal cracks (after Dyer et al., 2009)

A summary the various field and laboratory methods to find cracks geometry is presented in Table 2.1

Table 2.1 Summary of the various field studies undertaken to determine crack geometry.

Author	**Year**	**Remarks**
EL Abedine and Robinson	1971	Developed mechanical insitu methods to determine the geometry of cracks. Observations were made on different kinds of soils under different conditions.
McKay et al.	1993	Developed an insitu method to determine the hydraulic conductivity of the soil. From the hydraulic conductivity data, they estimated the cracks aperture at different depths using the cubic law. The crack aperture was found to follow a lognormal distribution.
Hinsby et al.	1996	Calculated the permeability of a soil sample and used the cubic law to determine the crack aperture from the permeability.

Table 2.1 continued

Author	Year	Remarks
Konrad and Ayad	1997	Exposed marine clay to continuous evaporation for 35 hours and instrumented it with thermistors, settlement plates and TDR probes. The observed polygonal surficial geometry of the crack network and the presence of subhorizontal cracks.
Nahlawi and Kodikara	2006	Prepared soil samples in smooth long plates with different thicknesses of the soil sample. The sample was subjected to heating leading to desiccation cracks. The measurement of the crack aperture showed that they follow a lognormal distribution.
Li Jinhui	2007	Used digital photogrammetry to ascertain the aperture and spacing between the cracks of a soil slope under natural conditions. She found out that the crack spacing and crack aperture follow a lognormal distribution
Dyer at al.	2009	Conducted a field surveys on flood embankments in UK. They excavated trenches to find the geometry of crack network inside the embankment. Actual field data was gathered by making trenches in the embankment. They recorded vertical cracks as deep as 1.1 m. Also at places they confirmed the presence of subhorizontal cracks.

2.4.3 Geophysical methods

In practice, it can be difficult to detect desiccation fissuring only by visual observations, particularly if the surface vegetation is well developed. Even if cracking near the surface

is observed, it is not be possible to determine the depth to which the cracking penetrates without careful excavation and inspection. Such an approach is not usually advocated because the damage caused by the inspection may be worse than that caused by the cracking itself. Some of the past researchers (e.g. Pugh, et al., 1995; Chandler et al., 1995) proposed desiccation fissuring detection in clayey embankments, but these methods are only point-wise measurements and cannot cover the whole structure. So, a reliable technique to assess the presence of desiccation crack network, their geometrical characteristics (i.e. space between cracks, depth, aperture and morphology) and the whole integrity of earthworks was much needed. Indirect geophysical method can be very useful for such an endeavor.

One of the first successful studies on the use of geophysical investigations took place in Sweden, where a permanent monitoring system was designed and built at two dams (Johansson and Dahlin, 1998). The main aim of these investigations was to evaluate the seepage through the embankment (Dahlin et al., 2001). Another successful method was developed by the LCPC (French Public Works Research Laboratory) and the Cemagref in Aix en Provence, France, which consisted of a comprehensive experimental research from 1998 to 2004 that included the testing of different geophysical and geotechnical methods for improving the integrity assessment of embankments for flood protection. Their main interest was on evaluating the effect of internal erosion (Fauchard and Meriaux, 2004). In this study the cracks were artificially recreated and geophysical resistivity was measured by using only two electrodes. Samouëlian et al. (2003) were the

first in using miniature resistivity arrays to detect cracks of a few centimeters in size. They created cracks of 2 mm width artificially with a saw at varying depths (1, 2, 3, and 4 cm deep) in order to obtain four cracking stages. The resistivity images obtained from this study enabled the detection of discontinuities at the millimeter scale. More recently, Zielinski (2009) used a similar geophysical technique to detect the natural formation of desiccation cracks in soils (rather than in recreated artificial cracks). He used an array of 48 electrodes (which is normally used on a long distance, about 100 m), increasing the technique resolution and detected desiccation cracks in small-scale tests and on scaled flood protection embankments (Sentenac and Zielinski, 2009).

Nondestructive measurements of the desiccation crack network were carried out by using the geophysical technique developed by Zielinski (2009). The basic equipment used was composed of an ‘ARES’ earth meter equipment; forty eight non-corrosive 1.5 mm diameter and 6 cm long electrodes which were wired up and connected with the automatic resistivity system using double 24 ways connector. The electrodes were pushed 3 cm into the compacted clay keeping a 3 cm spacing between them. This technique has proved to be very useful to detect naturally formed discontinuities in the soil mass. Some results showing this type of investigation are presented in Figure 2.8 and Figure 2.9. ‘Boulder clay’ was compacted in a Perspex tank (Figure 2.8c) at water content near the optimum. An initial scan (Figure 2.8a) just after compaction showed that soil mass was quite homogeneous. Infra-red heaters (1.2 kW) were used to heat the soil. The scan after drying (Figure 2.8b) showed phase changes in color, from deep blue

to dark purple, which were due to the vertical and horizontal cracks developed during desiccation process, which resulted as response from changes in soil resistivity during desiccation. A deep blue color on the picture represents very low resistivity (~50mΩ); deep purple contour represents places with the high resistivity. The inversed resistivity map confirmed that the air space created inside the crack gave high resistivity response. The resistivity technique was also tested in a scaled embankment at the laboratory (1x1 m crest, slopes 1:2, and 2 m long, 20 cm high berm). Figure 2.9a showsa picture of the embankment just after construction and Figure 2.9c the same embankment after drying alongside two electrical resistivity images obtained in two perpendicular arrays. Figure 2.8 and Figure 2.9 show that the improved electrical resistivity nonintrusive technique provided a good image of the discontinuities in the soil mass.

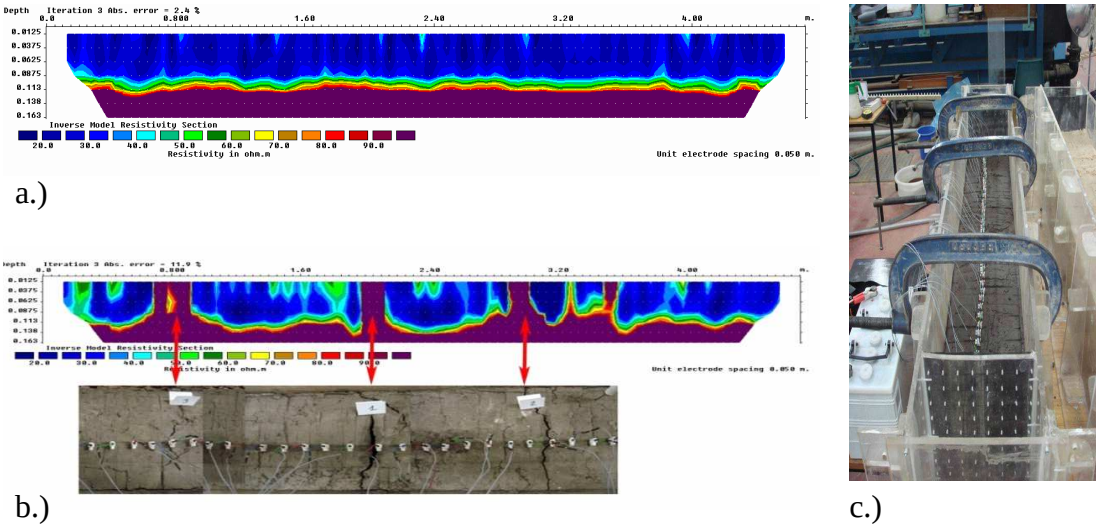

Figure 2.8. Geophysical scans: a) just after compaction; b) after drying-below picture of cracked soil. c) Picture of the scaled experiment

a)

b)

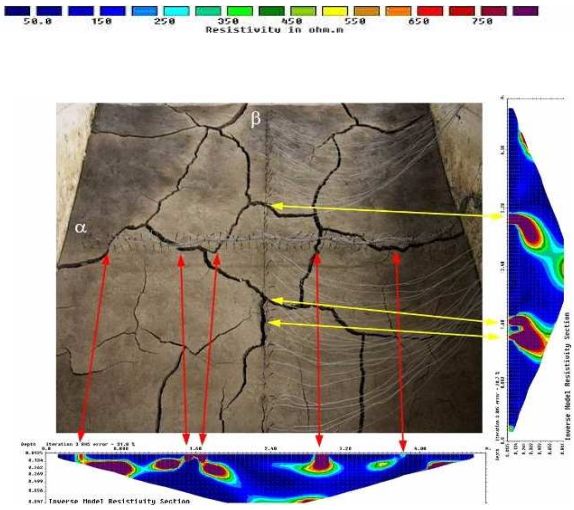

Figure 2.9. a) Scaled embankment; b) Geophysical scans and visual observation after 7 days of drying

2.5 Desiccation crack behavior during drying-wetting cycles

Soils in the field undergo repeated cycles of drying and wetting during summer seasons and rainy seasons, respectively. This repeated fluctuation in the water content causes cyclic soil swelling and depression with the consequence of opening and closing of cracks. This cyclic change in the geometry of the cracks induces changes in the mechanical and hydraulic behavior of the soil. The effect of repeated drying and wetting cycles on soil has been studied by various researchers e.g., Corser and Cranston (1991), Yesiller et al. (2000), Eigenbrod (2003), Rayhani et al. (2007), Zielinski et al. (2010). Yessiler et al. (2000) subjected compacted clay liners to repeated drying and wetting cycles and observed that the amount of cracking does not change after the second cycle. Rayhani et al. (2007) conducted some lab tests on cylindrical specimens to see the effect of repeated drying and wetting on the hydraulic conductivity of the soil. They found that after a wetting cycle when apparently the cracks seem to close on the surface, the hydraulic conductivity was 12-34 times higher than that of the intact clay. This suggested that the cracks did not close completely upon wetting. Eigenbrod (2003), on the other hand, suggested not all fine-grained soils show an increase in the hydraulic conductivity upon cyclic drying and wetting. Certain nonplastic or very low-plastic and even certain very highly swelling soils do not experience such drastic changes in permeability. The major causes for such self-healing due to crack closure upon wetting were identified as: (i) an increase of effective stress above the level of the undrained shear strength of the intact soil; (ii) clogging of fractures by particles eroded from the

fracture surfaces during permeation for non- or low-plastic soils; and (iii) swelling of the clay particles near the fracture surfaces in highly swelling clay.

2.6 Flow through a single crack

Fluid flow through cracks is commonly described by parallel plate model where the volume of the flow rate varies as the cube of the joint aperture. This relation is famously known as the cubic law (Snow, 1969) and is expressed in its general form as:

$$\frac{Q}{\nabla h} = Cb^3 \qquad (2.1)$$

where, ‘ Q ’ is flow rate, ∇h is hydraulic gradient, ‘C’ is a constant and ‘b’ is aperture width. The cubic law is valid for the laminar flow of a viscous incompressible fluid. However deviations from this law are expected as real crack surfaces are rough and contact each other at discrete points (Figure 2.10).

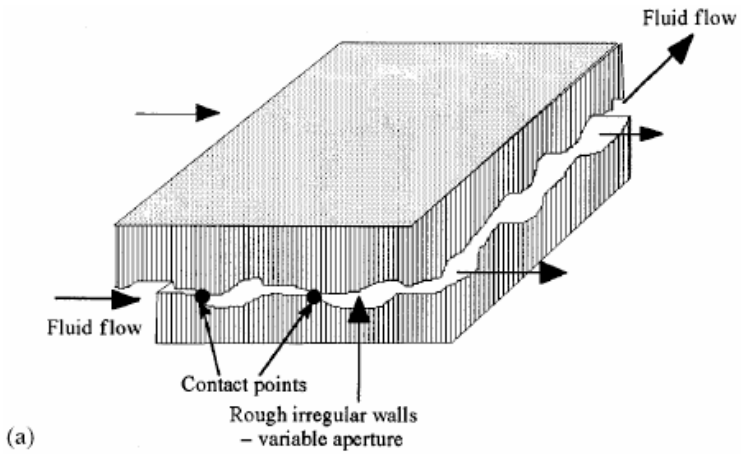

Figure 2.10. Flow through a single fracture: (a) Natural fracture; (b) Idealized fracture. (after Indraratna et al., 1999)

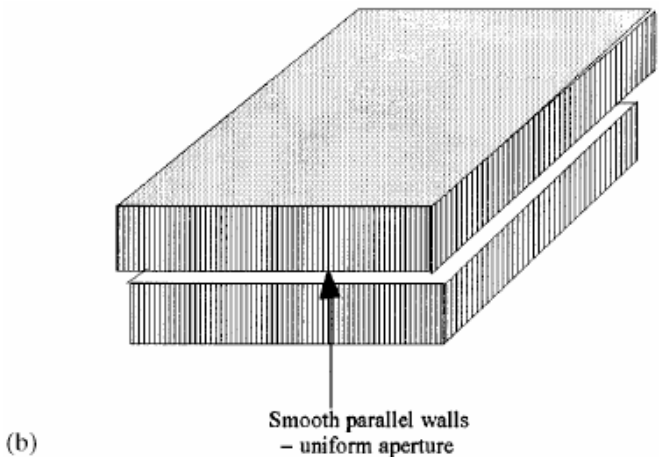

Figure 2.10. continued

Researchers in the past have studied the effect of crack surface roughness and variable aperture width on its hydraulic conductivity when the flow is steady as well as turbulent (Witherspoon et al., 1980; Brown, 1987; Indraratna et al., 1999). A generalized law for flow through fractures (Indraratna et al., 1999) was worked out in terms of the Reynolds number, 'Re', and friction factor, ' ψ ' such that for open fractures:

$$\psi = \frac{96}{Re} \tag{2.2}$$

However, to account for other variabilities in the crack geometry, Witherspoon et al., (1980) introduced a factor, ' f ' in the cubic law such that it takes the following form:

$$\frac{Q}{\nabla h} = \frac{C}{f}(b)^3 \tag{2.3}$$

In their study they found that the above expression held regardless of the different loading patterns and that 'f' varied from 1.04 to 1.65.

For generalized flow (both laminar and transient), the pressure drop coefficient is normally represented as:

$$\lambda = f(Re, k/2e) \qquad (2.4)$$

where, ' λ ' is pressure drop coefficient, 'k' is joint roughness and 'e' is joint aperture.

Table 2.2 gives the pressure drop coefficient and flow rate, established by different researchers, for a range of relative roughness, for both laminar and turbulent flow to express fluid flow through a single crack.

Table 2.2. Pressure drop coefficient and the unit flow rate in single joint (after Indraratna et al., 1999)

	Flow Type	Pressure drop coefficient	Flow rate	Comments
Relative roughness, $k/D_h \leq 0.033$ (Parallel flow)	Laminar	$\lambda = \frac{96}{R_e}$ Poiseuille	$q = \frac{g}{12v} e^3 J$	Overestimates the flow volumes Widely used in numerical models
	Turbulent	$\lambda = 0.316\ R_e^{-0.25}$ Blasius	$q = \left[\frac{g}{0.079}\left(\frac{2}{v}\right)^{0.25} e^3 J\right]^{4/7}$	
		$\frac{1}{\lambda} = -2 \log \frac{k}{3.7\ D_h}$ Nikuradse	$q = 4\sqrt{g}\left(\log \frac{3.7D_h}{k}\right) e^3 \sqrt{J}$	Need to know roughness of each joint Results may be better than flow rate values computed by cubic law, if correct roughness is used Yields low magnitude of flow rate than cubic law.
Relative roughness, $k/D_h > 0.033$ (Nonparallel flow)	Laminar	$\lambda = \frac{96}{R_e}\left[1 + 8.8\left(\frac{k}{D_h}\right)^{1.5}\right]$ Louis	$q = -\frac{g\ e^3\ J}{12v\ [1 + 8.8(k/D_h)^{1.5}]}$	
	Turbulent	$\frac{1}{\sqrt{\lambda}} = -2 \log \frac{k}{1.9\ D_h}$ Louis	$q = 4\sqrt{g}\left(\log \frac{1.9D_h}{k}\right) e^{1.5} \sqrt{J}$	

In the above table (Table 2.2) J is hydraulic gradient, 'D_h' is hydraulic aperture and ' ν ' is viscosity.

Brown (1987) plotted the ratio $(d_h/d)^3$ for different mechanical apertures where, 'd_h' is hydraulic aperture and 'd' is the average aperture. The plot is shown in Figure 2.11. He found out that the cubic law works well for larger apertures, however, for small aperture widths the flow rate as predicted by the cubic law was 40-70% higher than the actual flow rate.

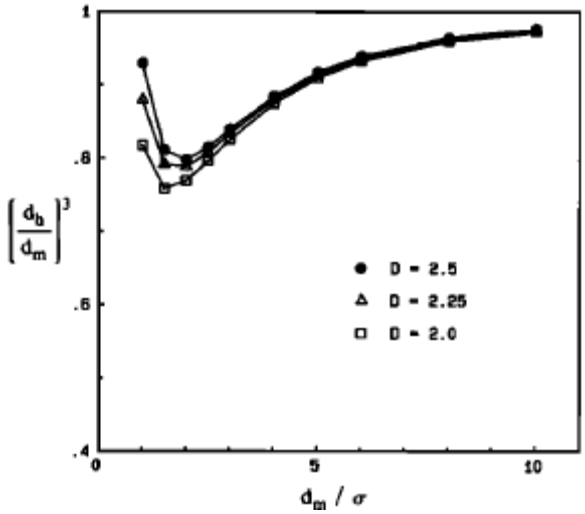

Figure 2.11. Hydraulic aperture d_h compared to the mechanical aperture d_m for all fractal dimensions (after Brown, 1987)

Indraratna et al. (1999) also summarized the comments of various researchers (Table 2.3) on the application of the cubic law.

Table 2.3. Application of cubic law in research purposes and in numerical models (after Indraratna et al., 1999)

Studies	Applications	Comments
Engelder and Scholz (1981)	Experimental investigation of flow through artificial fractures	Cubic law is found to be valid
Gale and Raven (1980)	Radial fluid flow through natural fractures – Experimental	Not in agreement
Pyrak-Nolte *et al.* (1987)	Flow through natural low permeability rocks – Experimental	Cubic law is valid for effective stress below 20 MPa
Brown (1987)	Effects of surface roughness on flow – Numerical	Cubic law estimates 40–70% larger flow rate
Amadei and Illangasekre (1992)	Transient flow in single joint	Cubic law was used but modified to account for surface roughness
Iwai (1976)	Fundamental studies of fluid flow through a single joint	Cubic law is followed
ITSCA (1996)	Universal Distinct Element Code (UDEC)	Cubic law is used for flow calculation
Wilcock (1996)	NAPSAC fracture network code	Cubic law is used for flow calculation

Greco (2002) attempted to numerically model the flow through cracks using VIMAC (Vertical Infiltration through a Macroporous Clay) model. The macroporous swelling soil was divided into three parts: soil matrix, shrinkage cracks and permanent macropores (Figure 2.12). The shrinkage cracks changed their aperture according to the moisture content of the soil matrix while the macropores size remained constant with time. Apart from that, there were internal catchments of water inside dead end macropores. The flow of water through the soil matrix followed Darcy's equation. Infiltration experiments were conducted to calibrate the flow equations used to model the flow through the cracks and to validate the model. The proposed infiltration model was adequately able to simulate water infiltration through macroporous swelling and

shrinkage soils. However, due to the complexity of the model, a large number of parameters had to be estimated or guessed.

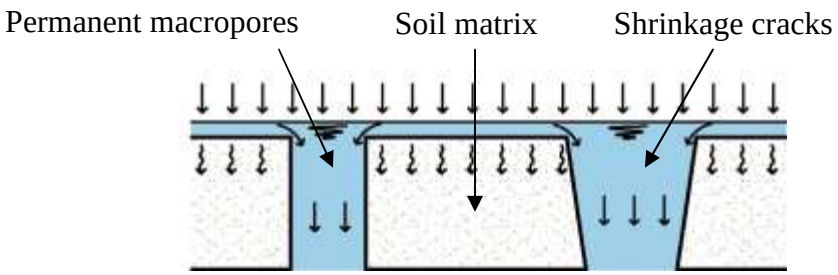

Figure 2.12. Schematic representation of the porous media divided into soil matrix, permanent macropores and shrinkage cracks in the VIMAC model (after Greco, 2002)

2.7 Flow through a crack network

Flow through a cracked porous media is affected not only by a single crack but also the connectivity of the crack network, as they provide multiple flow paths for the fluid to flow. Brady and Brown (1993) and Ohnishi et al., (1996) studied the effect of crack network on fluid flow. Ohnishi et al., (1996) summarized the work done on this topic by various researchers. Most of the expressions derived to describe flow through a crack network are too complex even after involving various simplifying assumptions.

A summary of the work done by researchers on flow through crack network is presented in Table 2.4.

Table 2.4. Various hydro-mechanical models for joints (after Ohnishi et al., 1996)

Constitutive models	Relationship	Comments
Walsh and Grosenbaugh (1979)	$K / K_0 = \left[(1 - 2\sqrt{2}(b / E_0)\ln(\sigma_n / \sigma_0)\right]^3$ K_0 = joint conductivity at σ_0 effective pressure E_0 = aperture at σ_0 effective pressure b = standard deviation of asperity height distribution	• Analytical expression deduced on the basis of elastic deformation and analogy between heat flow in a sheet and fluid flow in a planar joint • Moderate to weak results (Gale, 1993)
Gangi (1978)	$k(\sigma_n) = k_0\left[1 - (\sigma'_n / Y_n)^m\right]^3$ k_0 = permeability at zero applied stress Y_n = Y A_n, where Y is Young's modulus and A_n is contact area at effective stress σ'_n $m = 1/n$, $1 \le n < \infty$	• Rough surface was replaced by a nail bed • Experimental data show that it is valid for some rocks only
Swan (1980, 1983)	$\sqrt{K / K_0} = (1 - a_b / E) - (b / E_0)\ln(\sigma'_n)$ K_0 = hydraulic conductivity at zero stress a_b = constant and other notations are same as Walsh model described earlier	• Assuming the validity of parallel plate joint flow, the conductivity was expressed in terms of stress and roughness • No clear evidence for the validity of model
Tsang and Witherspoon (1981)	$\langle e^3(\Delta u, \sigma'_n)\rangle = \int_0^{e_0 - \Delta u_n} (e_0 - \Delta u_n - h)^3 n(h)dh \Big/ \int_0^{e_0} n(h)dh$ where, Δu_n = joint deformation e_0 = aperture at zero stress $n(h)$ = asperity height distribution σ'_n = effective stress h = asperity height	• Joint was simulated as a collection of voids, and the closure of joint is due to the deformation of voids • Model treats both loading and unloading parts of stress-joint flow curve • Validity of the model is acceptable but not totally convincing.
Barton *et al.* (1985)	Hydraulic aperture $e = \min\left[E, E^2 / (JRC)^{2.5}\right]$ Fracture permeability $k = e^2/12$ Where JRC = joint roughness coefficient E = mechanical aperture	• Modified the cubic law to account for roughness and tortuosity

2.8 Suction-moisture content relation of a crack

The relationship between the suction and moisture content is called the retention curve. The physics underlying the retention curve has been explained in detail in section 3.3. Much work has been done to characterize the relation between the soil moisture content and soil suction (e.g., Brooks and Corey, 1964; van Genuchten, 1980; Fredlund and Rahardjo, 1993). Fractures exhibit capillary pressure because of their rough walled surfaces (Firoozabadi and Hauge, 1990; Pruess and Tsang, 1990; Kueper and McWhorter, 1991; McDonald et al., 1991; Reitsma and Kueper, 1994).

Preuss and Tsang (1990) proposed the retention curve for a fracture. Their model was based on capillary allowability criterion, however, they assumed the fracture behaves like a parallel plate locally and they disregarded the hysteresis phenomenon of the water retention curve. Reitsma and Kueper (1994) developed a laboratory technique to study the hysteresis in the water retention curve of rough walled fracture. They compared the Brooks and Corey (1964) retention curve and the van Genuchten model (1980) with their experimental data and found that the Brooks and Corey model fits the data better. Figure 2.13 gives the comparison between the two models as observed by Reitsma and Kueper (1994).

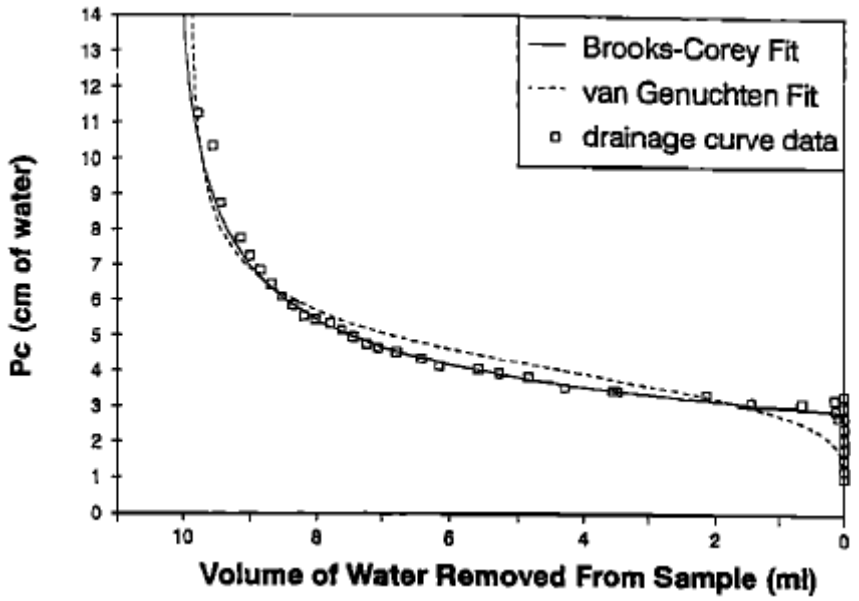

Figure 2.13. . Brooks-Corey and van Genuchten fits to the capillary pressure curve for laboratory data. Pressure expressed in equivalent height of water.

It can be noted that more research needs to be done to develop a reliable and practical water retention behavior model for cracks.

2.9 Conclusion

In this section a thorough literature review about the morphology, geometry and flow properties of the crack network was done with a special emphasis on desiccation cracks. For the current research, there was a special interest in modeling the flow of water through desiccation cracks in unsaturated soils. In the next section, all the theory and formulations required to understand flow through unsaturated porous media have been described. A joint model has also been presented to model the effect of cracks on flow in soils.

3. MODELING UNSATURATED FLOW IN POROUS MEDIA

3.1 Overview of the section

The section contains theoretical background pertaining to flow in porous media. A special emphasis has been given to unsaturated flow and all the governing phenomena and equations associated with the unsaturated flow have been described in detail. Finally, the joint model to simulate fluid flow through cracks has been presented.

3.2 Porous media

Porous media (Bear, 1972) is a portion of space occupied by heterogeneous or multiphase matter in which at least one of the phases comprising the matter is not a solid. The solid phase is called the solid matrix and the space within the porous medium that is not a part of the solid matrix is referred to as void space (pore space). Some of the basic characteristics of a porous media are:

- The solid phase should be distributed throughout the porous medium within the domain occupied by the porous medium.
- The various openings comprising the void space should be relatively narrow.
- At least some of the pores comprising the void space must be interconnected, referred to as the effective pore space.

In order to describe the motion of fluid in a porous media there can be two approaches: microscopic approach and macroscopic approach. A very large number of molecules in a

fluid particle and the equations involved to describe the motion of these molecules, forces to abandon the microscopic approach to describe fluid motion at molecular level (microscopic approach). Instead of adopting the molecular viewpoint, a different approach which is statistical in nature is adopted to describe the motion of a system composed of many molecules. By statistical approach it is implied that the results of an analysis or an experiment are presented only in statistical form. This means the average value of successive measurements can be determined but to predict the outcome of a single measurement with certainty is not possible. When the purpose of abandoning the molecular level treatment is the description of the phenomena as a fluid continuum, the statistical approach is referred to as the macroscopic approach.

The concept of particle is essential for treatment of fluids as continua. A particle is an ensemble of many molecules contained in a small volume, the size of which is much larger than the mean free path of a single particle. It should, however, be sufficiently small as compared to the considered fluid domain that by averaging fluid and flow properties over the molecules included in it, values relevant to the description of bulk fluid properties will be obtained. So the basic concept of a continuum is the particle, or the physical point, or the representative volume over which an average is performed. The representative elementary volume (REV) is the smallest volume over which a measurement can be made that will yield a value representative of the whole. The concept of REV is explained in Figure 3.1. The small volumes V1 and V2 randomly selected do not characterize the entire volume of the site, thus they are not

representative. Beginning with V3 the porosity becomes relatively constant and thus representative.

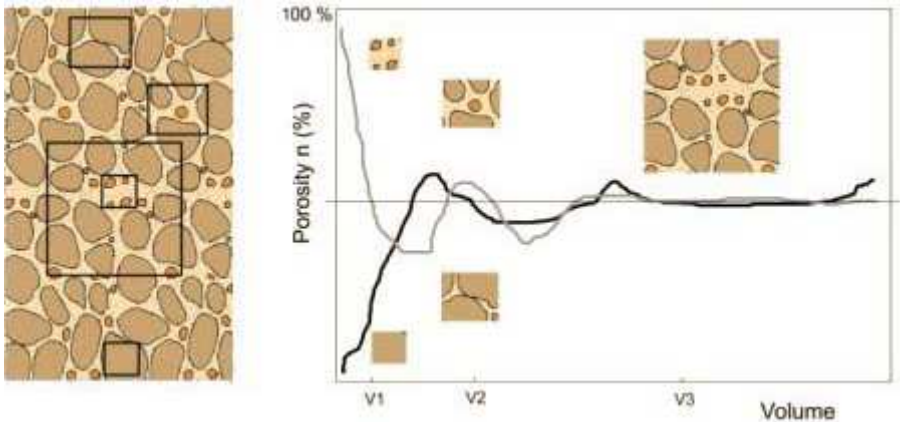

Figure 3.1. Definition of porosity and representative elementary volume.

3.3 Flow in porous media

A saturated porous media is one in which all the voids of a porous media (e.g. soil) are occupied by a single fluid (generally water). Thus flow through a saturated porous media or simply saturated flow is essentially a two phase problem (solid and liquid). However, as the liquid recedes giving way to gas (generally air) into the void space, the porous media becomes unsaturated. So, unsaturated flow is a three phase problem (solid, liquid and gas). Figure 3.2 shows the development of unsaturated soil by withdrawal of water from the void space.

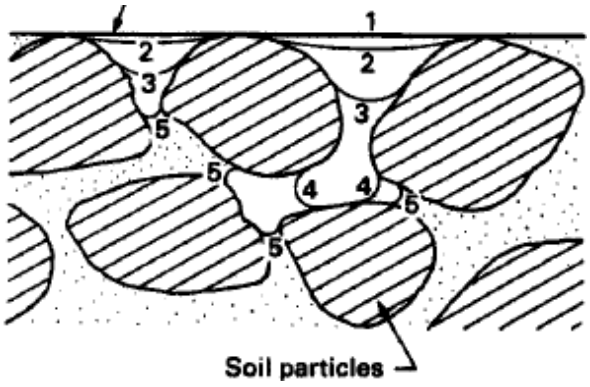

Figure 3.2. Development of unsaturated soil by withdrawal of water at different stages (1-5)

If the hydraulic head gradient in a specific fluid phase is the driving potential in that phase, then such a flow is called an advective flow (or flux). This is equally true for saturated and unsaturated porous media. The main equations associated with the saturated and unsaturated flow are presented in the following sections.

3.3.1 Flow under saturated conditions

Saturated flow in porous media is a two phase problem. To describe flow in saturated medium, in general, the continuity equation, the Darcy's law and liquid density are sufficient. Continuity equation is basically a mass balance equation. Darcy's law is an equation that describes the flow of a fluid through a saturated porous medium. It is based on conservation of momentum. It relates the discharge velocity to the hydraulic gradient through a coefficient called Darcy's permeability or simply permeability. The basic assumptions of Darcy's law are:

- Fluid flow is laminar

- Soil is saturated
- Rigid soil skeleton (no pore-structure changes)
- Soil is homogenous
- Soil is isotropic

Under the last two assumptions the Darcy's permeability is a scalar. However, Darcy's law can be generalized for situations where above conditions cannot be assumed.

The experimentally derived Darcy's law (for homogenous incompressible fluids) was limited to one-dimensional flow and has the form:

$$q=-Ki \tag{3.1}$$

where, 'q' is the discharge velocity (one-dimensional), 'i' is the hydraulic gradient, and 'K' is the Darcy's permeability.

When the flow is three-dimensional the obvious formal generalization of Darcy's law is:

$$\mathbf{q} = -\mathbf{K}\nabla h \tag{3.2}$$

where, '**q'** is the specific flux vector, ∇h is the hydraulic gradient and '**K'** is the permeability tensor. When the flow takes place in homogenous, isotropic medium, **K** takes the following form:

$$\mathbf{K} = K\mathbf{I} \tag{3.3}$$

where, 'K' is a constant scalar and '**I**' is the identity matrix.

For fluid flow in a non-deformable saturated medium, the continuity equation can be written as:

$$\frac{\partial(\rho_l \phi)}{\partial t} + \nabla \cdot (\rho_l \mathbf{q}) = 0 \tag{3.4}$$

where, 'ρ_l' is the fluid density and 'ϕ' is the porosity of the porous media.

Substituting **q** from the Darcy's law in the continuity equation, one gets the general equation of fluid flow in saturated porous media:

$$\frac{\partial(\rho_l \phi)}{\partial t} + \nabla \cdot (-\rho_l \mathbf{K} \nabla h) = 0 \tag{3.5}$$

For the case of non-deformable medium (ϕ=constant) and incompressible fluid (ρ_l=constant), equation 3.5 reduces to

$$\nabla \cdot (\mathbf{K} \nabla h) = 0 \tag{3.6}$$

If the reference system corresponds to the permeability tensor principal directions, then:

$$\mathbf{K} = \begin{bmatrix} K_x & 0 & 0 \\ 0 & K_y & 0 \\ 0 & 0 & K_z \end{bmatrix}$$

So equation (3.6) can now be written as:

$$\frac{\partial}{\partial x}\left(K_x \frac{\partial h}{\partial x}\right) + \frac{\partial}{\partial y}\left(K_y \frac{\partial h}{\partial y}\right) + \frac{\partial}{\partial z}\left(K_z \frac{\partial h}{\partial z}\right) = 0 \tag{3.7}$$

3.3.2 Flow under unsaturated conditions

3.2.2.1 Suction in soil

Unsaturated conditions render the flow problem in porous media a three phase problem (solid, liquid and gas). As the liquid degree of saturation of porous media reduces below unity, gas occupies the porous space along with liquid. The pressure difference between the gas pressure and the liquid pressure gives rise to surface tension. The phenomenon of surface tension results from the intermolecular forces acting on molecules on the liquid surface. The surface tension causes the liquid surface to behave like an elastic membrane. Figure 3.3 shows the phase diagram of an unsaturated soil.

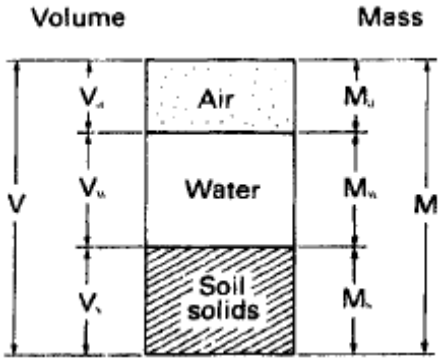

Figure 3.3. Phase diagram of an unsaturated soil system (after Fredlund and Rahardjo, 1993)

Soil suction is commonly referred to as the free energy state of soil water (Edlefsen and Anderson, 1943). The soil suction as quantified in terms of relative humidity is called total suction. It has two components: matric suction and osmotic suction. The total, matric and osmotic suction can be defined as (Aitchison, 1965):

"Matric or capillary component of free energy- In suction terms, it is equivalent suction derived from the measurement of partial pressure of the water vapor in equilibrium with the soil water, relative to the partial pressure of the water vapor in equilibrium with a solution identical in composition with the soil water

Osmotic (or solute) component of free energy- In suction terms, it is equivalent suction derived from the measurement of the partial pressure of the water vapor in equilibrium with a solution identical in composition with the soil water, relative to the partial pressure of water vapor in equilibrium with the pure water.

Total suction or free energy of soil water- In suction terms, it is equivalent suction derived from measurement of the partial pressure of water vapor in equilibrium with a solution identical in composition with the soil water, relative to the partial pressure of water in equilibrium with free pure water."

The water potential ' ψ ' can then be defined as the work required to transport a unit mass from a reference pool of pure water to the soil water under consideration, such that:

$$\psi=\psi_c+\psi_o+\psi_g+\psi_z \tag{3.8}$$

where, $\psi_c=(u_a-u_w)$: Matric (capillary) potential

ψ_o: Osmotic potential

$\psi_c=(u_a-u_{atm})$: Gas pressure potential

$\psi_z = \rho_w g z$: Gravitational potential

'u_a' is the gas pressure, 'u_w' is the water pressure, 'u_{atm}' is the atmospheric pressure, 'g' is the acceleration due to gravity, 'z' is the height above a fixed datum and 'ρ_w' is the water density.

Also, $S=-\rho_w \psi_c$: Matric suction; $\pi=-\rho_w \psi_o$: Osmotic suction

So that total suction S_t is:

$$S_t = S + \pi \tag{3.9}$$

Osmotic suction component is included as a component of the total suction only when the flow involves reactive species.

3.3.2.2 Water retention behavior

In an unsaturated soil, the liquid surface is subjected to an air pressure 'u_a', which is greater than the water pressure 'u_w'. Thus the water is in tension. The pressure difference $(u_a - u_w)$ is referred to as the matric suction (or capillary pressure, 'p_c'). The pressure difference causes the liquid surface to curve according to the equation:

$$(u_a - u_w) = \frac{2T_s}{R_s} (= p_c) \tag{3.10}$$

where, 'T_s' is the surface tension and 'R_s' is the radius of curvature of the contractile skin.

The connected soil pores can be considered as rough and twisted capillary tubes allowing the water to rise. The capillary pressure (p_c) varies with mean curvature of the (microscopic) menisci within the pores. As the curvature varies with saturation the capillary pressure is also a function of liquid degree of saturation (S_l). The relationship $p_c = p_c(S_l)$ must be determined experimentally.

The retention curve gives the relationship between the matric suction and liquid degree of saturation. The shape of the retention curve depends on the pore size distribution and on pore shapes. The retention curve obtained for a sample is different for drying and wetting because of the hysteresis phenomena. The non-uniform pore size distribution in soil can result in hysteresis in the retention curve. This geometry of the void space with bottlenecks causes different degree of saturation in the soil for the same matric suction. This phenomenon is called the ink-bottle effect. The phenomenon is explained in Figure 3.4a.

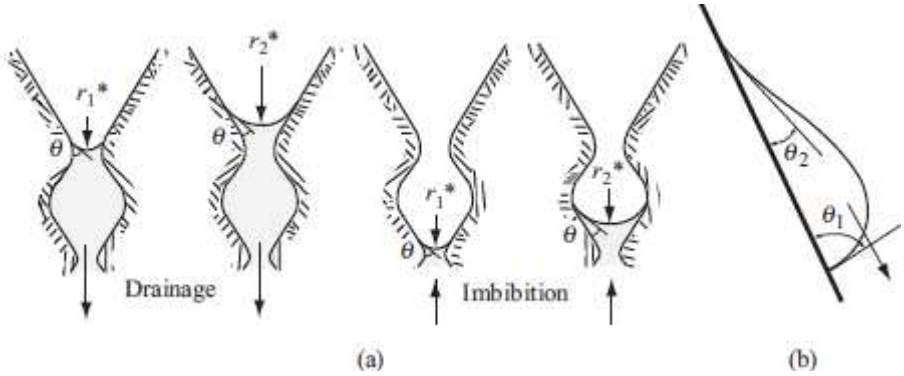

Figure 3.4. (a) Ink bottle effect and (b) rain drop effect causing difference in capillarity during wetting and drying

In addition, the contact angle may have different values if equilibrium is approached by advancing trace of a water-air interface on a solid than at the receding one because of impurities and variability in the mineral that compose the surface, roughness of the solid, gravity and polar nature of the liquid (Bear and Alexander, 2008). This phenomenon called the rain drop effect also causes hysteresis of the retention as shown in Figure 3.4b above. Figure 3.5 shows a typical retention curve exhibiting hysteresis.

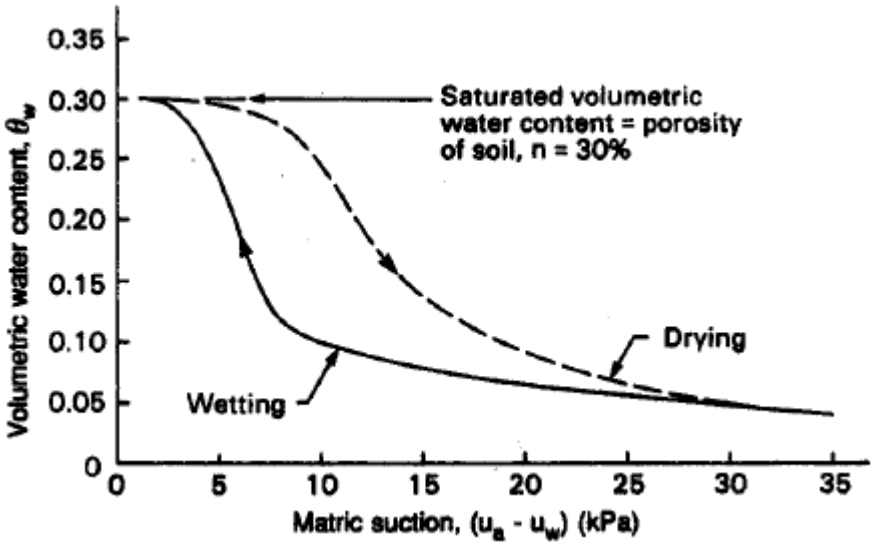

Figure 3.5. A typical retention curve (after Fredlund and Rahardjo, 1993)

3.3.2.3 Darcy's law for unsaturated flow

Darcy's law can also be extended for the advective flow of water through unsaturated soil. However, the coefficient of permeability is a variable which is predominantly a function of the liquid degree of saturation or the matric suction of the unsaturated soil. The Darcy's permeability can be modified for unsaturated flow as:

$$K_{unsat} = K k_{r\alpha} \tag{3.11}$$

where, 'K_{unsat}' is modified Darcy's permeability for unsaturated soil and '$k_{r\alpha}$' is the relative permeability (subscript 'α' is to distinguish between the relative permeability of liquid, $\alpha = l$ from gas $\alpha = g$). Underlying the extension of the motion equation of a single fluid to the simultaneous flow of two or more fluids is the concept of relative permeability. It is natural to assume that when flow of one of the fluids at a point is being considered, since the part of the pore space in the vicinity of that point is occupied by another fluid, the permeability of the porous medium would be reduced with respect to the fluid considered. Relative permeability takes into account this reduced pore space of the porous medium for the fluid in question as shown schematically in Figure 3.6.

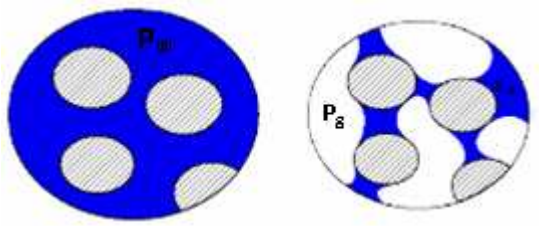

Figure 3.6. Reduced pore space for liquid flow due to reduced liquid degree of saturation

In particular, in an unsaturated soil, water can be visualized as flowing only through the space filled with water. The air filled pores are non-conductive channels to the flow of water and therefore can be considered as behaving similar to the solid phase, and the soil can be treated as saturated soil having a reduced liquid degree of saturation. Figure 3.7

shows that as liquid degree of saturation approaches 1, k_{rl} approaches 1 and k_{rg} approaches 0 and vice versa as liquid degree of saturation approaches 0.

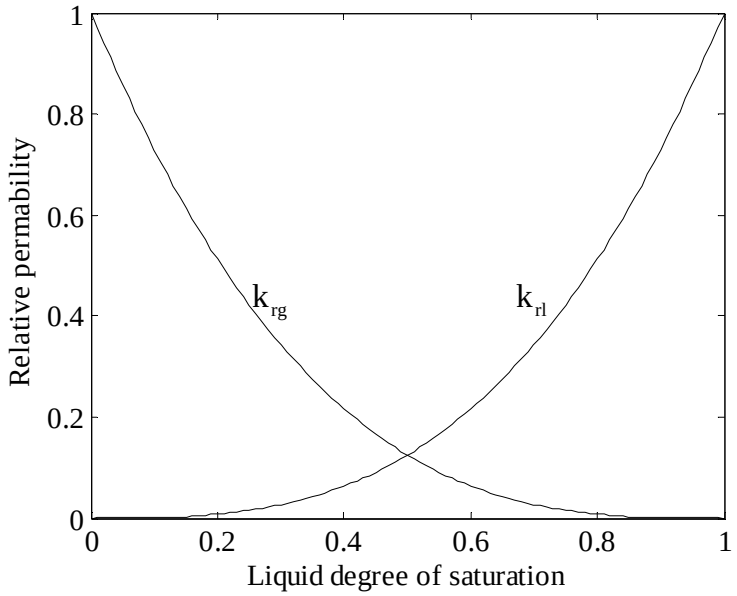

Figure 3.7. Effect of liquid degree of saturation on the relative permeability of liquid and gas

In unsaturated conditions water is also present in the gas phase as vapor. As explained below in the next section, vapor transfer in the gas phase is due to the gradient of vapor concentration which can be calculated by Fick's law. Similarly, undissolved air is also present in the liquid phase. The transfer of air in the liquid phase is due to the gradient of concentration of air in liquid phase, which is again calculated using the Fick's law.

3.4 Modeling unsaturated flow in porous media

For this thesis the finite element program CODE_BRIGHT was adopted to perform the numerical simulations. It is a tool designed to handle thermo-hydro-mechanical (THM) coupled problems in geological media. This code has been extensively applied and validated in different simulation involving complex coupled geomechanical applications (e.g. Olivella et al., 1996; Alonso and Alcoverro, 1998, 2005; Sanchez et al., 2005, 2008, 2010, 2011; Gens, 2009)

3.4.1 Governing equations used to model unsaturated flow

CODE_BRIGHT uses a macroscopic approach developed in the context of the continuum theory for porous media for the analyses (Olivella et al., 1994). It is assumed that the porous medium is made up of three phases: solid (s), liquid (l) and gas (g). The liquid phase contains water (w) and dissolved air (a) whereas the gas phase is made up of dry air and water vapor. The hydraulic component should be understood in a generalized way, i.e. including both liquid and gas flow. In the present work, a constant temperature has been maintained for solving the problems. The mathematics of this macroscopic approach for solving flow of liquid under isothermal conditions is expressed in terms of the following governing equations:

- Balance equations
- Constitutive equations
- Equilibrium restrictions

Table 3.1 summarises these equations. Note that each of them is associated with one variable, as proposed in the original work by Olivella et al. (1994). This association is not unique as each equation is related to several variables. Hence, the variable shown in Table 3.1 should be understood as the one employed in subsequent derivations.

Table 3.1. Summary of constitutive equations, balance equations and equilibrium restrictions for flow problem

Balance equations	**Variable name**	**Symbol**
Water mass balance	Liquid pressure	u_l
Air mass balance	Gas pressure	u_g
Constitutive equations	**Variable name**	**Symbol**
Fick's law (vapor and air)	Vapor and air non-advective flux	
Darcy's law (liquid and gas)	Liquid and gas advective flux	$\mathbf{q_l}$, $\mathbf{q_g}$
Retention curve	Liquid phase degree of saturation	S_l
Liquid density	Liquid density	ρ_l
Gas law	Gas density	ρ_g
Equilibrium restrictions	**Variable name**	**Symbol**
Henry's law	Air dissolved mass fraction	ω_l^a
Psychrometric law	Vapor mass fraction	ω_g^w
Constraints	**Variable name**	**Symbol**
$\omega_l^w + \omega_l^a = 1$	Mass fraction of water in the liquid phase	ω_l^w
$\omega_g^w + \omega_g^a = 1$	Mass fraction of air in the gas phase	ω_g^a

3.4.1.1 Mass balance equations

The mass balance equation accounts for a given specie in a phase, in the flux of the specie as well as in the source and the sink of the specie. The compositional approach has been adopted in CODE_BRIGHT to establish the mass balance equations and it consists of balancing the species (water and air) instead of balancing phases (solid, liquid and gas). The subscripts are used to identify the phase ('s' for solid, 'l' for liquid and 'g' for gas) and the superscripts indicate the species: 'w' for water and 'a' for air. In the case of unsaturated flow, two sets of balance equations need to be satisfied:

1. Water mass balance
2. Air mass balance

They water mass balance equation can be generally expresses as:

$$\frac{\partial}{\partial t}\begin{pmatrix}\text{mass of water in liquid}\\ \text{and gas phases}\end{pmatrix}+\nabla\cdot\begin{pmatrix}\text{total advective and non}\\ \text{advective fluxes of water}\end{pmatrix}=\text{external supply of water}$$

and similarly, air mass balance equation is expressed as:

$$\frac{\partial}{\partial t}\begin{pmatrix}\text{mass of air in liquid}\\ \text{and gas phases}\end{pmatrix}+\nabla\cdot\begin{pmatrix}\text{total advective and non}\\ \text{advective fluxes of air}\end{pmatrix}=\text{external supply of air}$$

A more formal description of the above equations as used in CODE_BRIGHT is given below:

Water mass balance equation

$$\frac{\partial}{\partial t}\left(\theta_l^w S_l\phi+\theta_g^w S_g\phi\right)+\nabla\cdot(\mathbf{j}_\mathbf{l}^\mathbf{w}+\mathbf{j}_\mathbf{g}^\mathbf{w})=f^w \qquad (3.12)$$

where, ‘ θ_l^w ’and ‘ θ_g^w ’ are the masses of water per unit volume of liquid and gas phase respectively, ‘ $\mathbf{j}_l^w$ ’and ‘ $\mathbf{j}_g^w$ ’ denote the total mass fluxes of water in the liquid and gas phases with respect to a fixed reference system, ‘ f^w ’ is the external mass supply of water per unit volume of medium and ‘$S_\alpha^{'}$ is the volumetric fraction of pore volume occupied by the ‘α’ phase (α=l, g).

Air mass balance equation

$$\frac{\partial}{\partial t}\left(\theta_l^a S_l \phi + \theta_g^a S_g \phi\right) + \nabla \cdot (\mathbf{j}_l^a + \mathbf{j}_g^a) = f^a \qquad (3.13)$$

where, ‘ θ_l^a ’ and ‘ θ_g^a ’ are the masses of air per unit volume of liquid and gas phase respectively, ‘ $\mathbf{j}_l^a$ ’ and ‘ $\mathbf{j}_g^a$ ’ denote the total mass fluxes of air in the liquid and gas phases with respect to a fixed reference system and ‘ f^a ’ is the external mass supply of air per unit volume of medium. Dry air is considered as a single species in spite of the fact that it is a mixture of gasses. The gaseous phase is assumed as a mixture of air and water vapor. Air is also dissolved in the liquid phase.

3.4.1.2 Constitutive Equations

Constitutive equations relate a state variable with a dependent variable, for example in the Darcy’s law, the state variable, ‘pressure’ relates the dependent variable ‘flux’.

Advective fluxes are computed using generalized Darcy's law, can expressed as (Gens and Olivella, 2001):

$$\mathbf{q}_{\alpha} = -\mathbf{K}_{\alpha}\left(\nabla P_{\alpha} - \rho_{\alpha}\mathbf{g}\right); \qquad \alpha = l, g \tag{3.14}$$

where, 'P_{α}' is the phase pressure, '$\mathbf{K}_{\alpha}$' is the permeability tensor of 'α' phase and '**g'** is the gravity vector. The permeability tensor is not constant but, in turn, it depends on other variables:

$$K_{\alpha} = \mathbf{k}\frac{k_{r\alpha}}{\mu_{\alpha}} \qquad \alpha = l, g \tag{3.15}$$

where, 'μ_{α}' is the dynamic viscosity of the 'α' phase, '$k_{r\alpha}$' is the 'α' phase relative permeability and '**k**' is the intrinsic permeability tensor that depends on pore structure. The intrinsic permeability tensor, **k** of the soil represents the characteristics of the porous medium and is independent of the fluid properties. For a purely hydraulic problem (no mechanical effect), **k** remains constant with time.

The relative permeability for the liquid phase was calculated using the generalized power law:

$$k_{rl} = AS_{l}^{\lambda} \tag{3.16}$$

where, A is a constant (generally equals 1) and λ is the power (generally equals 3)

The retention curve relates degree of saturation to the suction. The retention curve followed the van Genuchten Model which has the following form:

$$S_l = \left(1 + \left(\frac{u_a - u_w}{P_0} \right)^{\frac{1}{1-\lambda}} \right)^{-\lambda} \tag{3.17}$$

where,

S_l: Liquid degree of saturation

$u_a - u_w$: Suction

λ, P_0: van Genuchten Model Parameters

Non-advective fluxes of species inside the fluid phases are computed using Fick's law, which expresses these fluxes in terms of gradients of mass fraction of species through a hydrodynamic dispersion tensor that includes both molecular diffusion and mechanical dispersion (Olivella et al., 1994; Gens and Olivella, 2001):

$$\mathbf{i}_{\alpha}^{i} = -\mathbf{D}_{\alpha}^{i} \nabla \omega_{\alpha}^{i}; \qquad i=w, a \qquad \alpha=l, g \tag{3.18}$$

where, '$\mathbf{D}_{\alpha}^{i}$' is the dispersion tensor of the medium and 'ω' the mass fraction of 'i' species in 'α' phase.

The properties of the fluid phase appear in the balance equations and in the constitutive laws. In general, they depend on the composition of the phase and on the state variables (temperature and pressures). Some of them are introduced below:

The function of density for the liquid phase 'ρ_l' can be expressed as:

$$\rho_l = 1002.6 \exp\left[4.5 \times 10^{-4} (P_l - 0.1) - 3.4 \times 10^{-4} T \right] \tag{3.19}$$

where, ‘T’ is temperature in ^{o}C.

The air density is obtained from the law of ideal gases:

$$\theta_g^a = \frac{M_a P_a}{R(273.15+T)} \tag{3.20}$$

where, ‘M_a’ is the molecular mass of air.

The density of the gas phase ‘ρ_g’ is obtained adding the partial densities of the two species:

$$\rho_g = \theta_g^w + \theta_g^a \tag{3.21}$$

Finally, the viscosity of the liquid ‘μ_l’ and gas phase ‘μ_g’ are, respectively:

$$\mu_l = 2.1\times10^{-12}\exp\left(\frac{1808.5}{273.15+T}\right) \tag{3.22}$$

$$\mu_g = 1.48\times10^{-12}\exp\left(\frac{(273.15+T)^{1/2}}{1+\frac{119}{273.15+T}}\right) \tag{3.23}$$

where, μ_α is in $MPa\cdot s$.

3.4.1.3 Equilibrium restrictions

The term ‘equilibrium restrictions’ generally comprises the relationships that establish the link between the state variables with the amount of the species in the phase, phase changes or other relationships that have to be fulfilled in a multiphase porous medium in equilibrium. It is generally assumed that phase changes are rapid in relation to the characteristic times typical of the problem under consideration in porous media. So, they can be considered in local equilibrium, giving rise to a set of equilibrium restrictions that must be satisfied at all times. For example, the vapor concentration in the gaseous phase is governed by the psychometric law and the amount of air dissolved in water is given by Henry’s law.

Psychometric law

The vapor concentration in the gaseous phase is governed by the psychometric law, which can be expressed as:

$$\theta_g^w = (\theta_g^w)^0 \exp\left(-\frac{\psi M_w}{R(273.15+T)\rho_l} \right) \tag{3.24}$$

where, ‘θ_g^w’ is the vapor concentration in the gas phase, ‘$(\theta_g^w)^0$’ is the vapor concentration in the gas phase in equilibrium with a liquid at flat surface (at the sample temperature), ‘Ψ’ is the total water potential of water (excluding gravity terms), in this case it is related to suction, $\psi = (u_a - u_w)$, ‘M_w’ is the molecular mass of the water (0.018 kg/mol) and ‘R’ the gas constant (8.314 J/mol/ºK). The gas laws relate vapor density and vapor pressure:

$$(\theta_g^w)^0 = \frac{M_w P_{v(T)}}{R(273.15+T)} \tag{3.25}$$

For pure water the vapor pressure is approximated as:

$$P_{v(T)} = 136075 \exp\left(-\frac{5239.7}{273.15+T}\right) \tag{3.26}$$

Henry's law

Henry's law is adopted to define the amount of air dissolved in water. This law expresses a linear relationship between the concentration of air in dissolution and the partial pressure of air (P_a) in the gaseous phase:

$$\theta_g^a = w_a^i \rho_l = \frac{P_a}{H} \frac{M_a}{M_w} \tag{3.27}$$

where, 'M_a' is the molecular mass of the air (0.02895 kg/mol), and 'H' is Henry's constant (1000 MPa).

3.4.2 Description of the FEM package: CODE_BRIGHT

The numerical solver that integrates all the equation presented before is CODE_BRIGHT (Olivella et al., 1996; CODE_BRIGTH User's Guide, 2011). The equations are solved in a fully coupled way (monolithic) and the Newton-Raphson method is used to solve the non-linear problem. Finite differences are adopted to solve the evolution in time. One main unknown (state variable) is associated to each one of the mass balance equations. For the problems solved in this dissertation liquid pressure 'P_l' is

associated with the mass balance water and gas pressure 'P_g' is associated with the mass balance of air. Dependent variables are calculated from state variables through the constitutive equations and equilibrium restrictions. It uses Newton-Raphson method to solve partial differential equations. CODE_BRIGHT uses GiD (GiD, 2010) system for preprocessing and post-processing. GiD is an interactive graphical user interface that is used for the definition, preparation and visualization of all the data related to numerical simulations. This data includes the definition of the geometry, materials, conditions, solution information and other parameters. The program can also generate a finite element mesh and write the information for a numerical simulation program in its adequate format for CODE_BRIGHT.

3.5 Joint model to simulate flow in cracked soil

Many researchers have worked on the problem of laminar flow of a viscous incompressible fluid through fractures. Boussinesq (1868), Snow (1965), Louis (1969), Bear (1972), and Witherspoon (1980) are only a few of the many researchers who have derived the basic equations describing flow through a fracture. For laminar flow, if one adopts the analogy of planar plane plates to represent the fracture surfaces, the saturated flow law for a crack can be derived. In the present work the formulation for the laminar flow through crack was used. The derivation of flow through crack has been given, similar to the one presented by Li Jinhui, 2007 in her Phd dissertation.

For saturated laminar flow through a crack with aperture, ‘b’ and a pressure difference of ΔP between A and B (Figure 3.8)

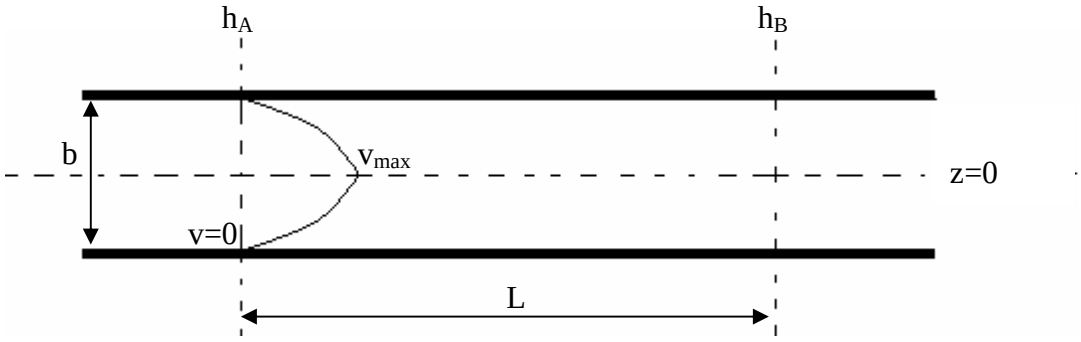

Figure 3.8. Laminar flow through a parallel crack

$$\Delta P = \gamma_w \left(h_A - h_B \right) \qquad \left[\frac{N}{m^2} \right]$$

where, h_A and h_B are the total hydraulic heads at point A and B respectively.

Force difference between A and B for a crack of unit extension is,

$$\Delta F = \Delta P \times 2z \qquad [N]$$

The shear stress, τ on the sides is,

$$\tau = -\mu \frac{dv}{dz} \qquad \left[\frac{N}{m^2} \right]$$

where, μ is the dynamic viscosity and v is the velocity.

From force balance,

$$2L\tau = \Delta F$$

$$2L\tau = \gamma_w \left(h_A - h_B \right) \times 2z$$

$$-2L\mu\frac{dv}{dz}=\gamma_w\left(h_A-h_B\right)\times 2z$$

$$dv=-\frac{\gamma_w}{\mu}Jzdz \qquad \left[\frac{m}{s}\right]$$

where, J is the hydraulic gradient, $J=\frac{\left(h_A-h_B\right)}{L}$

On integration,

$$\int_{b/2}^{z}\frac{\gamma_w}{\mu}Jzdz=-\int_{0}^{v}dv$$

$$\frac{\gamma_w}{2\mu}J\left[\frac{b^2}{2}-z^2\right]=v \qquad \left[\frac{m}{s}\right]$$

Now, rate of flow ‘Q’ is

$$Q=\int_{-b/2}^{+b/2}vdA \qquad \left[\frac{m^3}{s}\right]$$

where, *A* is the area of cross-section

On substitution,

$$Q=\int_{-b/2}^{+b/2}\frac{\gamma_w}{2\mu}J\left[\frac{b^2}{2}-z^2\right]dz$$

$$Q=\frac{\gamma_w}{12\mu}Jb^3$$

For, a two-dimensional flow cross-sectional area, '*A*' equals the aperture width, 'b'. So that:

$$Q = \left(\frac{\gamma_w}{12\mu} b^2 \right) JA$$

Upon comparison with the Darcy's law it can be shown that the permeability of a fracture, 'K_f' is:

$$K_f = \frac{(b)^2 \rho g}{12\mu} \tag{3.28}$$

According to Witherspoon et al. (1980), the cubic law can be applied with good degree of reliability irrespective of the shape of the crack (U or V). In order to account for the roughness of the cracks a factor 'f' is multiplied to the above equation. It was found my many comparative studies done by Indraratna et al. (1999) that cubic law overestimates the permeability of crack in soil by 40%-70%. In order to account for this bias the permeability so obtained from the cubic law was divided by a factor of 2 for modelling the cracks in an embankment, presented later in section 4 and section 5.

3.6 Instructions to use input/output files of CODE_BRIGHT

CODE_BRIGHT was used to model the cracks. It reads data from two files: *ROOT*_GEN.DAT and *ROOT*_GRI.DAT. These files are identified by the *ROOT* argument (previously read in a file called *ROOT*.DAT). The name of these two files is composed by the extension .DAT which indicates that these files contain input data, a

suffix _GEN or _GRI that follows the *ROOT* , indicates a file with general information and a file with grid information respectively, with *ROOT* being the name assigned by the user. *ROOT* _GEN.DAT file contains all the general information about the problem, i.e. information not related to the geometry of the problem. It contains information about the material properties, the constitutive laws used, boundary conditions, solver type, etc. *ROOT*_GRI.DAT on the other hand contains all the information about the geometry of the problem, such as, the location of the nodes, their connectivity and types of elements used. To numerically model the hydraulic effect of cracks in the porous media, there is a provision of using joint elements in CODE_BRIGHT. Joint elements are linear elements that can be assigned to the finite element mesh without introducing any new nodes. These elements have to be assigned material properties like intrinsic permeability, etc and follow constitutive equations like the van Genuchten model. To impose the cracks on the finite element mesh, joint elements are added in the *ROOT*_GRI.DAT file and their aperture is specified there as well. The intrinsic permeability of the crack is calculated according to the Cubic law and this information is passed to the *ROOT*_GEN.DAT file. In order to check the influence of the joint elements for a flow model response, a synthetic case was set up as discussed in section 3.7.

3.7 Application of the joint model

A model was developed in CODE_BRIGHT to check the response of the joint elements. A very simple square geometry of $1\times1\ m^2$ was constructed. Figure 3.9a shows the geometry of the model with three cracks. Meshing of the model was done using 4-node

quadrilateral elements. A structured mesh type was employed using 441 nodes and 400 quadrilateral elements. The mesh is shown in Figure 3.9b. Additional joint elements were introduced directly in the *ROOT*_GRI.DAT file to model the cracks as required to simulate the effect of the cracks.

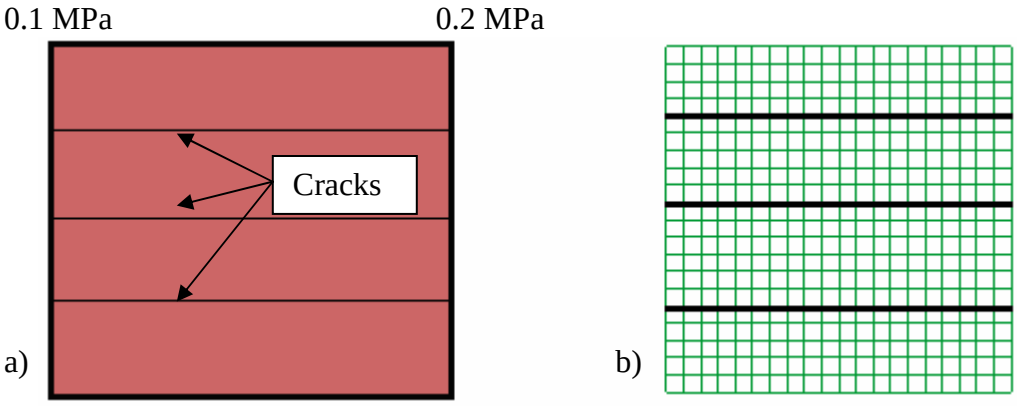

Figure 3.9. (a) Geometry of the model with three cracks (b) Finite element mesh

Using this model a comparative study was done to assess the nature of the joint element by measuring the flow at the left side boundary for the three cases:

1. Without any cracks.
2. With a single crack running through the middle of the geometry from left to right.
3. With three cracks running through the three quartiles of the geometry from left to right.

3.7.1 Initial conditions, boundary conditions and material properties.

Initially the soil mass was at a liquid pressure of 0.1 MPa (saturated), gas pressure zero and a temperature of $20\ ^{\circ}C$. A liquid pressure of 0.2 MPa was imposed on the left boundary and a liquid pressure of 0.1 MPa was imposed on the right, so that the flow is from left to right. The top and the bottom boundaries were impervious. The soil properties are summarized below in Table 3.2.

Table 3.2. Summary of the soil properties/model parameters used in the model

Material	**Property/Model**	**Value**
Soil	Porosity, ϕ	0.3
	Intrinsic Permeability	$1.0\times10^{-15}\ m^2$
	van Genuchten Model	P_0=50 kPa; λ=0.3
	Power Law	A=1; λ=3

As only the effect of the width of the joint element and the effect of its presence on the neighboring nodes was sought from this model, the intrinsic permeability of the cracks was kept constant at $1.0\times10^{-11}\ m^2$. All the other material properties were same for cracks (joint elements) and the soil. Analysis was done for three different widths (0.01 m, 0.05 m and 0.1 m).

3.7.2 Results of the analysis

The analysis showed that the joint elements do not have any bearing on the adjacent nodes as far as flow is concerned. The effect of the width of the joint elements on the total flow at the left boundary is presented below:

Figure 3.10 shows the total flow at the left boundary of the geometry with a single crack against time. When the total flow for three widths was divided by the width of the aperture, a constant value was observed. Table 3.3 summarizes the above mentioned observations.

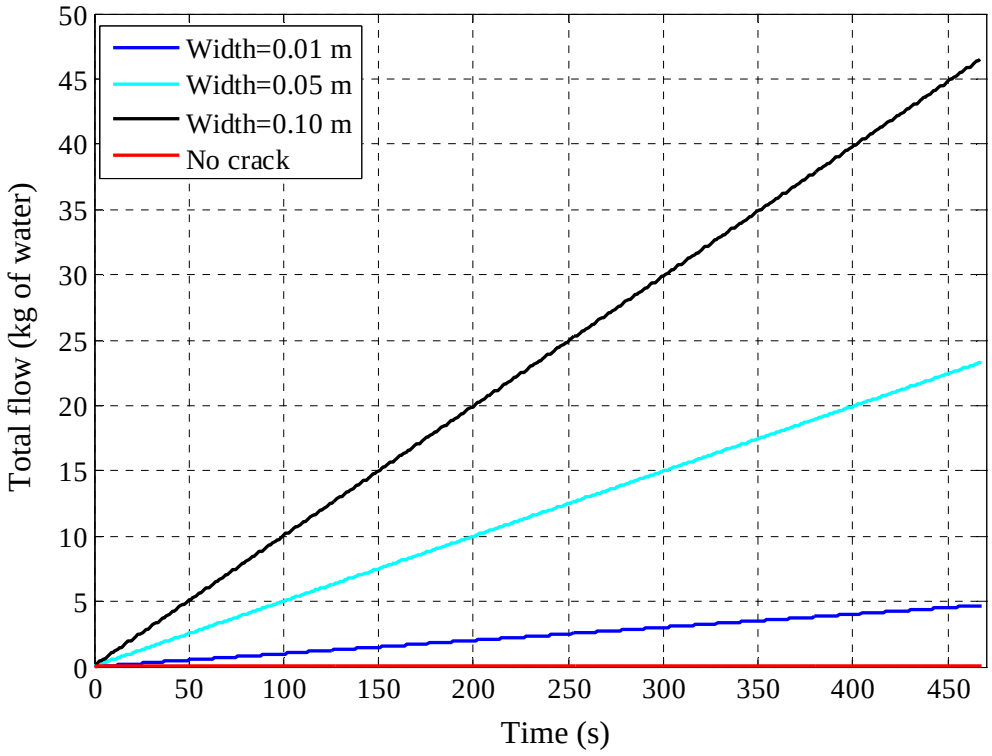

Figure 3.10. Total flow v/s time at the right boundary for single crack

Darcy's law can also be written as:

$$Q=KiA \tag{3.29}$$

where, Q is flux and A is cross-sectional area.

For identical soil properties and head,

$$\frac{Q}{A} = \text{constant}$$

So for the two dimensional joint model, where the cross-section of the cracks equals, 'b':

$$\frac{Q}{b} = \text{constant, must be true}$$

Column 3 of Table 3.3 demonstrates the above mentioned expression

Table 3.3. Summary of the flow at the boundary with single crack

Crack width	**Total flow (kg of water)**	**Flow/aperture (kg/m)**
No crack	0.46422	--
0.01m	4.6911	464.709
0.05m	2.3270×10^{1}	464.520
0.1m	4.6494×10^{1}	464.500

Similar analysis was done for a case with three cracks. Again, when the total flow for three widths was divided by the width of the aperture, a constant value was observed. Table 3.4 summarizes the above mentioned observations.

Table 3.4. Summary of the flow at the boundary with triple cracks

Crack width	**Total flow (kg of water)**	**Flow/aperture (kg/m)**
No crack	0.46422	--
0.01m	1.3981×10^{1}	1.3981×10^{3}
0.05m	6.9718×10^{1}	1.3943×10^{3}
0.1m	1.3939×10^{2}	1.3939×10^{3}

Figure 3.11 shows that under identical condition and same crack aperture (0.01 m), the flow was thrice for the case with three cracks as compared to the case with a single crack.

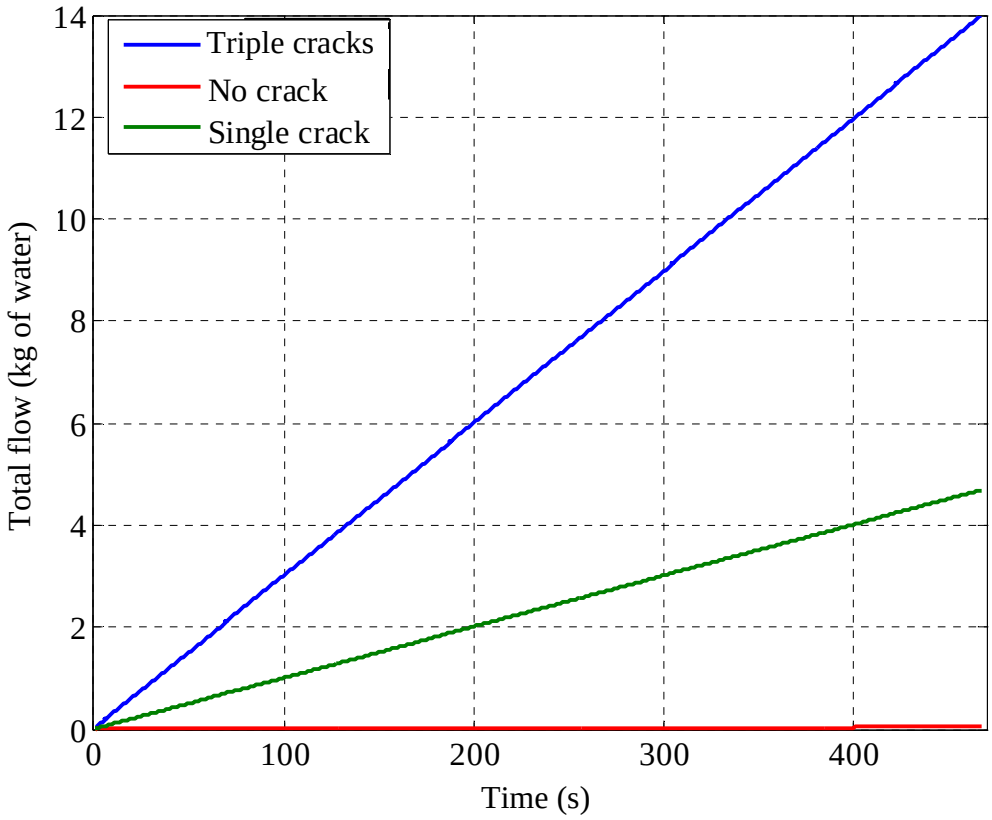

Figure 3.11. Comparison of total flow for no, single and triple cracks under identical conditions

Hence, from the results summarized in Table 3.3 and Table 3.4, it can be inferred that the flow is directly proportional to the aperture of the joint element if the permeability assigned to the joint element is very high compared to the soil. If 'W' is the width of the joint element and 'Q' is the total flow, then the following proportionality can be expressed between the two:

$$Q \propto W$$

3.8 Conclusions

In this section all the concept pertaining to the flow in porous media were described. The set of equations used by CODE_BRIGHT to solve flow problems in unsaturated soils were also discussed. Along with that the use of joint elements to simulate the effect of cracks in soil was also discussed. However, it is very important to validate the joint model presented in this section. The validation of the joint model has been discussed in the next section, where data from a small scale embankment was used and compared with the predictions of the joint model.

4. DESICCATION CRACKS IN LEVEES

4.1 Overview of the section

This section starts with a note on the importance of flood protection followed by the various mechanisms by which they might fail. A scaled embankment experiment has been discussed in the following sub-section. Subsequently, a finite element model developed to capture the data acquired by the sensors in a scaled embankment has been described followed by a comparison between the predicted and the actual values of the relevant state variables.

4.2 Importance of levees

Flood embankments or levees are essentially low level dams of short retention period. The main purpose of a levee is to prevent flooding. They are used to confine rivers and lakes and even seas from the adjoining inhabited areas. Levees have also been used to confine natural or man-made landfills filled with contaminated substances.

There has been an increased interest in the performance of flood embankment in recent years due to two main factors: (i) inclement weather causing huge damages to levees and (ii) global climatic shift predictions. In recent years, especially in the aftermath of the flooding from Hurricanes: Katrina, Rita, Gustav and Ike which caused huge loss of life and property has accentuated the important role of flood embankments in providing public safety during storm events. Flooding during the summers of 2007 caused an

estimated loss of £ 3.1 billion in the UK (Defra, 2008). As a direct consequence of this event, in the following year, the investment in managing the risks of coastal and river flooding was increased to £ 2.1 billion for a period of three years.

The rise of sea levels as a result of global warming has triggered an alarm particularly in the South-East Asian countries like Indonesia, etc. as such an eventuality will lead to greater pressure on the coastal defense of these countries. Moreover, in parts of the world such as northern and central Europe there has been an increase in the magnitude and frequency of precipitation Christensen et al. (2007) that will put an increased pressure on the fluvial embankments. Therefore, it is imperative for these countries to upgrade their flood protection embankments in order to prevent the loss of life and property from more intense flooding events. To counter these challenges, it is of utmost importance that more research be done to better understand the different modes of failures of a flood embankment system.

4.3 Hydraulic behavior of a flood embankment

For most of the time, embankments are subjected to low hydraulic heads or even no hydraulic heads and remain largely unsaturated. However, this situation changes within a matter of days due to rapid rise of water level during storms or heavy precipitation. This results in building up of internal pore water pressures under high hydraulic gradients.

While designing the height of the embankment is considered the single most important design parameter. However, experience has shown that the most flood embankments do not fail by overtopping but by structural weaknesses. Bogardi et al. (1971) have identified four common modes of failure. These are:

1.) Overtopping: The elevation of wave exceeds that of the levee.
2.) Structural failure of a levee by water saturation or loss of stability: The flood wave causes increased saturation of the levee and an increased pressure gradient through the levee. Decease in soil strength is associated with increased saturation, which with increase in the pressure gradient causes failure through slumping.
3.) Boils and hydraulic soil failures: The height of the flood wave and its resulting pressure is transmitted through the foundation soil under the levee and can cause soil failure through rupturing. The ensuing failure usually leads to a large inflow of water into the protected area and the undermining of the levee foundation.
4.) Wave action: High flood levels give rise to wave action which scours the top of the levee. Such scouring reduces levee strength and causes premature failure.

Cooling and Marsland (1953) observed that a seepage failure of a different kind might also occur in levees made of highly shrinkable clays. The surface of such levees is often found highly fissured due to desiccation cracking, owing to removal of moisture by

vegetation and atmospheric drying. These cracks generally appear during the dry seasons, when the water levels are low and the embankment is mostly unsaturated. But in the event of flooding, large amount of water can flow through the cracks in this highly fissured zone. This can cause sufficient downdrag resulting in the mechanical failure of the levee or can provide a preferential pathway to water to reach the other side of the embankment.

4.4 Scaled Embankment Experiment

4.4.1 Introduction

An experiment was conducted at University of Strathclyde, Glasgow to understand the hydraulic behavior of a fill used to build a flood protection embankment in Glaston, Scotland. Figure 4.1 shows the actual embankment at Glaston.

Figure 4.1. A flood protection embankment in Glaston, Scotland

To better understand the behaviour of the fill material and the embankment, a physical model of the embankment was constructed in the laboratory in a chamber, allowing full control of the environmental conditions. Tensiometers and ThetaProbes were placed at strategic points in the “as-constructed” scaled embankment. By “as-constructed” it is implied that care was taken to construct the scaled embankment just like the actual embankment. The embankment was then subjected to controlled drying and wetting cycles and the evolution of main variables of the problem (suction and water content) were monitored for a period of 20 days. In the course of the experiment, the scaled embankment developed desiccation cracks. The data collected by some of the probes could only be explained by preferential path that the cracks would have provided to the water flow. Therefore, the experiment was ideal for validating the numerical model developed to simulate effect of cracks in soil, required for this thesis.

4.4.2 Soil characterization

The soil used in the experiment is called Glaston Clay. Both wet/dry sieve analysis and hydrometer analysis were performed in accordance to the British Standards (BS 1377-2:1990 and BS 1377-1:1990). The gradation curve for the particle size analysis done is shown in Figure 4.2.

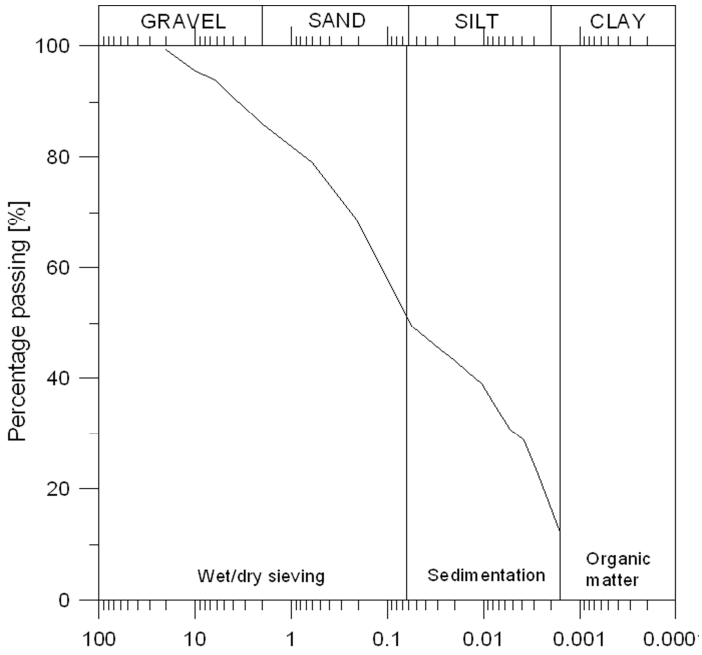

Figure 4.2. Gradation curve for the fill material (after Zielinski, Sanchez, et al., 2010)

Tests were also performed to find the index properties of the soil. Table 4.1 summarises the results of these test. The soil was classified as clay of intermediate plasticity (BS 5930:1990).

Table 4.1 Summary of the properties of the soil (after Zielinski, Sanchez, et al., 2010)

Soil property	**Value**
Natural moisture content *MC*: %	17.9 (*)
Shrinkage limit *SL*: %	10 (*)
Liquid limit *LL*: %	36 (*)
Plastic limit *PL*: %	16 (*)

Table 4.1 continued

Soil property	**Value**
Plasticity index I_D: %	19 (*)
Optimum moisture content *OMC*: %	11.5
Maximum dry density ρ_d: Mg/m^3	1.95
Particle density (<2 mm) ρ_s: Mg/m^3	2.66 (*)
Particle density (>2 mm) ρ_s: Mg/m^3	2.77 (*)
On-site undrained shear strength c_u: kN/m^2	138 (**)
Estimated suction of the natural soil: kPa	100
(*) Average from 3 independent tests (**) Average from 4 independent tests	

4.4.3 Embankment preparation

The scaled embankment was built in order to achieve the actual embankment from where the fill was taken. The scaled embankment was built in ten 0.1 m thickness layers. This ensured that a high degree of homogeneity is achieved along with the required density of the fill. Before construction, the soil was placed in 0.12m high shuttering and then broken down to smaller lumps. Figure 4.3a and Figure 4.3b show the plan view and cross-section of the embankment, respectively.

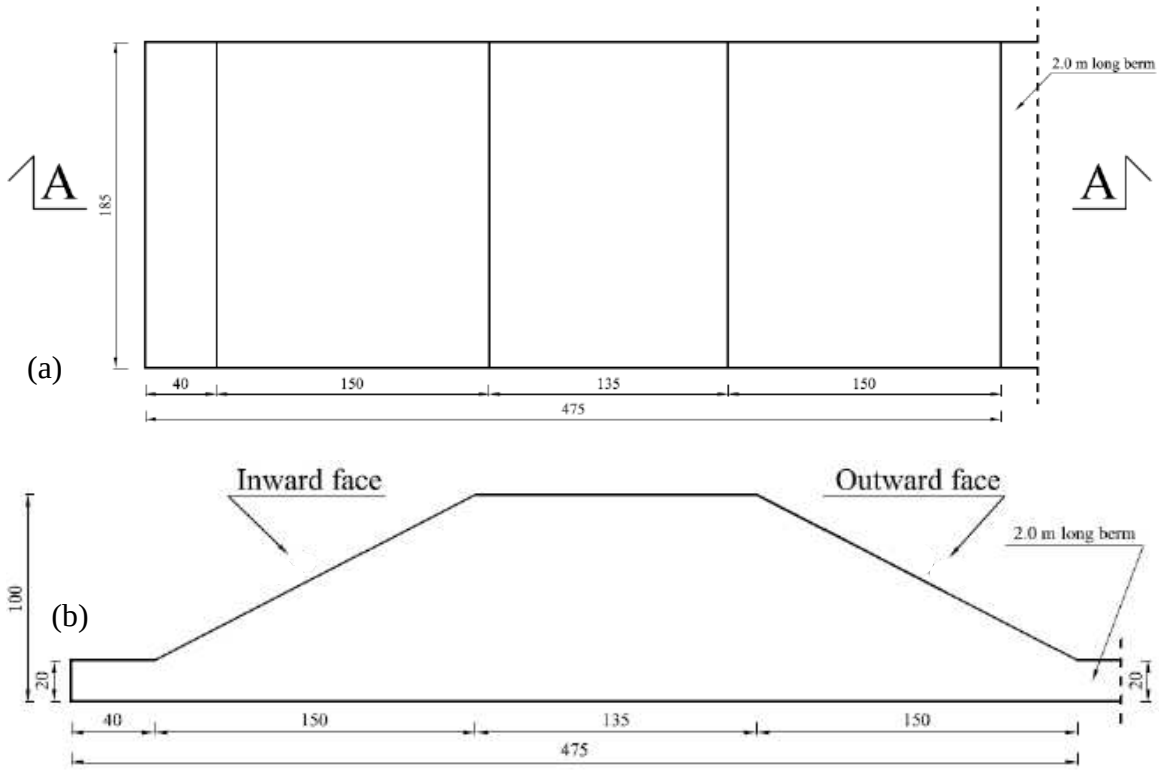

Figure 4.3. (a) Plan view (b) Cross-section A-A of the embankment (all dimensions in cm)

4.4.4 Description of the experiment

The physical model of the embankment was covered in an environment chamber to fully control the environmental conditions. It was built with an aim to assess the influence of environmental conditions (rain, intense drying and flooding) inside the chamber on the soil variables (water content, suction and temperature) and to further see how changes in these parameters affect the embankment (such as formation of desiccation cracks, etc.). There were arrangements inside the chamber to simulate rain (through sprinklers), impose drying (through infra-red heaters) and control the temperature of the chamber

(through fans and thermostats). The scaled embankment inside the environment chamber is shown in Figure 4.4

Figure 4.4. Picture of the scaled embankment inside the environment chamber

As for the embankment, four Time Domain Reflectrometry (TDR) sensors (ThetaProbe) were inserted inside the soil to measure the water content of the soil. Eight Soil Water Tensiometers (TS) were inserted strategically at depths of 0.2 m, 0.4 m, 0.6 m and 0.8 m to measure the matric suction. Apart from that, two arrays of resistivity sensors were inserted vertically and horizontally into the embankment to monitor the changes in the resistivity of the soil. The position of the sensors is shown in Figure 4.5.

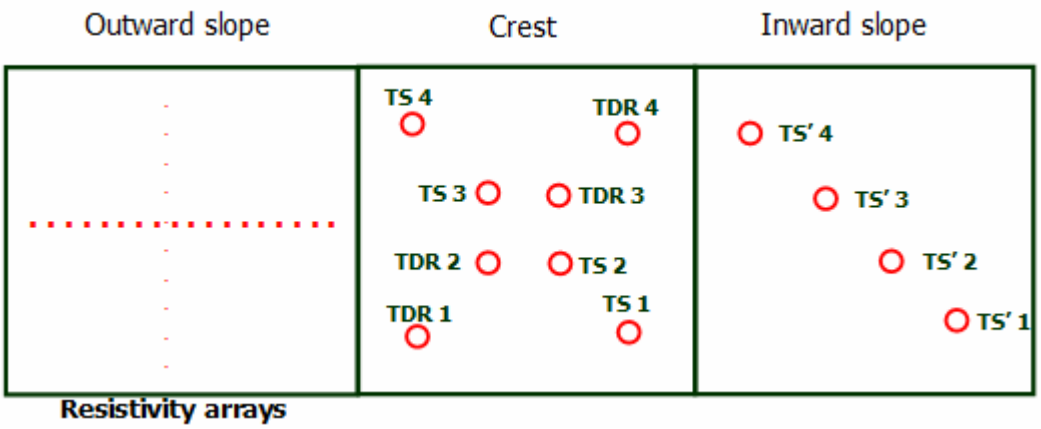

Figure 4.5. Plan view of the positions of tensiometers (TS) and ThetaProbes (TDR)

The experiment was conducted for a period of twenty days. Data collection was started when the suction and the moisture content was 4 kPa and 21.5% respectively. Three drying cycles of about one week each were separated by two wetting cycles of half an hour. The precipitation rate during wetting cycles was maintained at a rate of 55mm/h. Figure 4.6 shows the evolution of air temperature inside the chamber with time. The bold line indicated the average air temperature inside the chamber. Figure 4.7 shows the evolution of relative humidity inside the chamber with time. In Figure 4.7, the dotted lines indicate wetting spell and the bold line indicate the average value of relative humidity during that drying cycle.

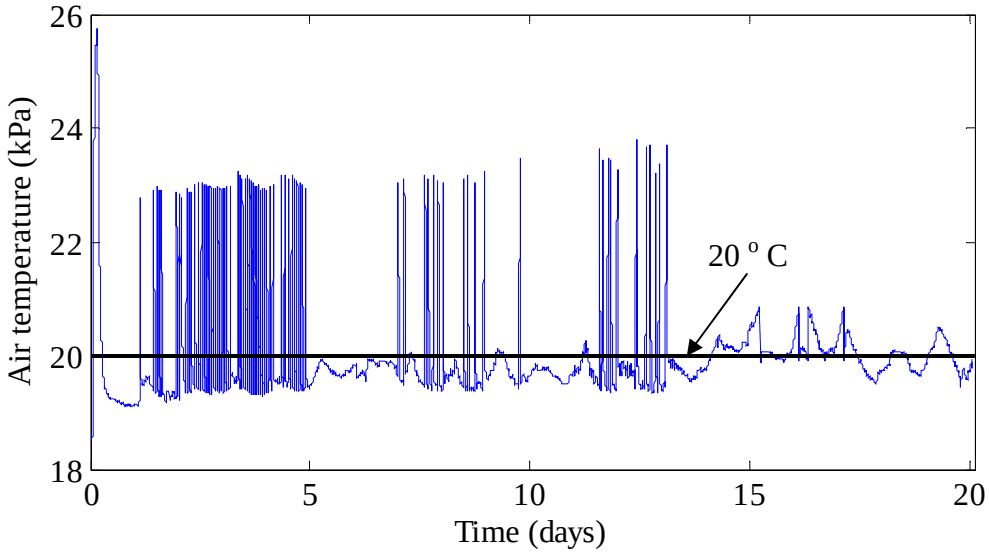

Figure 4.6. Air temperature inside the chamber

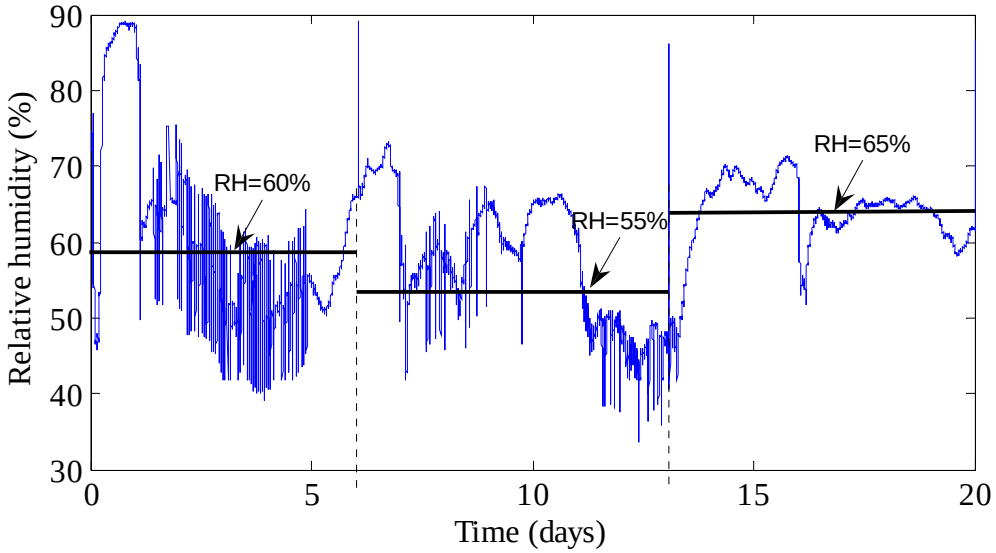

Figure 4.7. Relative humidity inside the chamber

4.4.5 Experiment results

The retention curve of the soil was found using three different techniques, viz. contact filter paper, high-range psychrometer and mercury intrusion porosimetry (MPI). The retention curve so obtained is shown in Figure 4.8.

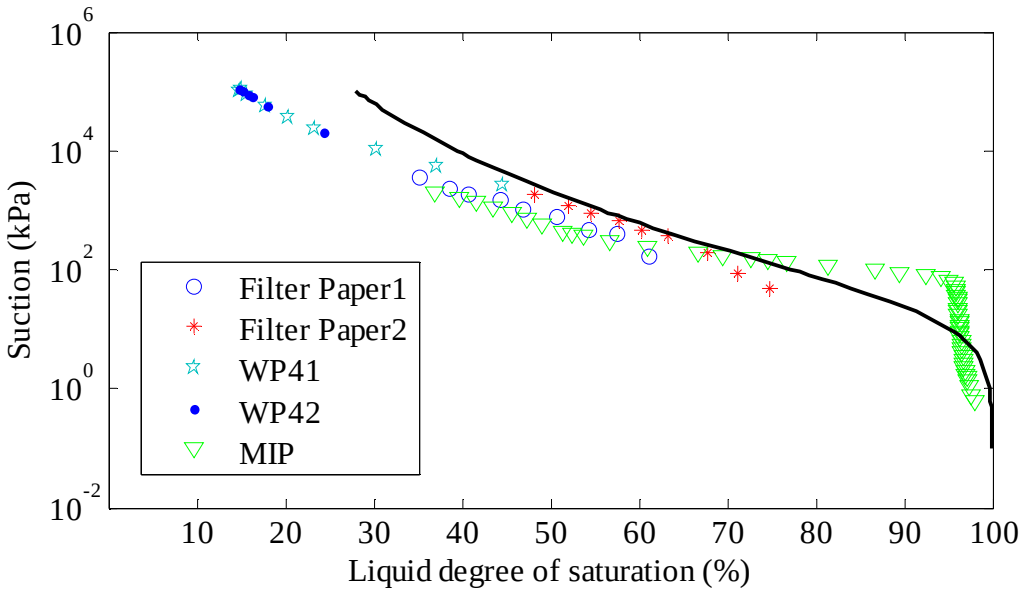

Figure 4.8. Plot between suction and liquid degree of saturation

Pictures of the embankment were taken each day using cameras from three different angles. Based on these pictures, evolution of the superficial pattern of cracks with time could be seen. Figure 4.9 (a) shows a picture of the embankment at day 7. The superficial cracks can be seen in the figure.

(a)

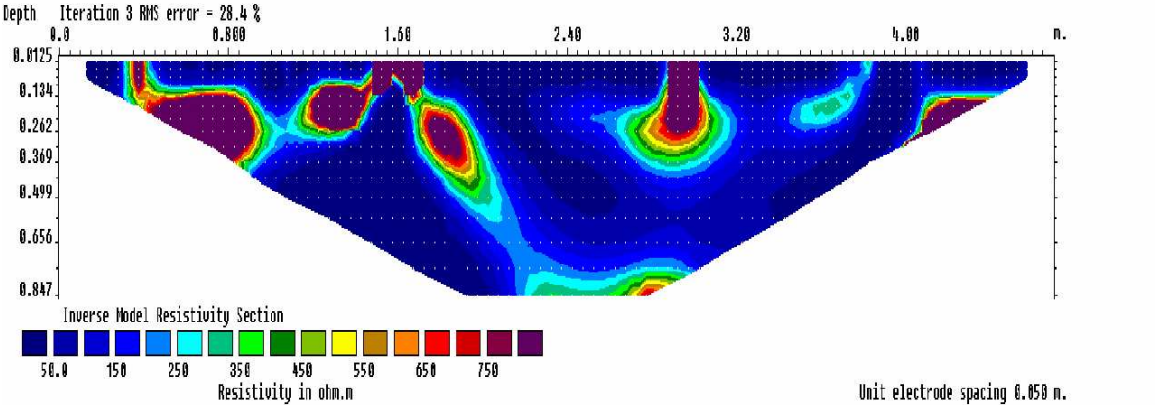

(b)

Figure 4.9 (a) Picture of the outward face of the embankment at day 7, (b) Electrical resistivity map of the embankment at day 7

Electrical resistivity maps gathered from the resistivity arrays were used to study dielectric properties of the embankment. This in turn helped to ascertain the depth of the cracks, as cracks are filled with air which is a poor conductor of electricity.

For the purpose of modeling, the suction data collected at 0.2 m, 0.6 m and 0.8 m depth form crest was used. Figure 4.10 show the evolution of suction at different depths with time as captured by the tensiometers.

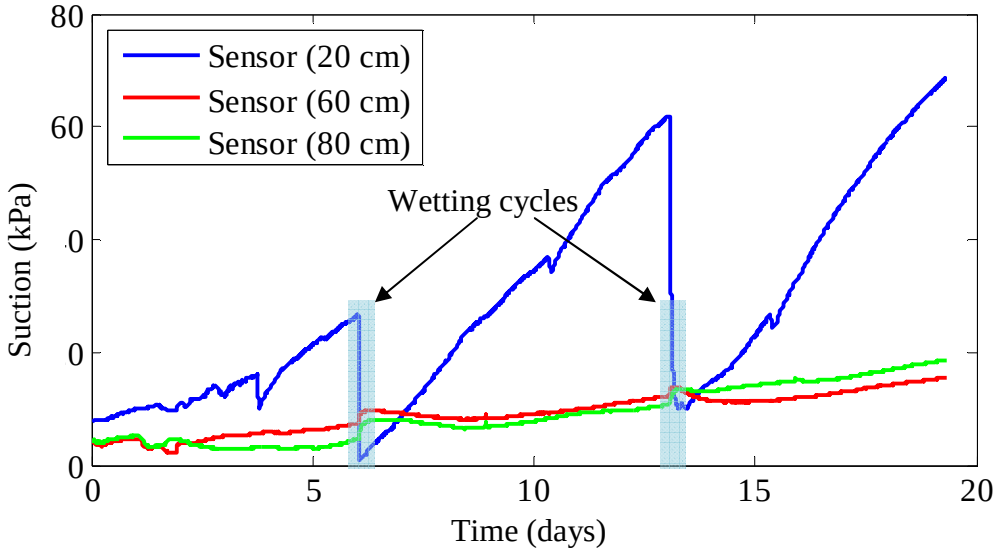

Figure 4.10. Plot of the data from the suction sensor

4.5 Numerical modeling of the scaled embankment

4.5.1 Model description

A 2-D numerical model was developed to simulate the experiment mentioned in section 4.4. For the purpose of preprocessing, i.e., development of the geometry, initial condition, final conditions and meshing, a pre and post processing software GiD was used. The model geometry was in accordance with the dimensions of the model shown in Figure 4.3a and Figure 4.3b. The meshing of the model was done using 4-node quadrilateral elements. A structured mesh type was employed, with 1436 nodes and

1366 quadrilateral elements. The concentration of elements was high near the boundary because of the high hydraulic gradient. Element concentration was high near the sensor as well, in order to get more accurate results there. Figure 4.11 shows the mesh generated for the model. 126 joint elements were used introduced into the finite element mesh to simulate the effect of desiccation cracks. The meshing information was then passed to the FEM package-CODE_BRIGHT.

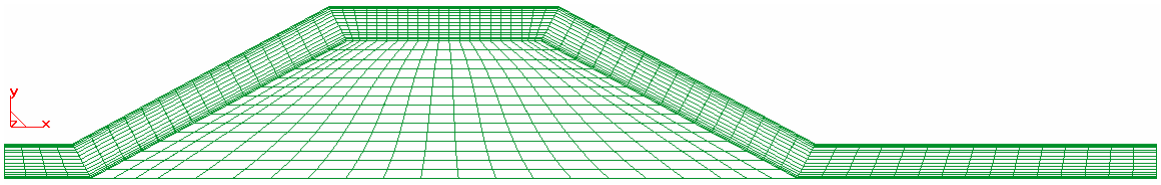

Figure 4.11. Mesh generated to model the scaled embankment

4.5.2 Initial and boundary conditions

A constant temperature of 20 °C for the air in the chamber and 18 °C for the embankment was maintained. A gas pressure of 0.1 MPa was also maintained. Apart from that, an initial liquid pressure of 96.0 kPa was imposed on the soil embankment. This corresponded to an initial suction of 4 kPa and a water content of 21.8 %.

The boundary conditions were imposed in the light of the relative humidity and temperature data (as shown in Figure 4.7 and Figure 4.8) gathered by the sensors inside the chamber. An average relative humidity of 60 %, 55 % and 65 % was used for the three drying cycles, respectively. Based on this data, suctions of 70 MPa, 60 MPa and 80

MPa, respectively was calculated for the three drying cycles at 20 ^{0}C, using the psychometric law.

According to Rodriguez, Sanchez et al., (2007), the total flux of water vapor in gas phase, $\mathbf{j}_{\mathbf{g}}^{\mathbf{w}}$ at the boundary can be prescribed as the difference between the vapor mass fraction in air , $(\theta_g^w)^*$, and the vapor mass fraction in the gas phase of the fill material, (θ_g^w), so that:

$$j_g^w = \beta_g \left[(\theta_g^w)^* - (\theta_g^w) \right]$$

where, β_g is the leakage coefficient to allow boundary condition of the Cauchy type (Wilson et al., 1994).

The quotient $(\theta_g^w)/(\theta_g^w)^0$ represents the relative humidity and can be calculated using the psychometric law (equation 3.24).

Thus, the above mentioned formulation was used to impose the boundary conditions on the embankment during the drying cycles. For the two wetting cycles, in order to simulate the raining conditions, a relative humidity of 100 % was imposed on the boundary by setting $P_1=P_g=0.1$ Mpa (i.e., suction =0)

Table 4.2 summarizes the value of the different parameters used at different drying cycles.

Table 4.2 Summary of the boundary conditions during drying cycle

Condition	**Relative Humidity (%)**	**Suction (MPa)**	**Vapor mass fraction (kg/m^3)**
1st Drying cycle	60	70	0.0103
1st Wetting cycle	100	0	--
2nd Drying cycle	55	60	0.0111
2nd Wetting cycle	100	0	--
3rd Drying cycle	65	80	0.0096

The value of the leakage coefficient, β_g used for the simulation was 0.005 m/s. During the two wetting cycles a liquid pressure of 0.1 MPa was imposed at the boundary (so that the suction is zero) to simulate the raining conditions. The bottom of the geometry was treated as an impermeable boundary.

4.5.3 Soil properties

The soil properties used were in accordance to the experiments done to ascertain soil properties (permeability, retention curve, etc.). Table 4.3 summarizes the soil property parameters used for modeling the embankment.

Table 4.3 Summary of the soil properties and model parameters used

Material	**Property/Model**	**Value**
Soil	Porosity, ϕ	0.37
	Intrinsic Permeability	1.0×10^{-16} m^2
	Power Law	A=1; λ=3
	van Genuchten Model	P_0=75kPa; λ=0.13

4.5.4 Imposing the crack geometry

From the pictures of the embankment taken each day, the evolution of the superficial pattern of cracks with time could be seen. The cross-section of the embankment going right across the sensor TS1 was selected for the 2-D numerical analysis. These images of the cracks were used to find the location of the crack on the embankment. A total of nine cracks were present in the above mentioned cross-section. One of the cracks ran right through sensor at 0.2 m.

Apart from location of the cracks, an estimate was made regarding the average aperture of the cracks from the photographs taken. It was found that the average aperture of the cracks was about 12 mm.

From the images of the embankment taken each day, it was realized that the cracks did not start opening up until the 4^{th} day of the experiment. So till the 3^{rd} day the material properties of the soil and the joint elements of the crack were assigned the same values.

4.5.5 Modeling the cracks

The cracks were modeled using the joint element. The joint element needs to be assigned material properties just as soil. The intrinsic permeability of the cracks was calculated using equation (3.28) for an aperture width of 12 mm. All the other properties of the cracks were maintained same as that of the soil.

4.5.6 Comparison of the experimental results with the model

4.5.6.1 Homogenous model

For the sake of comparison, a homogenous case (with no cracks) was run with identical initial and boundary conditions as well as the same soil properties. Figure 4.12 shows the value of suction at 20 cm depth, as captured by the sensor as well as the one predicted by the model. It can be seen that the model completely fails to capture the effect of the wetting cycles. Though, during the three drying cycles the slope of the suction curve of the model matches closely the slope of the suction data captured by the sensor, establishing the fact that the soil properties and boundary conditions imposed matched the actual conditions very well.

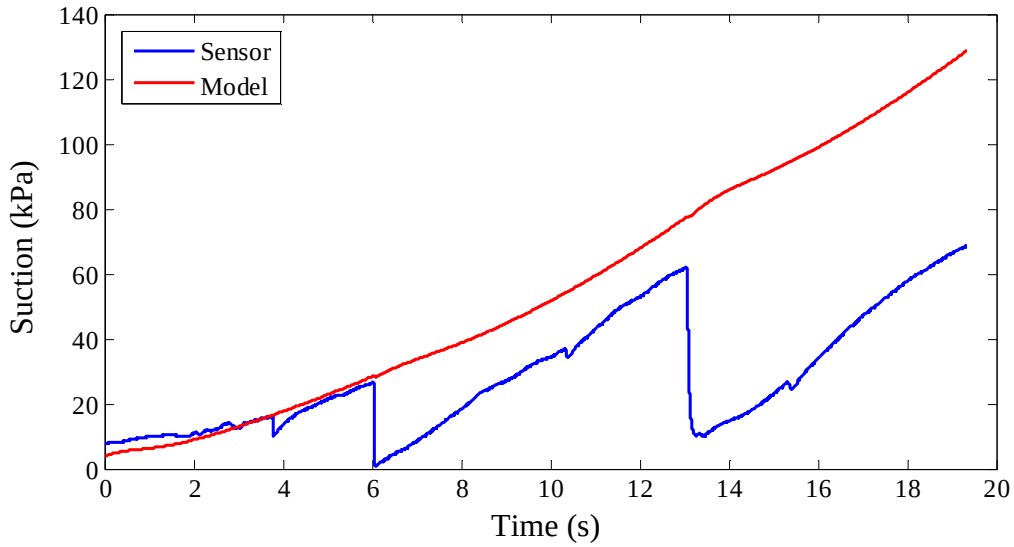

Figure 4.12. Comparison between the suction values by the homogenous model and the tensiometer at 20 cm depth

As one go down from the crest of the embankment, where there are no cracks, the model should predict suction values close to that of the sensors. Figure 4.13 shows the suction value at 60 cm depth as captured by the sensor as well as the one predicted by the model. The value of the suction predicted by the model matched closely the data gathered by the sensor. Again, this confirms that the boundary conditions and the value of soil properties used matched the actual conditions closely.

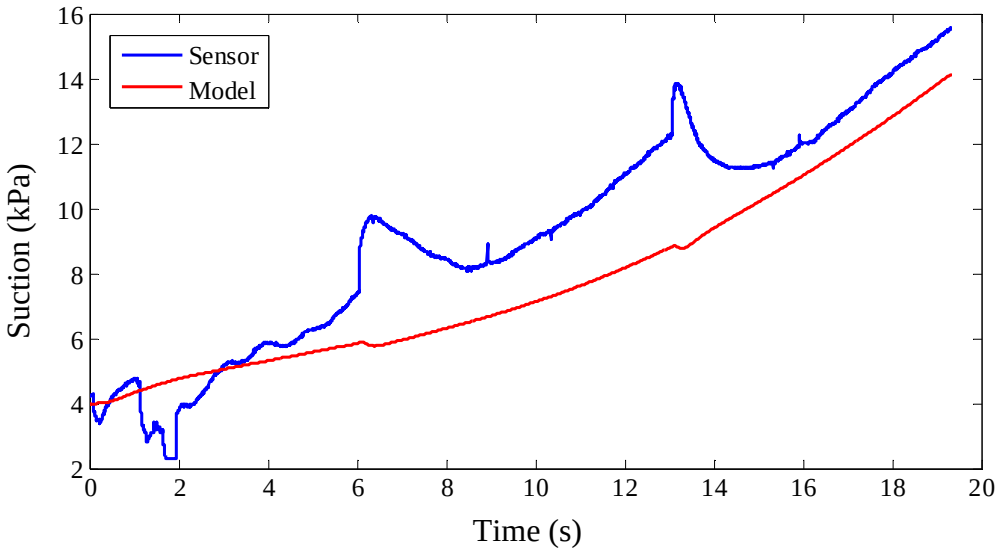

Figure 4.13. Comparison between the suction values by the homogenous model and the tensiometer at 60 cm depth

Figure 4.14 shows the value of suction at 80 cm depth as captured by the sensor as well as the one predicted by the model. In this case the homogeneous model did not perform very well and underpredicted the suction measured by the sensors.

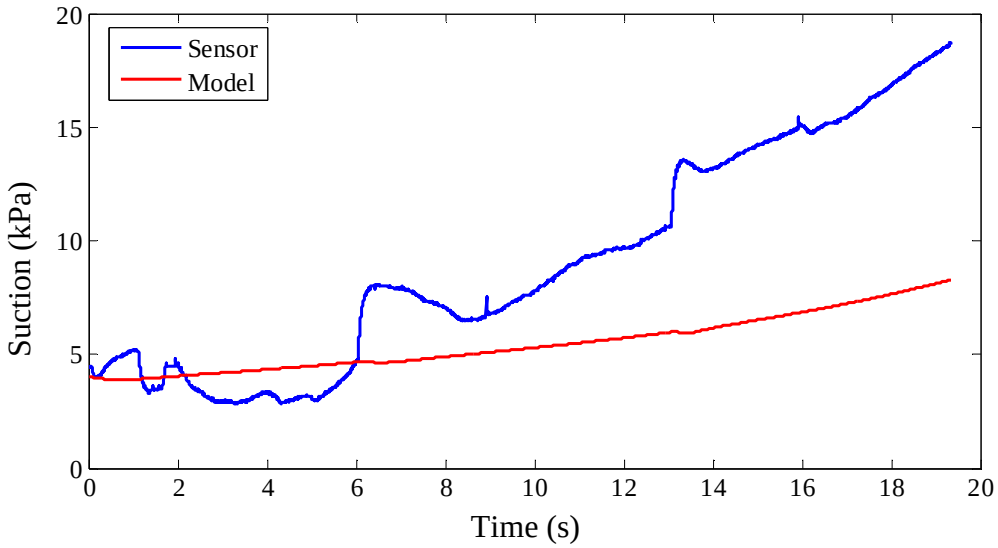

Figure 4.14. Comparison between the suction values by the homogenous model and the tensiometer at 80 cm depth

Thus the homogenous model failed to capture the wetting due to cracks in the soil. But at 60 cm depth the homogenous model captured the suction values at least qualitatively. For depths far from the cracks (80 cm) the homogenous model underpredicted the suction values measured by tensiometer.

4.5.6.2 Embankment model with cracks

The crack geometry as observed from the pictures was then imposed on the numerical model. The results of the analysis are discussed below:

Figure 4.15 shows the comparison between the suction values from the model and the sensor at 20 cm depth. It can be seen that the prediction of suction values by the model are in close agreement with that of the tensiometer. Though, a slight deviation can be

seen during the period of 2nd wetting and 3rd drying cycles, where both the wetting and drying were slightly overpredicted.

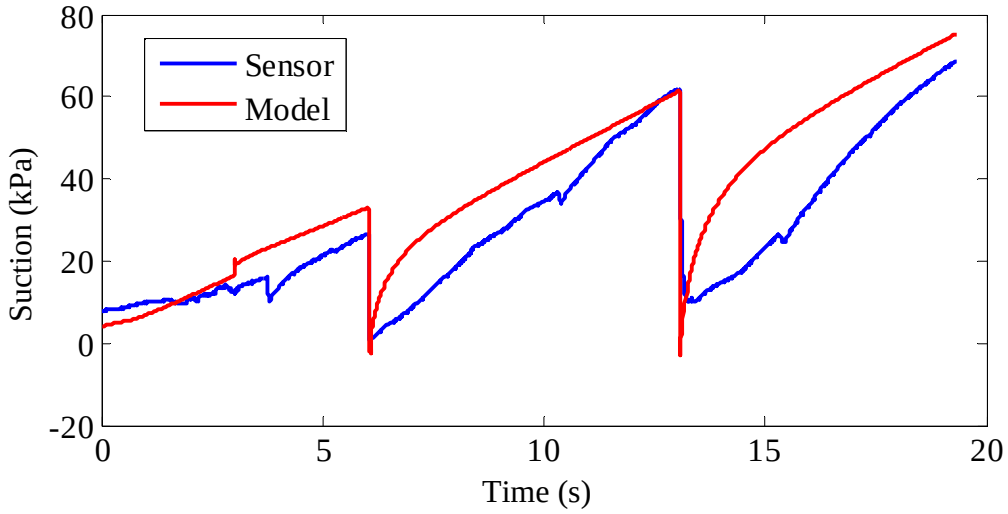

Figure 4.15. Comparison between the suction values by the model and the tensiometer at 20 cm depth

Figure 4.16 shows the comparison between the suction values from the model and the sensor at 60 cm depth. There was a peculiar observation recorded by the sensor, when at the time of wetting, the tensiometer recorded an increase in the suction. It can be seen that the prediction of suction values by the model are in very close agreement with that of the tensiometer, except for the higher suction values (meaning drying) during the wetting cycles as recorded by the sensor.

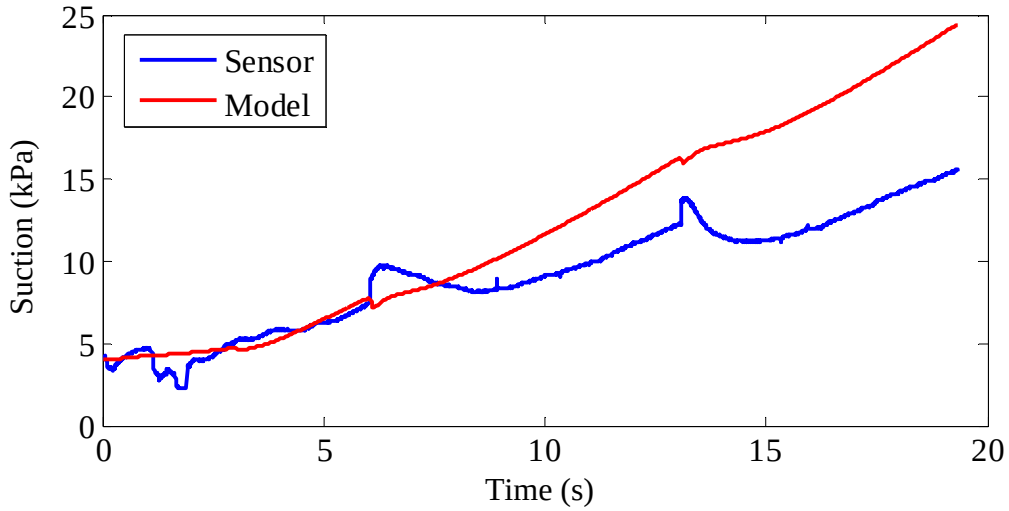

Figure 4.16. Comparison between the suction values by the model and the tensiometer at 60 cm depth

Figure 4.17 shows the comparison between the suction values from the model and the sensor at 80 cm depth. Slight deviation is observed between the model predicted suction values and the suction from the tensiometer. But, the model predicts the evolution of suction with time very closely.

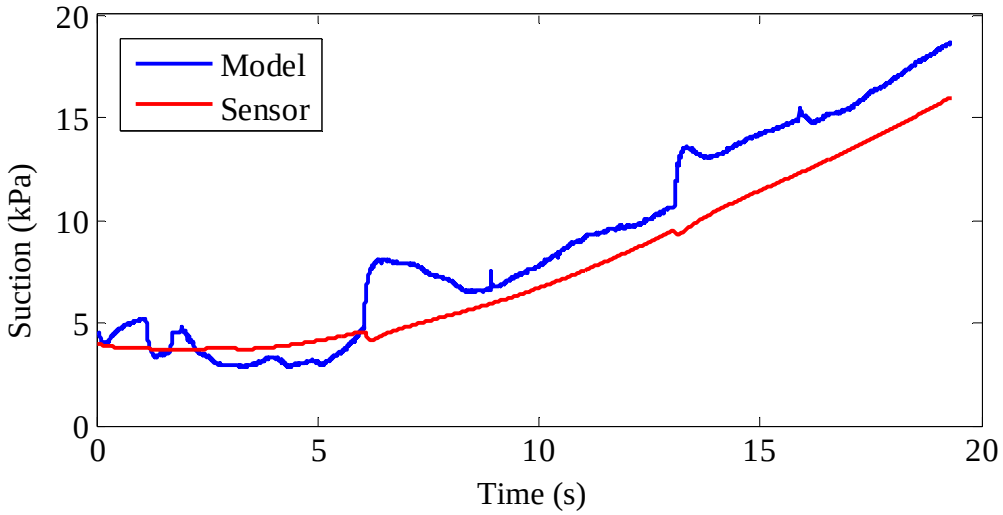

Figure 4.17. Comparison between the suction values by the model and the tensiometer at 80 cm depth

Thus the joint model was able to capture the suction as recorded by the sensors qualitatively as well as quantitatively.

4.6 Conclusions

Thus it is clear from section 4.5 that it is very difficult to model flow through an unsaturated embankment with desiccation cracks without taking into account cracks. So, to model the flow of water in an embankment with cracks a homogenous soil model cannot be used. Some technique must be used to take into account the effect of cracks. From the results presented above, it can be said that by the introduction of the joint elements implemented in CODE_BRIGHT for the analysis, it was possible to predict very well the flow of water through cracks in an unsaturated embankment. However, as explained in section 2, the phenomenon of desiccation cracking is random. A thorough

probabilistic analysis was much needed to better understand the effect of desiccation cracks in unsaturated embankment. In the next section a random field model was developed for the crack geometry. A Monte-Carlo analysis was done to probabilistically assess the effect of crack geometry on flow of water through a full scale unsaturated embankment.

5. MODELING A FULL SCALE EMBANKMENT WITH DESICCATION CRACKS

5.1 Overview of the section

In this section a synthetic earth embankment with random crack geometry was analyzed numerically. The description of the problem and the finite element model are discussed in section 5.2 and section 5.3. A random model was developed to capture the variability in the geometry of the crack network. The random model has been discussed in section 5.4. Finally, the results obtained from Monte Carlo simulations have been presented and discussed in section 5.5.

5.2 Problem description

The purpose of this analysis is to study the effect of the desiccation cracks (randomly distributed) on the hydraulic behavior of an earth embankment. The embankment is initially unsaturated and a flooding event is simulated. The analysis focuses on two main variables associated with the steady state condition: time of saturation (Ts) and flow rate (Q) of water at the outward slope. The footing of the embankment is 28 m wide, the crest is 4 m wide and the height of the embankment is 7 m. Figure 5.1 shows the geometry of the embankment.

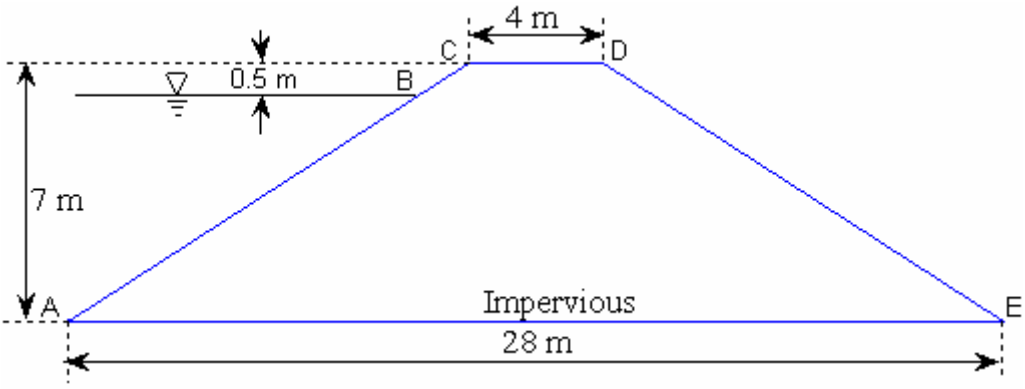

Figure 5.1. Geometry of the embankment

The embankment is initially unsaturated with water level at the bottom. Then over a period of the next 10 days the water level reaches its maximum height of 6.5 m from the bottom. All this while, the relative humidity of the atmosphere is assumed just below 100% (i.e., not raining).

5.3 Finite element model

5.3.1 Model description

A finite element model was used for the two-dimensional plain flow numerical analysis of the problem described in section 5.2. As in the case of modeling the scaled embankment, GiD was used for the purpose of preprocessing (defining the geometry and meshing). Meshing of the model was done using 4-node quadrilateral elements. An unstructured mesh type was employed using 2128 nodes and 2000 quadrilateral elements. Additional joint elements were introduced to model the cracks as required to

simulate the effect of the random crack geometry. Figure 5.2 shows the mesh generated for the finite element analysis of the embankment.

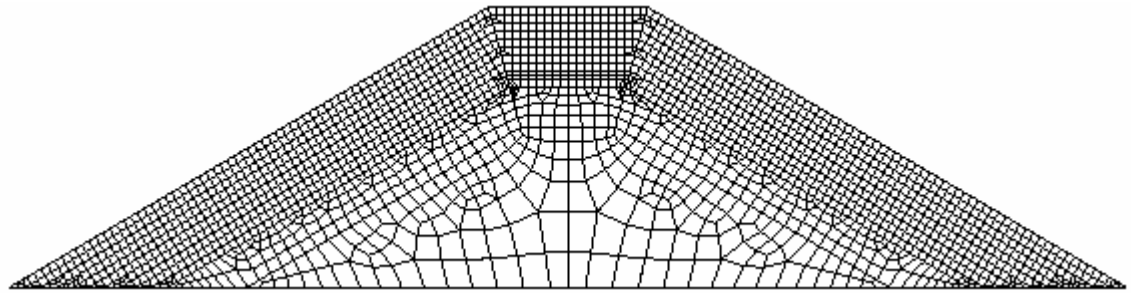

Figure 5.2. Mesh used for the finite element analysis of the embankment

The mesh is constructed in squares of 20 cm length till a depth of 2 m from the surface, wherever possible. This part of the mesh is where all the cracks can be located and the elements in this matrix of squares will be activated as joint elements to simulate the cracks. The location and geometry of these cracks was dictated by the probabilistic model developed to generate the random crack geometry. The advantage of designing such a mesh was that there was no requirement to create a separate mesh for different crack geometries. The interval of 20 cm can be reduced by using a finer mesh. But, a finer mesh increases the analysis time without any significant improvement in the results when one is trying to evaluate the effect of the crack geometry parameters on the slope. Furthermore, a crack depth greater than 2 m is seldom observed in the field.

5.3.2.1 Initial Conditions

A two-dimensional model was used to simulate the above mentioned problem. A 2-D analysis implies that the streamlines remain in the plane of analysis, which can only occur if the ends are impervious and the soil properties remain constant in the out of plane direction (Fenton and Griffiths, 1996).

Initially the soil embankment was unsaturated with a uniform suction of 50 MPa. The psychometric law (equation 3.23) gives the relation between suction in the soil and relative humidity in the atmosphere. The soil temperature was prescribed as $20\ ^{o}C$. A suction value of 50 MPa is equivalent of soil being in equilibrium with the atmosphere at a relative humidity of 70 % at $20\ ^{o}C$. An air pressure of zero was maintained throughout the simulations.

5.3.2.2 Boundary conditions

The boundary conditions were imposed in three stages emulating the transient state of water level rising up to a maximum height of 6.5 m and then maintaining steady state of the constant water head afterwards. The prescribed conditions are described below:

Stage 1 (from 0 to 0.01 days): A suction of 50 MPa was imposed on the open boundary ABCDE.

Stage 2 (from day 0.01 to day 10): The liquid pressure on boundary AB was linearly increased from a suction value of 50 MPa to a final value corresponding to the constant water level height shown in Figure 5.1. This was done to simulate the gradual rise of water under flood conditions over a period of 10 days. Simultaneously, the suction value on the boundary BCDE was decreased from 50 MPa to a value of zero. This boundary condition simulated a relative humidity condition of near 100 % (overcast but not raining).

Stage 3 (from day 10 to day 4000): the boundary conditions achieved in stage 2 were maintained. In all the above stages the boundary AE was prescribed as impervious.

5.3.2.3 Soil and crack material properties

The material properties for the soil used in the model were assigned to match that of compacted silty clay. Table 5.1 summarizes the soil properties and the model parameters used for this analysis.

Table 5.1 Summary of the soil properties/model parameters used in the model

Material	**Property/Model**	**Value**
Soil	Porosity, ϕ	0.3
	Intrinsic Permeability	1.0×10^{-15} m^2
	van Genuchten Model	P_0=50 kPa; λ=0.3
	Power Law	A=1; λ=3

The material properties of the cracks were the same as that of the soil except that the intrinsic permeability was calculated using the Cubic Law (equation 3.28). It was found by many comparative studies done by Indraratna et al. (1999) that cubic law overestimates the permeability of crack in soil by 40 %-70 %. In order to account for this bias the intrinsic permeability was divided by a factor of 2.

CODE_BRIGTH was used to numerically generate a liquid degree of saturation map for the above problem as shown in Figure 5.1. For the homogenous case the waterfront is very regular (as shown in Figure 5.3) and the water daylights at the bottom of the outward slope. This is the typical way most of the flood embankments are analyzed and no consideration is made to the fact that these structures are often subjected to desiccation cracking. Figure 5.3 shows the evolution of the waterfront at different times.

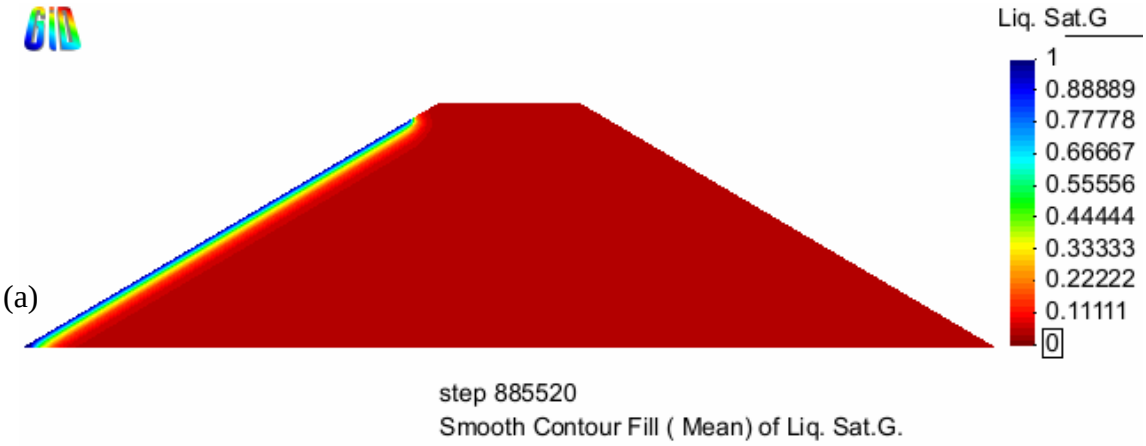

(a)

Figure 5.3. (a), (b) and (c) show the liquid degree of saturation for the homogenous case at subsequent time intervals

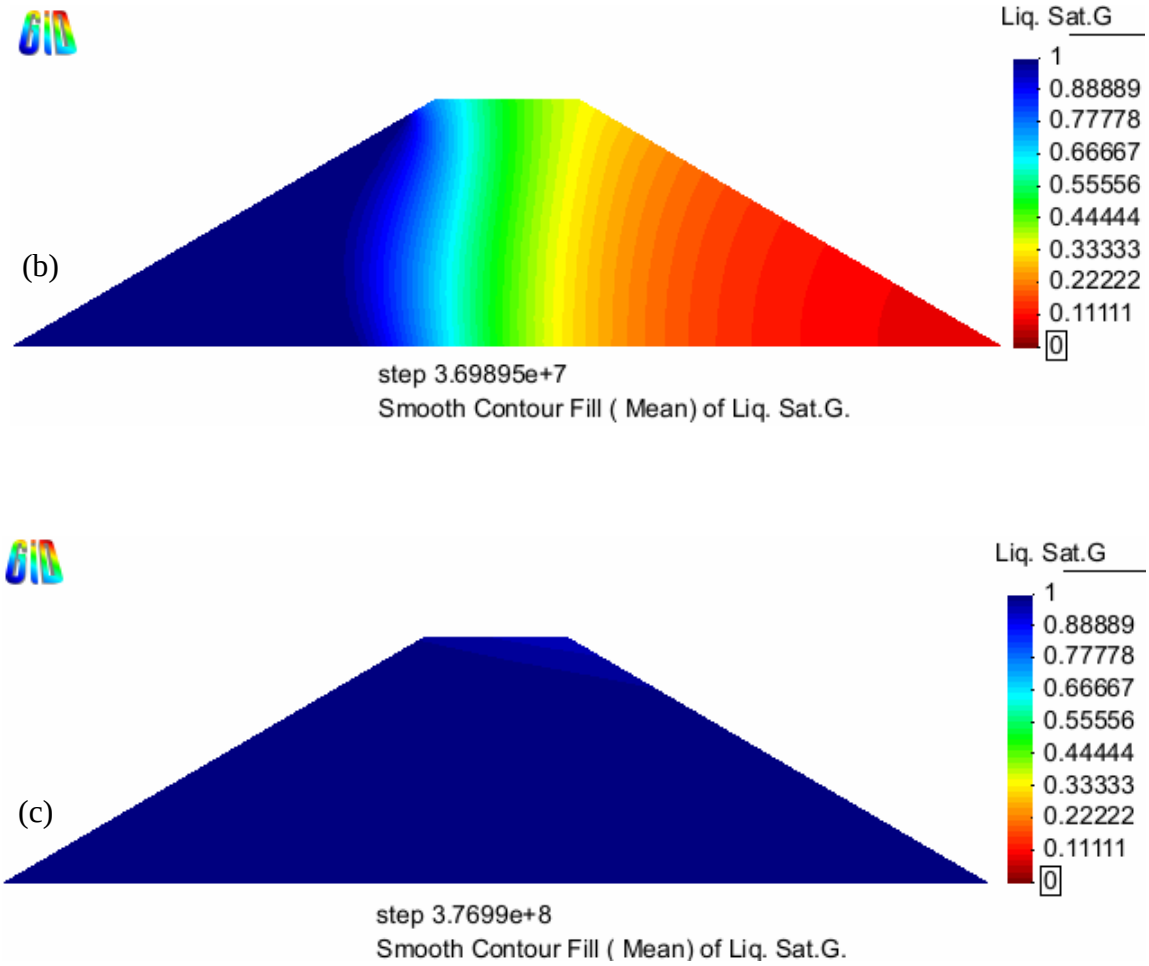

Figure 5.3. continued

However, earth embankments are often made of shrinkable clays which are prone to desiccation cracking. A single crack was introduced to the same embankment keeping all the other conditions intact. It can be easily from seen from Figure 5.4 that a single crack caused dramatic changes in the flow pattern of water in the embankment.

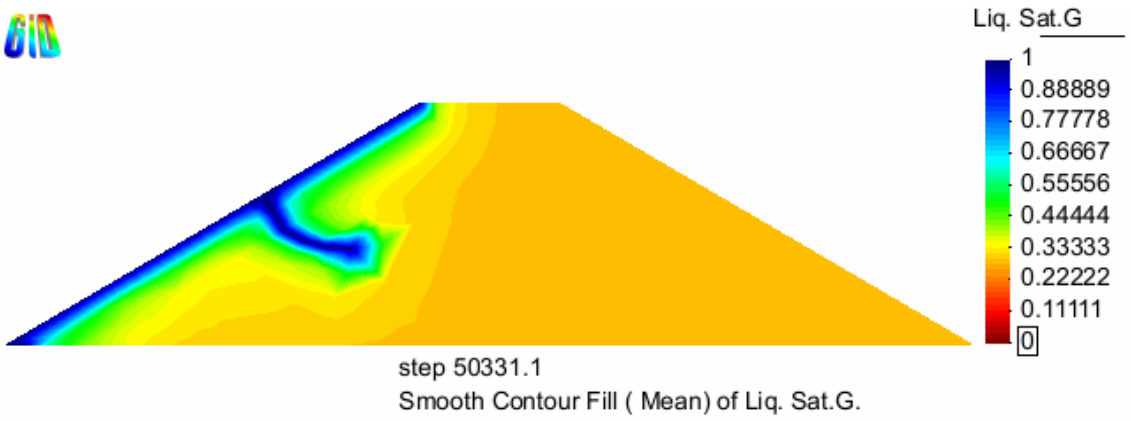

Figure 5.4. Liquid degree of saturation of flood embankment with a single crack

Generally, under actual field conditions, the embankments are subjected to myriad cracks that are present all over the surface of the embankment (Figure 5.5). Cooling and Marsland (1953), and Dyer et al. (2009) documented the presence of desiccation cracks on earth embankments made of shrinkable clays.

Figure 5.5. Picture depicting cracks on the surface of a flood embankment (after Cooling and Marsland, 1953)

A numerical analysis of the embankment was done to study the effect on the seepage pattern of the embankment when subjected to cracks using CODE_BRIGHT. Depth, spacing and aperture of the cracks are the three parameters that were identified to model cracks for the two-dimensional numerical analysis. The orientation of the cracks was always maintained normal to the surface (whether on top or on sides of the slope) as observed by Dyer et al. (2009) in the field survey that they conducted on an embankment. Sometimes vertical cracks are found to be connected by horizontal cracks (Cooling and Marsland, 1953; Konrad and Ayad, 1997; Lakshmikantha, 2009 and Zielinski et al., 2009). These subhorizontal cracks run parallel to the surface at about half the depth of the vertical cracks through which they pass. The horizontal cracks can highly affect the hydraulic properties of the soil as they provide interconnectivity between the crack network, thereby creating multiple flow paths for the fluid to flow.

The crack model was divided into two cases:

Case I: Crack geometry model without subhorizontal cracks

Case II: Crack geometry model with subhorizontal cracks

For modeling case II, the horizontal cracks ran in a single line parallel to the outer boundary. They were located at half the depth of the vertical cracks and had the same aperture as the vertical cracks.

For modeling Case I and Case II, the value of depth of the crack was 60 cm, spacing between the cracks was 60 cm and the aperture was 0.008 m. In these cases, as intuitively expected, the water tended to flow through the preferential paths provided by the cracks.

For Case I (without subhorizontal cracks), the waterfront was regular but the cracks at the edges got saturated much faster than the homogenous case (Figure 5.6).

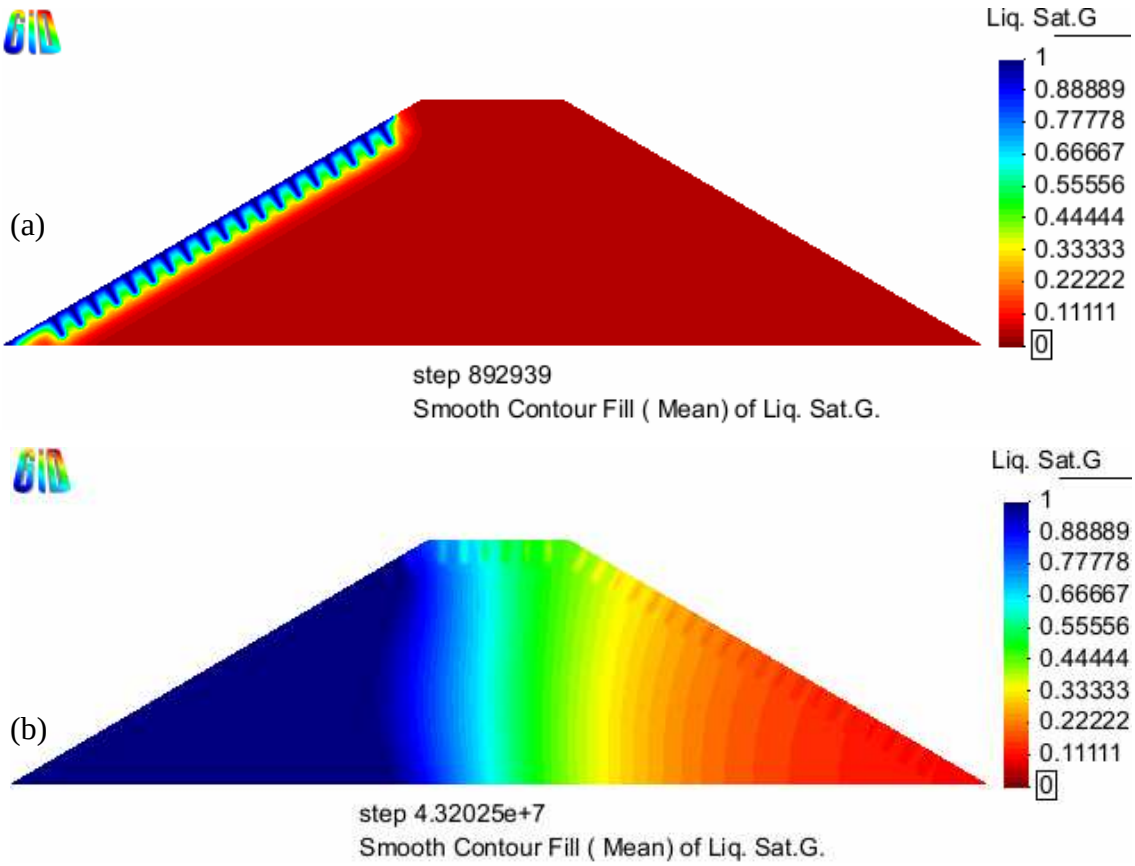

Figure 5.6. (a), (b) and (c) show the liquid degree of saturation for Case I at subsequent time intervals

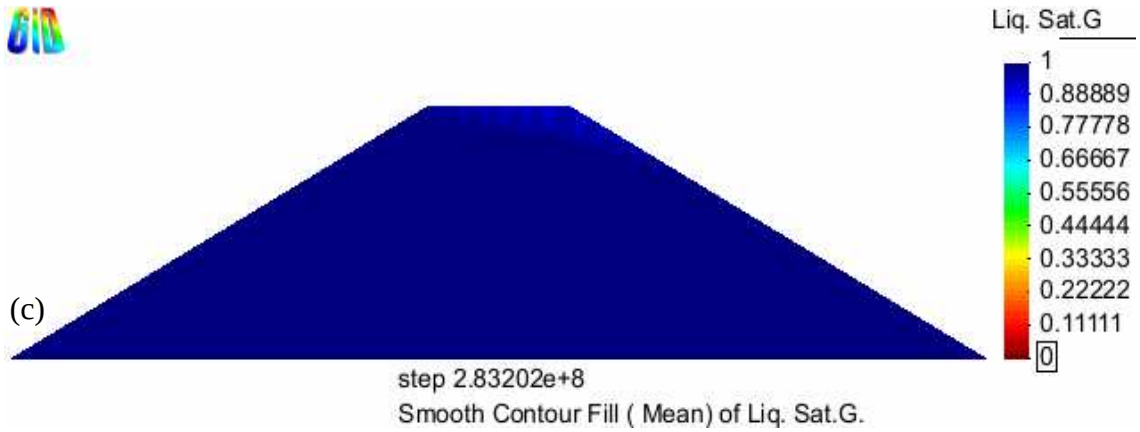

Figure 5.6. continued

In Case II, the seepage pattern was totally different. The edges got saturated very quickly and the top of the outward slope got saturated first. The core of the embankment in this case got saturated at last (Figure 5.7).

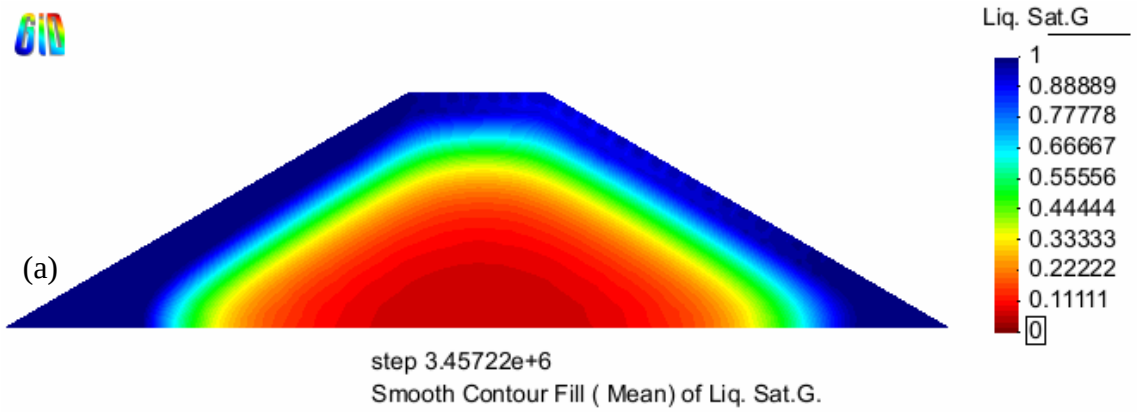

Figure 5.7. (a), (b) and (c) show the liquid degree of saturation for Case II at subsequent time intervals

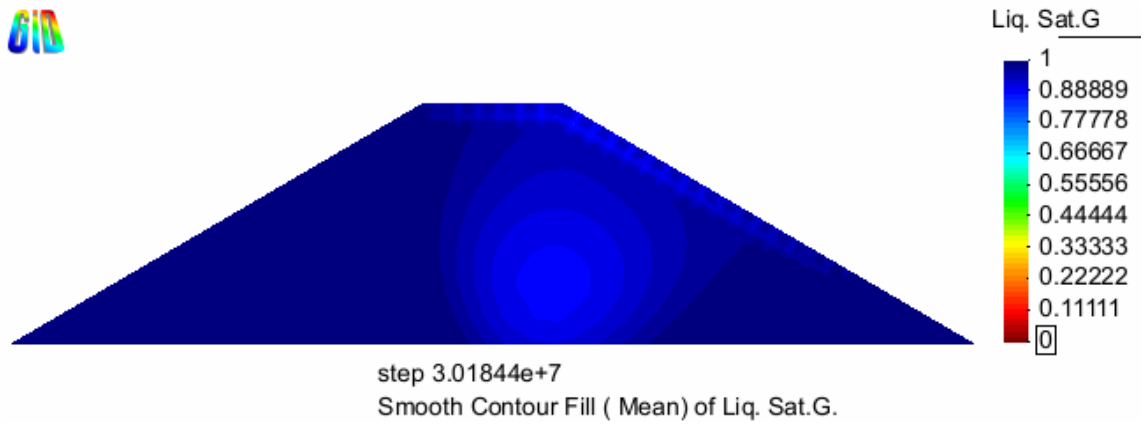

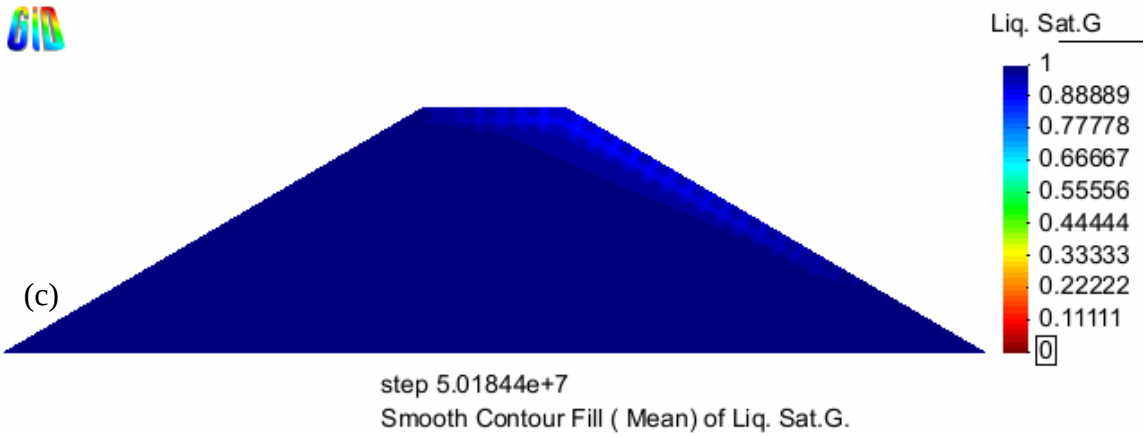

Figure 5.7. continued

The above cases showed the impact of desiccation cracks on the waterfronts in an unsaturated earth embankment. However, desiccation cracking is a highly random process and depends on parameters such as environmental conditions and properties of the soil which are difficult to control during and after the construction of the embankment. Therefore, a random model was developed to capture the uncertainty of the crack geometry which was imposed on the finite element mesh to see the effect of desiccation cracks on the seepage of the earth embankment.

5.4 Random model

5.4.1 Background

Monte Carlo method was used to find the effect of the random geometry of cracks on Ts and Q of the flood embankment. Monte Carlo methods are very useful for modeling phenomena with significant uncertainty in the inputs. A Monte Carlo analysis involves deterministic solution of a large number of randomly generated input parameters usually referred as “realizations”. For each realization identical conditions (embankment geometry, boundary conditions, soil properties, etc) are maintained except for the random input variable (crack geometry in this case) whose effect is sought on the system. The uncertainty of the input parameter is overcome by solving a large number of cases deterministically, each corresponding to a different randomly generated input. In general, the Monte Carlo method involves following steps:

1) Defining the domain of possible inputs.
2) Generating inputs randomly from the domain using a specified probability distribution.
3) Performing deterministic computation using inputs.
4) Aggregating the results of the individual computation into final result.

For the present analysis, the inputs and their distributions have been defined in section 5.4.2. The deterministic computation was done using a finite element model as discussed in section 5.3. Finally, the results obtained have been presented in section 5.5.

5.4.2 Probabilistic model

As desiccation cracking is a highly random process and varies dramatically with different environmental conditions and for different soils, a random model was developed to capture the variability in the geometry and the location of the desiccation cracks. Though some researchers Chertkov and Ravina (1998), and Horgan and Young (2000) came up with a probabilistic model for the geometry of the cracks, these models were not generic and too specific at times to implement. Various researchers have made an effort to find out the nature and geometry of cracks through various field (El Abedine and Robinson, 1971; Dasog et al., 1988; McKay et al., 1993; Li Jinhui, 2007; Dyer et al., 2009) and lab methods (Kleppe and Olson, 1985; Maerz et al., 1990; Hinsby et al., 1996; Samouëlian, 2003; Nahlawi and Kodikara, 2006; Rayhani et al., 2007).

In order to introduce variability in the geometry of the cracks, the data reported in the literature was used to generate the probability density functions (PDFs) for the depth, spacing and aperture of the cracks. The geometry of the cracks was kept the same for a single simulation i.e., the depth, spacing and aperture of all the cracks was the same for a single simulation. The location of the subhorizontal cracks was maintained parallel to the surface and at half the depth of the vertical cracks. All the other properties (material and geometry) of the subhorizontal cracks were maintained same as that of the vertical cracks.

On the basis of the laboratory observations, Nahlawi and Kodikara (2006) suggested that crack spacing follows a lognormal distribution. Li Jinhui (2007) did some field experiments and also came to the conclusion that crack spacing and aperture follow lognormal distribution. A lognormal distribution to represent the crack geometry parameter seems reasonable as it only takes positive value. The probability distributions for the three input variables are discussed below:

5.4.2.1 Depth

Depth of cracks can vary from a few inches to as deep as 3 feet inside the soil. Figure 5.8 shows the vertical cracks as observed by Dyer et al. (2009) in an earth embankment.

Figure 5.8. Picture showing cracks of different depth and aperture (after Dyer at al., 2009)

Researchers over the years have recorded the data for depth of the cracks. Abedine and Robinson (1971) and Dyer et al. (2009) collected data for the depth of cracks in soil under various field conditions. Based on these data a lognormal distribution was used to capture the variability in crack depth. Symbol ‘Z’ is used to denote the random variable associated with the crack depth and ‘z’ to denote a particular realization of Z. The lognormal PDF for the crack depth takes the following form:

$$f_Z(z) = \frac{1}{\sqrt{2\pi}\xi z}\exp\left[-\frac{1}{2}\left(\frac{\ln z - \lambda}{\xi^2}\right)\right]$$

here,

$\lambda = 4.3354$; ξ=0.5793 and z is in cm.

The mode of the above distribution is at 60 cm. Using the above PDF, four thousand random values for crack depth were sampled. The finite element mesh (section 5.3) was divided into squares of 20 cm in the zone where cracks were to be imposed. Accordingly, the depth of the crack sample was discretized in multiples of twenty cm, restricted to a maximum of 2 m. Figure 5.9 shows the empirical cumulative distribution of the crack depth sample and theoretical cumulative distribution for crack depth.

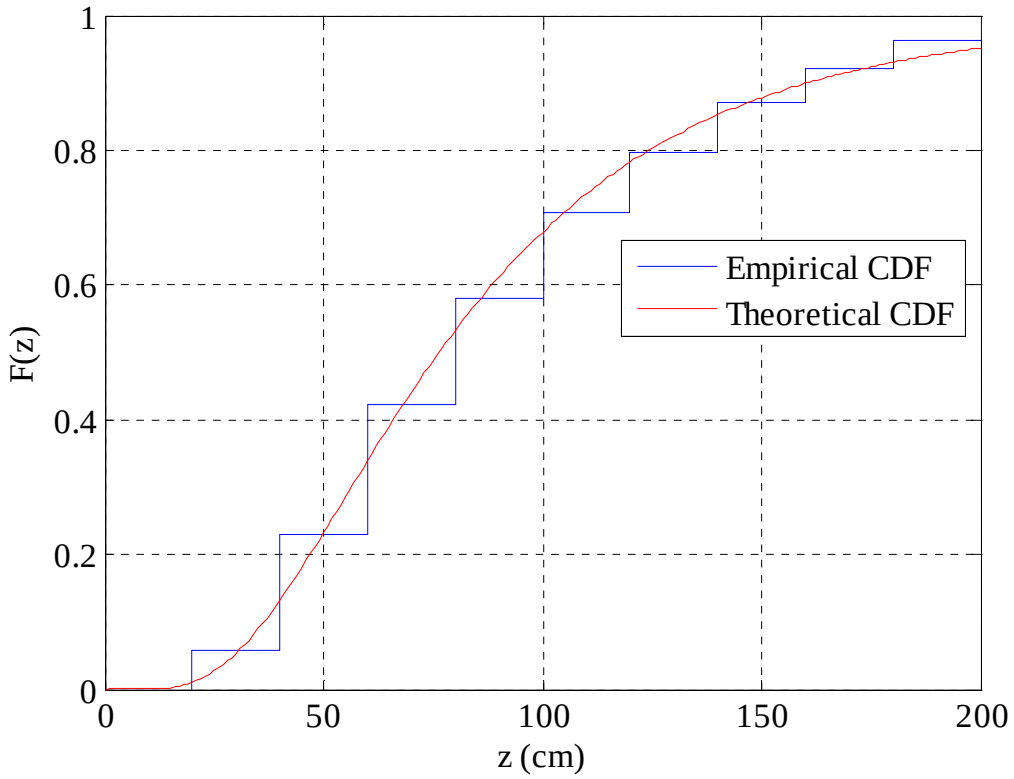

Figure 5.9. Empirical and theoretical cumulative distribution for depth (Z)

5.4.2.2 Spacing

Spacing between the cracks depends on the soil and environmental conditions which keep on changing continuously. Figure 5.10 shows the variable spacing between the cracks.

Figure 5.10. Picture depicting the surface of a cracked soil (after Dyer et al., 2009)

Based on the field data collected by Abedine and Robinson (1971), and Dasog et al. (1988), lognormal distribution parameters were found for spacing between the cracks. Symbol 'S' is used to denote the random variable associated with the crack spacing and 's' to denote a particular realization of S. The lognormal PDF for the crack spacing takes the following form:

$$f_S(s) = \frac{1}{\sqrt{2\pi}\xi s}\exp\left[-\frac{1}{2}\left(\frac{\ln s - \lambda}{\xi^2}\right)\right]$$

here,

$\lambda = 4.1964$; ξ=0.906 and s is in cm.

The mode of the above distribution is at 60 cm. Using the above PDF, four thousand random values for crack spacing were sampled. Again, because of the same reasons as

mentioned in section 5.4.2.1, the crack spacing sample was discretized in multiples of twenty cm, restricted to a maximum of 7 m. Figure 5.11 shows the empirical cumulative distribution for the sampled crack spacing and theoretical cumulative distribution for crack spacing.

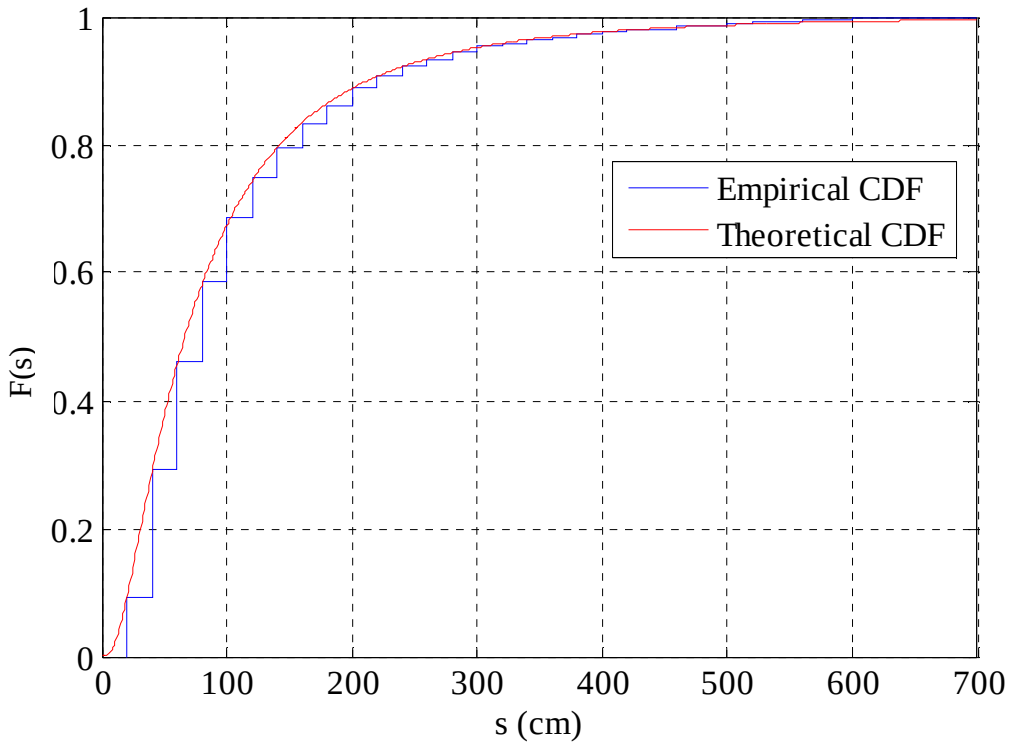

Figure 5.11. Empirical and theoretical cumulative distribution for crack spacing (S)

5.4.2.3 Aperture

Figure 5.8 shows the variability in the aperture of the crack. In order to capture the variability in the aperture of desiccation cracks a probabilistic model had to be developed. Based on the field data collected by Abedine and Robinson (1971), Dasog et

al. (1988) and Dyer et al. (2009) lognormal distribution parameters were found for the aperture of the cracks. Symbol ‘W’ is used to denote the random variable associated with the crack depth and ‘w’ to denote a particular realization of W. The lognormal PDF for the crack aperture takes the following form:

$$f_{\mathrm{W}}(\mathrm{w}) = \frac{1}{\sqrt{2\pi}\xi \mathrm{w}} \exp\left[-\frac{1}{2}\left(\frac{\ln \mathrm{w} - \lambda}{\xi^2} \right) \right]$$

here,

$\lambda = -4.4607$; ξ=0.5973 and w is in m.

The mode of the above distribution is at 0.008 m. Using the above PDF, four thousand random values for crack aperture were sampled. The aperture of the crack could be assigned any value in the finite element program; however, it was observed in the field that crack aperture takes value between 0.001 m and 0.03 m only. Therefore, the domain of the crack aperture was restricted between 0.001 m and 0.03 m. Figure 5.12 shows the empirical cumulative distribution of the sampled crack aperture and theoretical cumulative distribution for crack aperture.

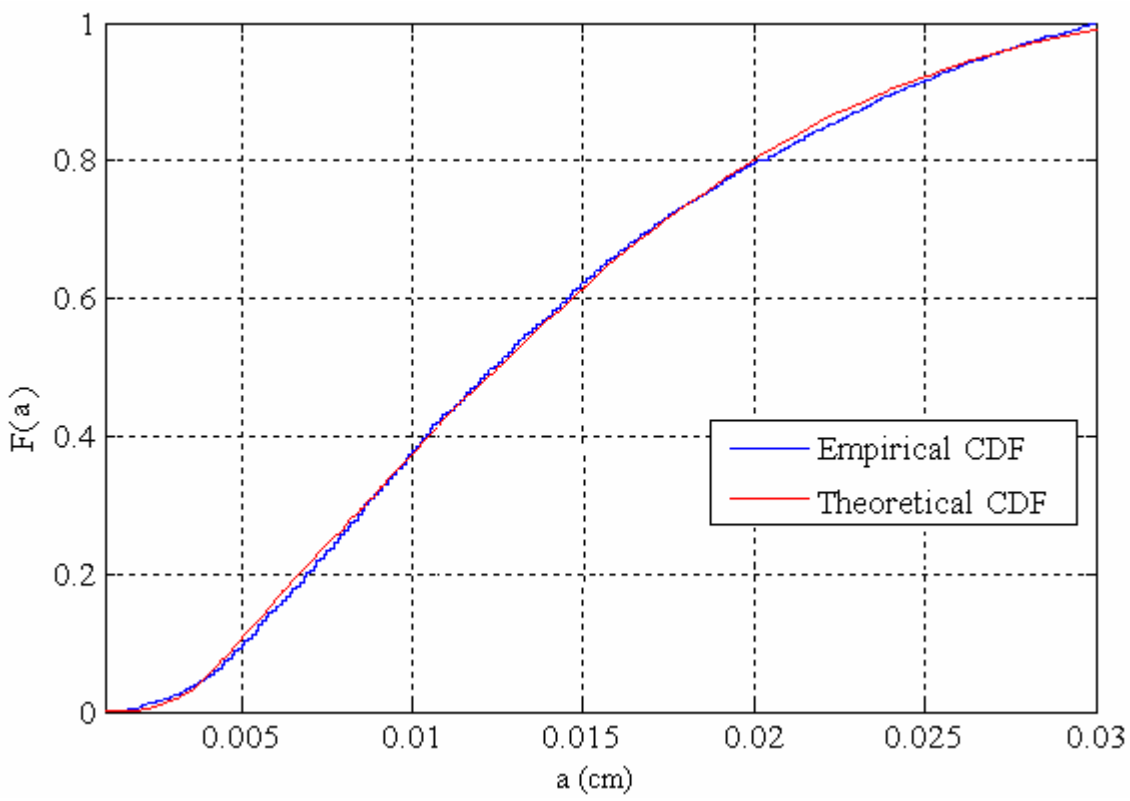

Figure 5.12. Empirical and theoretical cumulative distribution for crack aperture (A)

A summary for the modal values of the three input variables defining the crack geometry (Z, S and W) is given in Table 5.2

Table 5.2 Summary of the modal values of the crack geometry variables

Variable	**Modal value**
Depth of the crack (Z)	60 cm
Spacing between the crack (S)	60 cm
Crack aperture (W)	0.008 m

5.4.2.4 Joint probability distribution

In order to study the combined effect of Z, S and W in pair or all at once, on time to saturation (Ts) and flow rate (Q), joint probability distributions were defined. In the absence of any evidence, it was assumed that each of the three random variables (Z, S and W) are statistically independent. In general, a joint probability distribution for two random variables X and Y is defined as (Ang and Tang, 2007):

$$f_{X,Y}(x,y) = f_{X|Y}(x|y)\, f_Y(y) = f_{Y|X}(y|x)\, f_X(x)$$

where, $f_{X|Y}(x|y)$ and $f_{Y|X}(y|x)$ give the conditional distribution of Y given X and X givenY respectively, and $f_X(x)$ and $f_Y(y)$ give the marginal distributions for X and Y respectively.

If X and Y are statistically independent then:

$$f_{X|Y}(x|y) = f_X(x) \text{ and } f_{Y|X}(y|x) = f_Y(y)$$

So that, $f_{X,Y}(x,y) = f_X(x) f_Y(y)$

And so for the three random variables, their joint probability functions are as follows:

$$f_{Z,S}(z,s) = f_Z(z) f_S(s);\ f_{Z,W}(z,w) = f_Z(z) f_W(w);\ f_{S,W}(s,w) = f_S(s) f_W(w) \text{ and}$$

$$f_{Z,S}(z,s,w) = f_Z(z) f_S(s)\, f_W(w)$$

For the purpose of running finite element simulations, four thousand random realizations from each of the marginal distributions were sampled. The joint distributions for crack depth and crack spacing, crack spacing and crack aperture, and crack depth and crack aperture are shown in Figure 5.13, Figure 5.14, Figure 5.15 respectively.

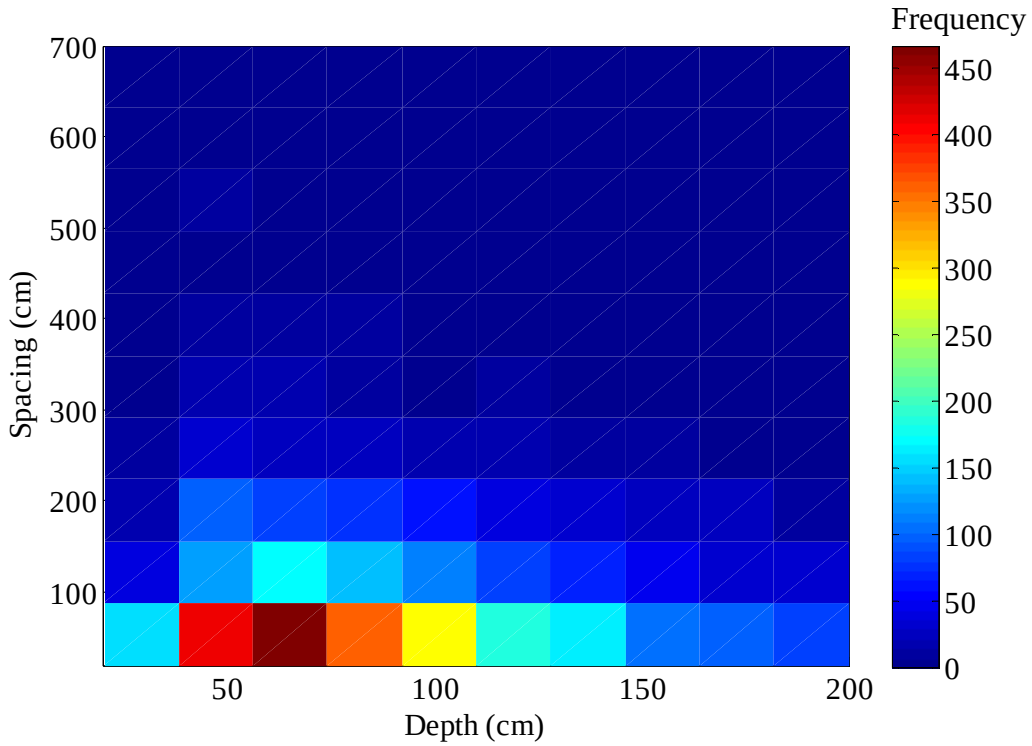

Figure 5.13. Joint empirical distribution for crack spacing and aperture

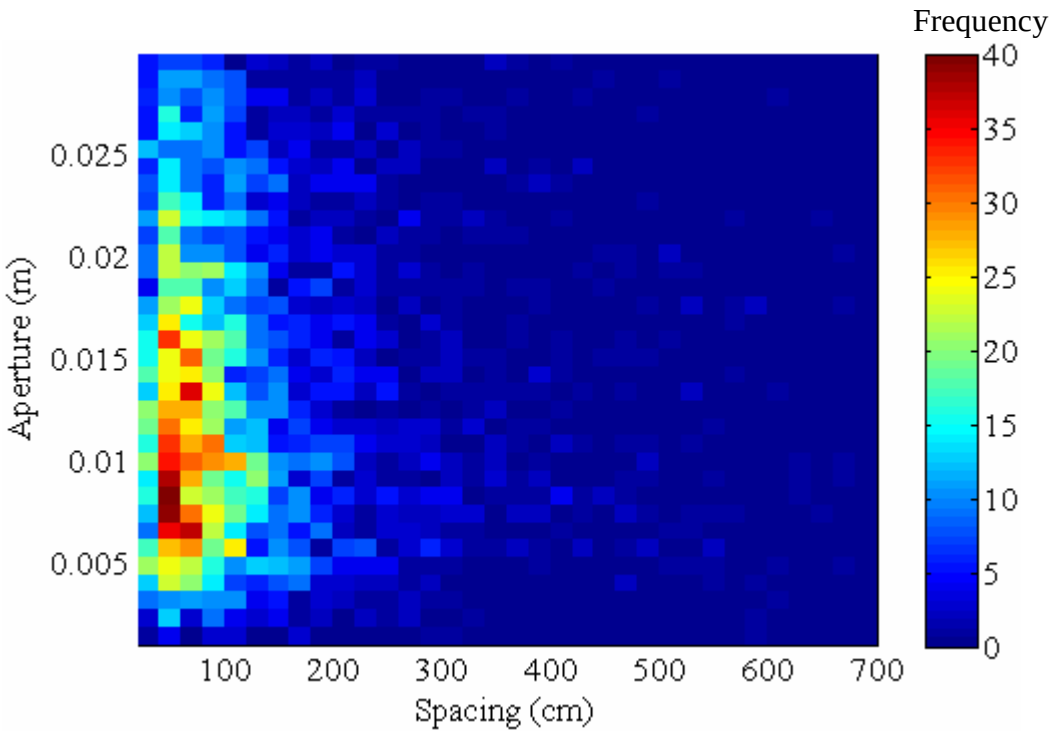

Figure 5.14. Joint empirical distribution for crack spacing and aperture

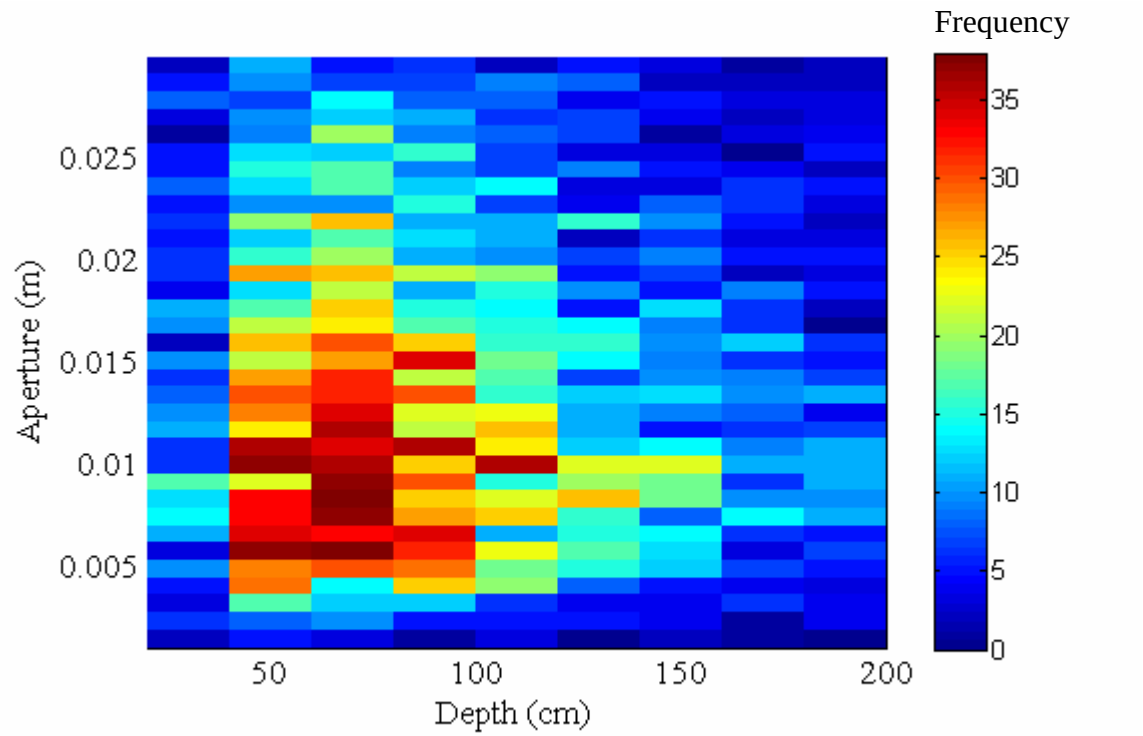

Figure 5.15. Joint empirical distribution for crack depth and aperture

5.5 Results

CODE_BRIGHT was used to perform the finite element computations. A MATLAB® code (see APPENDIX A) was written to generate the proper input files for CODE_BRIGHT. Details about the input files for CODE_BRIGHT have been discussed in section 3.6. The MATLAB® code basically prepares the geometry input file *ROOT*_GRI.DAT by adding the joint elements required for the crack geometry and assigning the aperture width to the joint elements. Based on the aperture width information the permeability of the cracks changes accordingly in *ROOT*_GEN.DAT file. CODE_BRIGHT is called through MATLAB® and once the simulation is over, the MATLAB® code reads the output files to find Ts and Q for each case. In the course of

research it was found that the pattern in which the embankment saturates for Case I (no subhorizontal cracks) and Case II (with subhorizontal cracks) was very different. In Case I, the element at the top right of the geometry gets saturated at last (Figure 5.6), while in Case II the element just above the bottom middle gets saturated last (Figure 5.7). The embankment was considered to have reached a steady state of saturation once the degree of saturation of the element that gets saturated last becomes constant. So a slightly different code was used to ascertain Ts for Case I and Case II. The results of the computational model are discussed below:

5.5.1 Comparison between homogenous case, Case I and Case II

With homogenous case (without cracks) as reference, the two main variables obtained from the probabilistic analysis viz., time to steady state saturation, Ts and flow rate at the outward slope, Q are used for comparison between Case I and Case II

From numerical simulation of the homogenous case, the time to saturation, Ts was calculated as 4400 days. Ts for Case I was in the range of 3300 days to 4100 days, which is comparable to the homogenous case. The cracks did not seem to decrease Ts significantly for case I as the vertical cracks only facilitated in the initial and final stages of wetting the soil. This was more like a skin effect and the kinetics of the waterfront was such that it had to move through the core of the embankment for the rest of the period just like the homogenous case. For Case II, Ts lied between 350 days to 430 days, which is one order of magnitude lower than the other two cases. The primary reason for

such a drastic shift is because of the subhorizontal cracks that took the flow of water to the other side of the slope in less than a day.

Flow rate, Q shows similar pattern as Ts. For the homogenous case the flow rate was 1.30×10^{-5} kg/s. For Case I, Q lied between 1.41×10^{-5} kg/s and 1.48×10^{-5} kg/s. Again, such a small increment from the homogenous case was because of the water losing its head while moving across the core of the embankment. In Case II, Q varies from 0.28 kg/s to 90 kg/s. Such a huge variation in Q for Case II is caused by the aperture of the cracks as explained through the corresponding CDF plots of Q in section 5.5.3.

5.5.2 Convergence of results

For a Monte Carlo simulation, a sufficiently large number of realizations have to be performed so that the calculated value of the mean and standard deviation of the output (Ts and Q) are not influenced by occurrence of extremely large or small events. In general, the analyses showed that the calculated mean and standard deviation of the output converged to stable values after 2000 realizations. (Note: In all the plots of the variable/variables shown below is the one that assumes random values. Other variables, if not mentioned, have been kept constant and are equal to the mode value as given in Table 5.2). The convergence results for only Ts value of Case I have been presented in section 5.5.2.1. Other convergence plots are described in APPENDIX B.

5.5.2.1 Time to saturation, Ts (Case I)

From the cumulative mean plot of Ts (Figure 5.16), the value of Ts corresponding to mean of the lognormal distribution assumed for the various random inputs (Z, S and W) and for their joint distribution can be easily seen. Ts for homogenous case is 4400 days, therefore it can be seen for the case where only W is varying (yellow line), that aperture of the cracks influences Ts the least. This can be explained by the fact that aperture of the crack will only facilitate the flow once the waterfront reaches the crack network. As mentioned in section 5.3, the reason for that is that cracks play a role only at the boundaries of the embankment, for the rest of its course the water has to flow through the homogenous core of the embankment losing most of its head. The fact that W does not influence Ts significantly can be further verified from Figure 5.17 that shows the standard deviation of Ts for each case. It is seen that the standard deviation is least in the case when only W is varying. Again from Figure 5.16 it can be inferred that Z (cyan line) has the highest influence on Ts and S (fuchsia line) has an intermediate effect between Z and W. A similar trend is shown in the standard deviation plot of Ts (Figure 5.17). The cumulative mean plot for the case when Z, S and W are varying in pairs, show intermediate effects corresponding to the individual parameters that are varying. For example, the values of Ts in the case where S, W are varying (blue line) is between the individual cases where S (fuchsia line) and W (yellow line) are varying. The value of Ts corresponding to the black line representing the case in which all three input variables (Z, S, W) are varying is basically the average response of the flood embankment when there is no knowledge about the geometry of the crack.

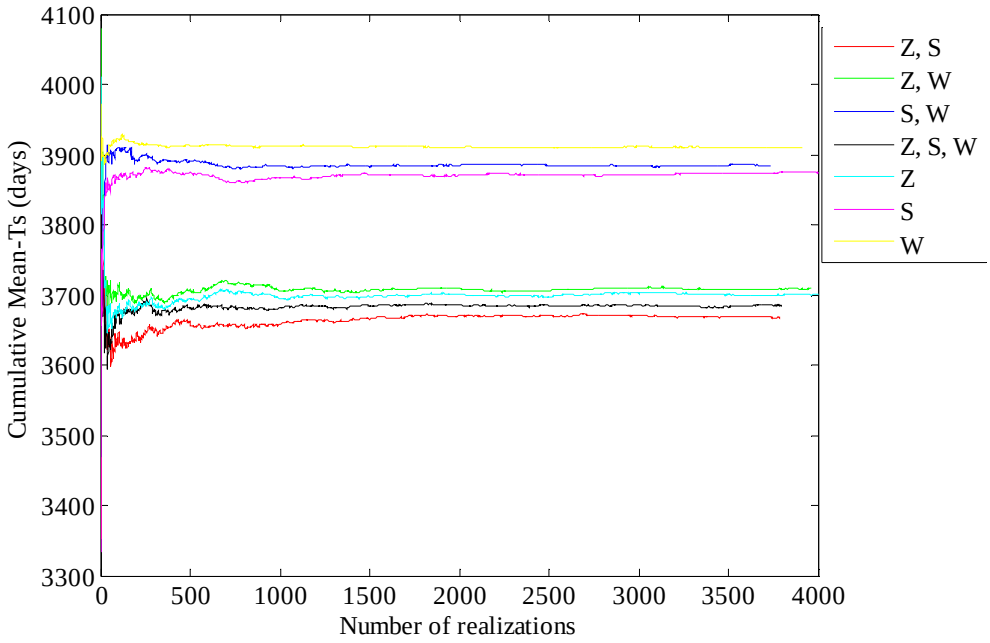

Figure 5.16. Cumulative mean plots of Ts for Case I

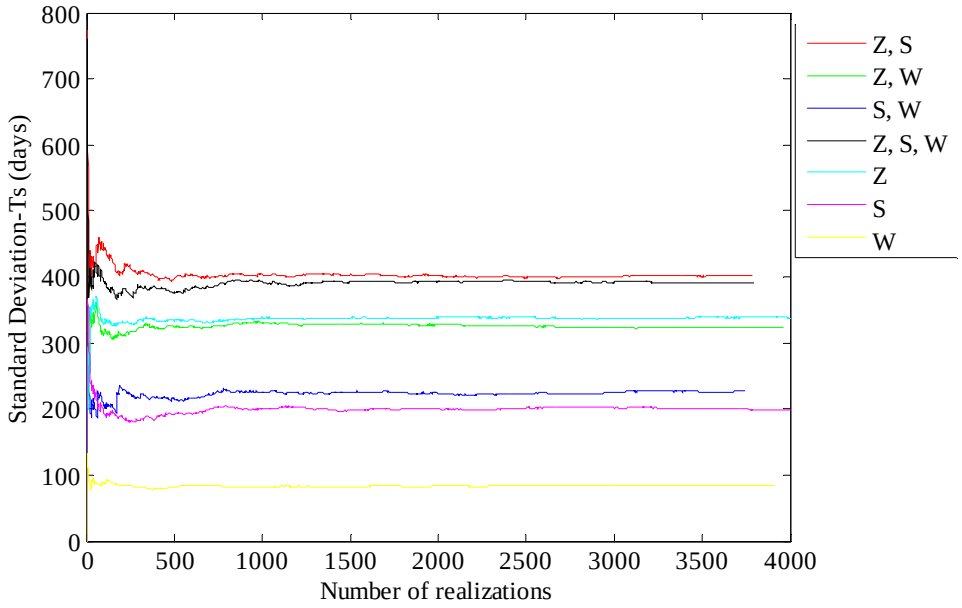

Figure 5.17. Standard deviation plots of Ts for Case I

5.5.3 Cumulative distribution functions of predicted quantities

Monte Carlo simulation when combined with random field finite element analysis leads to a random form of modeling. Such modeling is characterized by a distribution of responses rather than a single deterministic result. Finding the cumulative distribution of an output is much desirable for design purposes in geotechnical problems. For example, for a flood embankment it might be desirable to know the probability of flow rate exceeding a given threshold. This can be expressed mathematically for a random variable X, as:

$$P(X \leq x)=F_X(x) \tag{5.1}$$

where, $P(X \leq x)$ denotes the probability that the value of the random variable X is less than or equal to x and F is the cumulative distribution function.

As there is a range of possible values of a random variable, some central value of this range are of special interest. The median is one such quantity used to designate the central value of a random distribution. The median of a random variable X, denoted as x_m, is the value at which the CDF is 50% and thus larger and smaller values are equally probable, i.e.,

$$F_X(x_m)=0.5 \tag{5.2}$$

For the present case, ts_m and q_m represent the median value of Ts and Q, respectively.

5.5.3.1 CDF plots Case I

Figure 5.18 shows the CDF plots of Ts for cases where Z varies individually and in pairs. The CDFs and the median value of time to saturation, ts_m is almost same for all he cases. From this it can be inferred that the Z has the most influence on Ts for Case I.

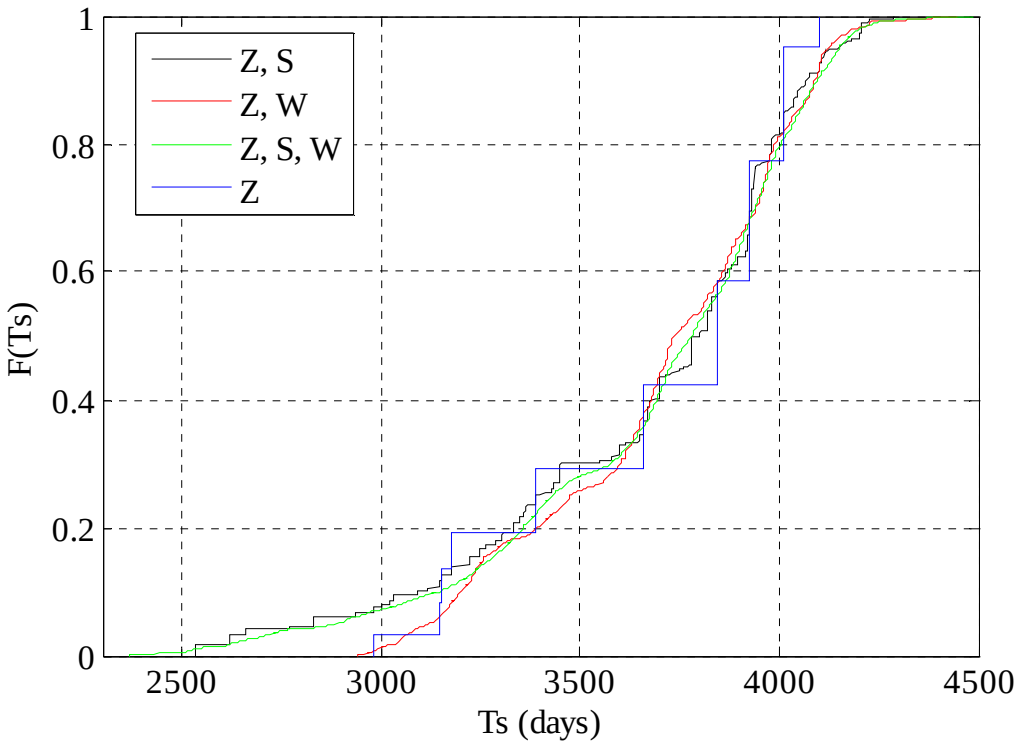

Figure 5.18. CDF plots for Ts when Z varies individually and in pairs for Case I

Figure 5.19 shows the CDF plots of Ts for cases where S varies individually and in pairs. The median value of time to saturation, ts_m is almost the same for the case when S alone varies (red line) and S, W (blue line) vary in pair and equals 3900 days. Also for

the case when S and Z vary (fuchsia) and, S, Z and W (green) vary in pair ts_m is close and equals 3800 days. Hence, it can be concluded that W does not has large effect on Ts.

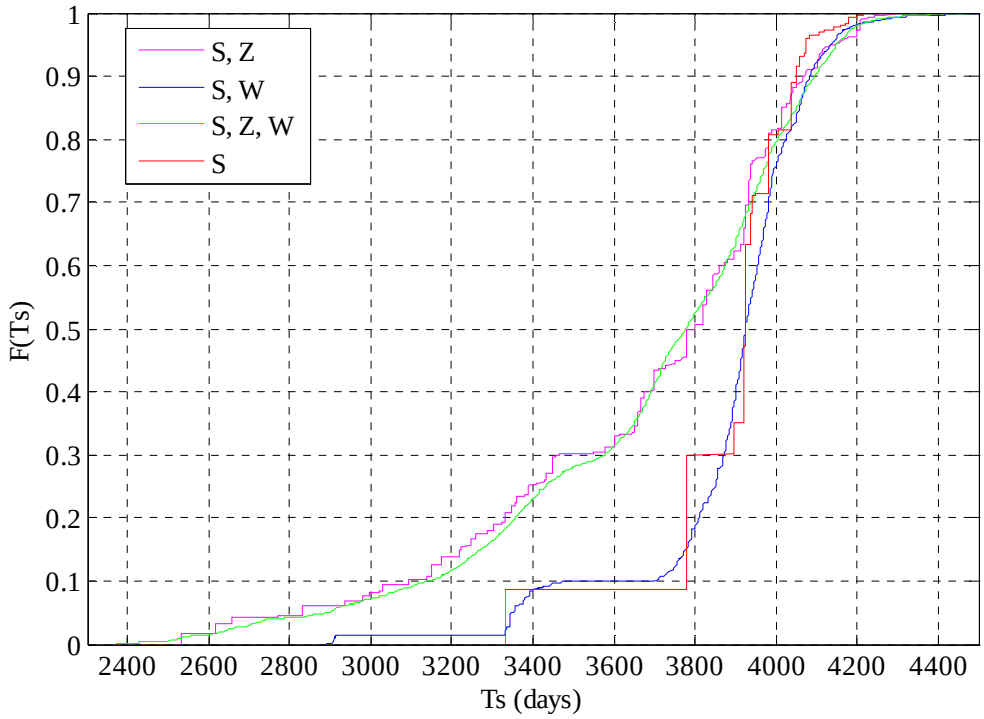

Figure 5.19. CDF plots for Ts when S varies individually and in pairs for Case I

Figure 5.20 shows the CDF plots of Ts for cases where W varies individually and in pairs. The median value of time to saturation, ts_m is almost same for the case when W varies alone (blue line) and W, S (red line) vary in pairs. Also for the case when W, Z vary (green line) and S, Z, W (black line) vary in pair, ts_m is close and equals 3800 days. Hence, it can be concluded that S has a small effect on Ts.

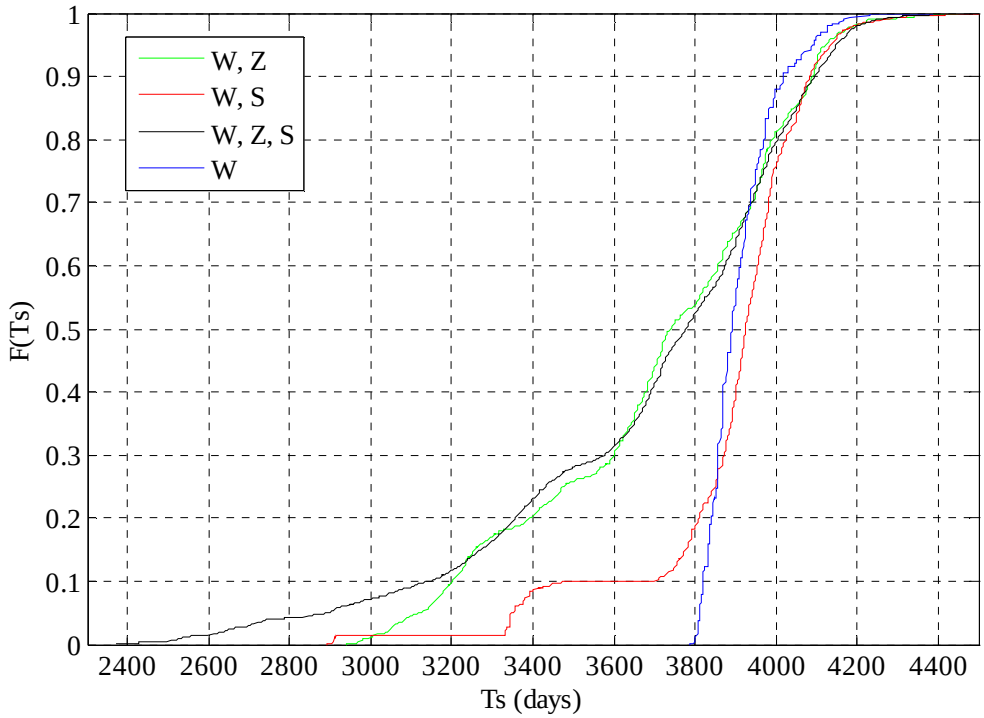

Figure 5.20. CDF plots for Ts when W varies individually and in pairs for Case I

Figure 5.21 shows the CDF plots of Ts, where Z, S and W vary individually. It can be seen that Z causes the most variation as far as Ts is concerned, followed by S and W causes the least variation in Ts.

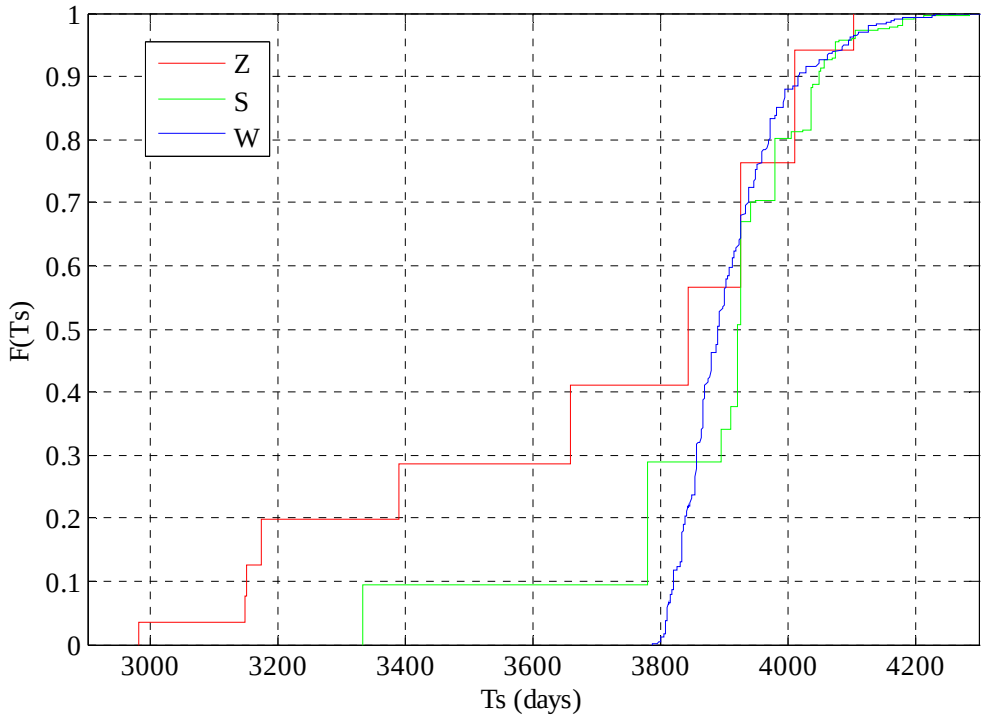

Figure 5.21. CDF plots for Ts when Z, S and W vary individually for Case I

Figure 5.22 shows the CDF plots of Q, where Z varies individually and in pairs. It can be seen from the figure that all the CDFs are very close. This implies that Z has the greatest effect on Q and variation in S and W contribute only marginally to Q.

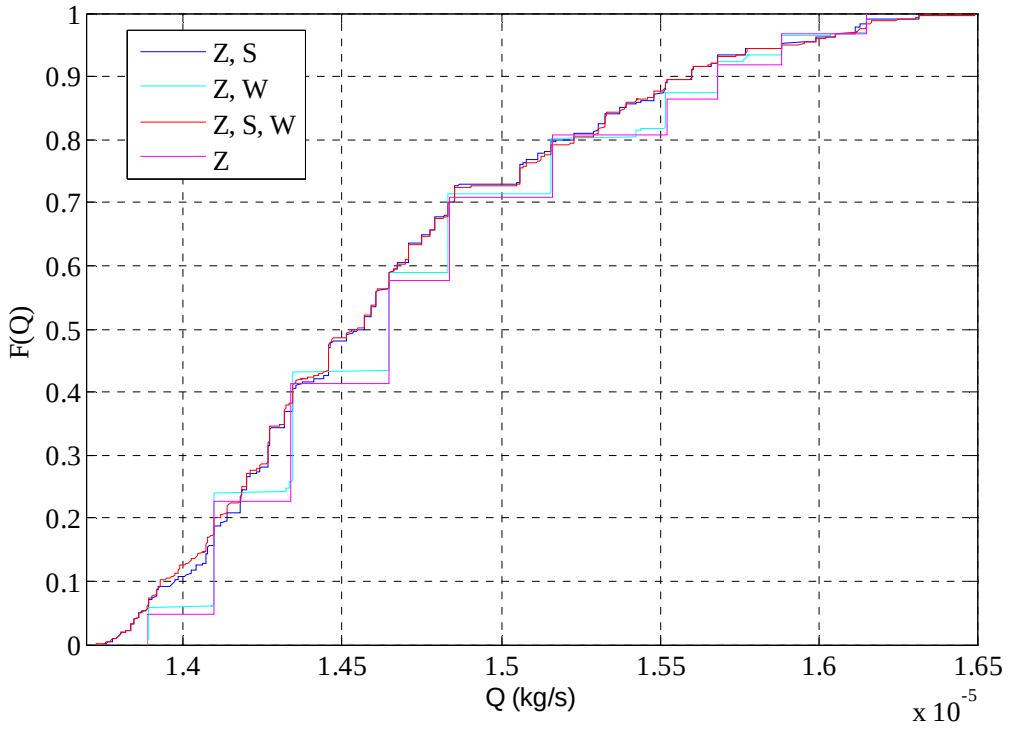

Figure 5.22. CDF plots for Q when Z varies individually and in pairs for Case I

Figure 5.23 shows the CDF plots of Q for cases where S varies individually and in pairs. The median value of time to saturation, q_m is almost the same for the case when S alone varies (blue line) and S, W (red line) vary in pairs and equals 1.43×10^{-5} kg/s. Also for the case when S, Z vary (black line) and S, Z, W (blue line) vary in pair q_m is close and equals 1.45×10^{-5} kg/s. Hence, it can be inferred that W has a small effect on Q.

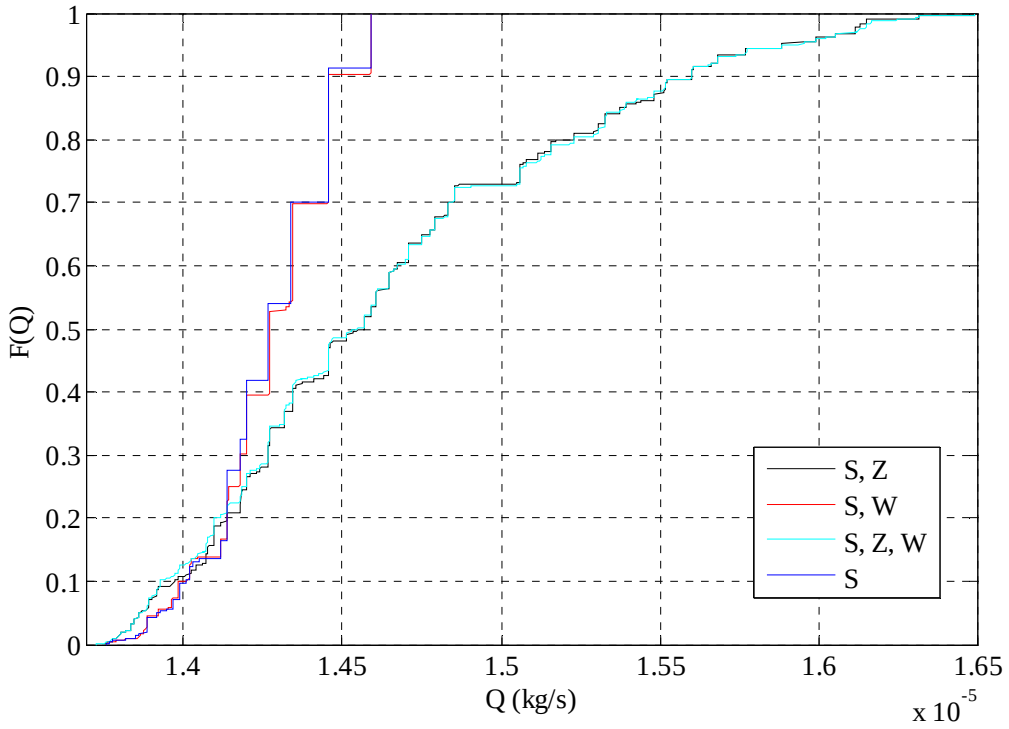

Figure 5.23. CDF plots for Q when S varies individually and in pairs for Case I

Figure 5.24 shows the CDF plots for Q when W varies individually and in pairs. A slight difference in q_m for W, S and W alone varying can be seen. Likewise, there is a small difference in q_m for W, Z, S and W, Z varying. This implies that W has slightly more effect on Q than S.

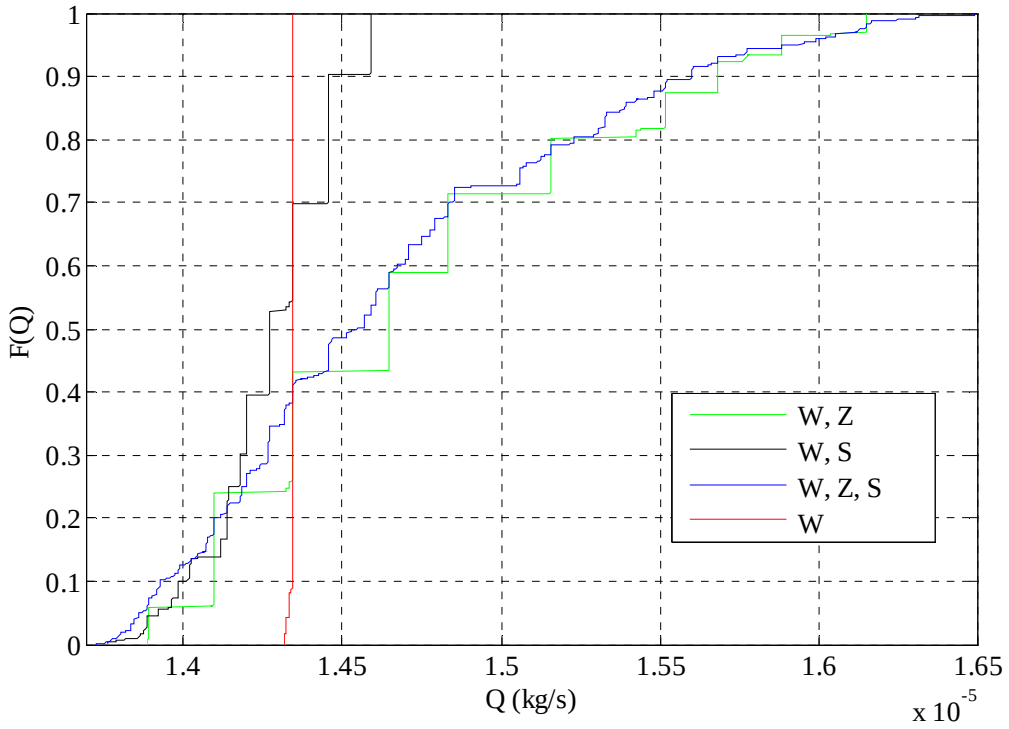

Figure 5.24. CDF plots for Q when W varies individually and in pairs for Case I

Figure 5.25 shows the CDF plots of Q when Z, S and W vary individually. As discussed earlier it can be seen from the figure that Z causes the most variation in Q followed by S and W.

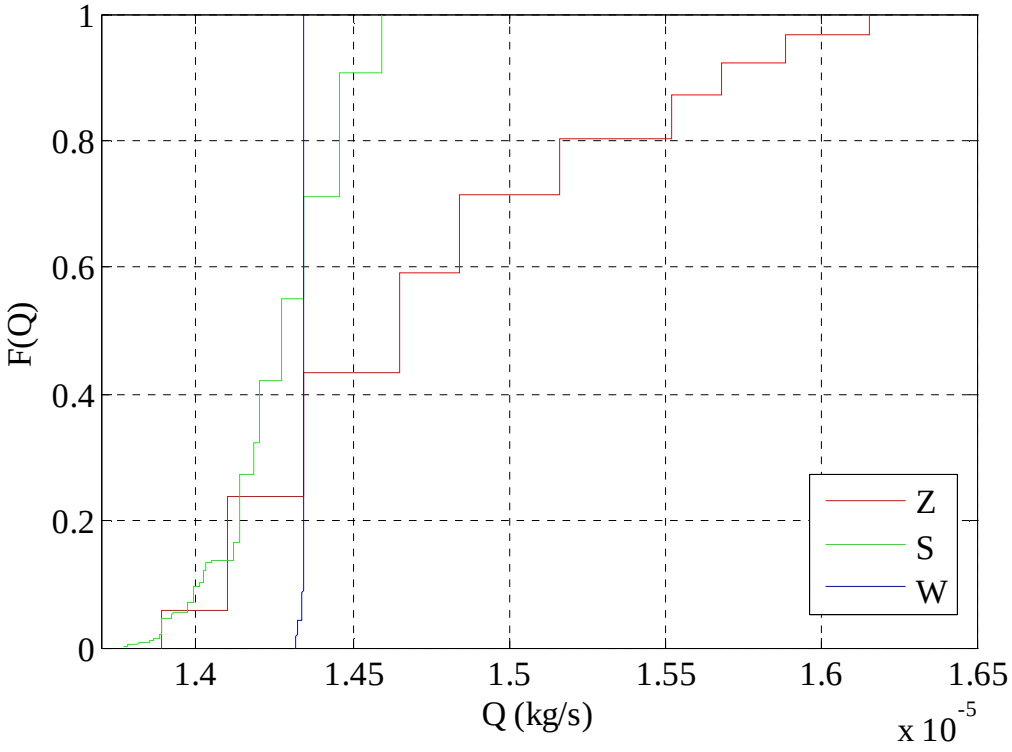

Figure 5.25. CDF plots for Q when Z, S and W vary individually for Case I

5.5.3.2 CDF plots Case II

Figure 5.26 shows the CDF plots of Ts when Z varies individually and in pairs. Again as all the CDF plots are close to each other, it can be said that Z has the most influence on Ts.

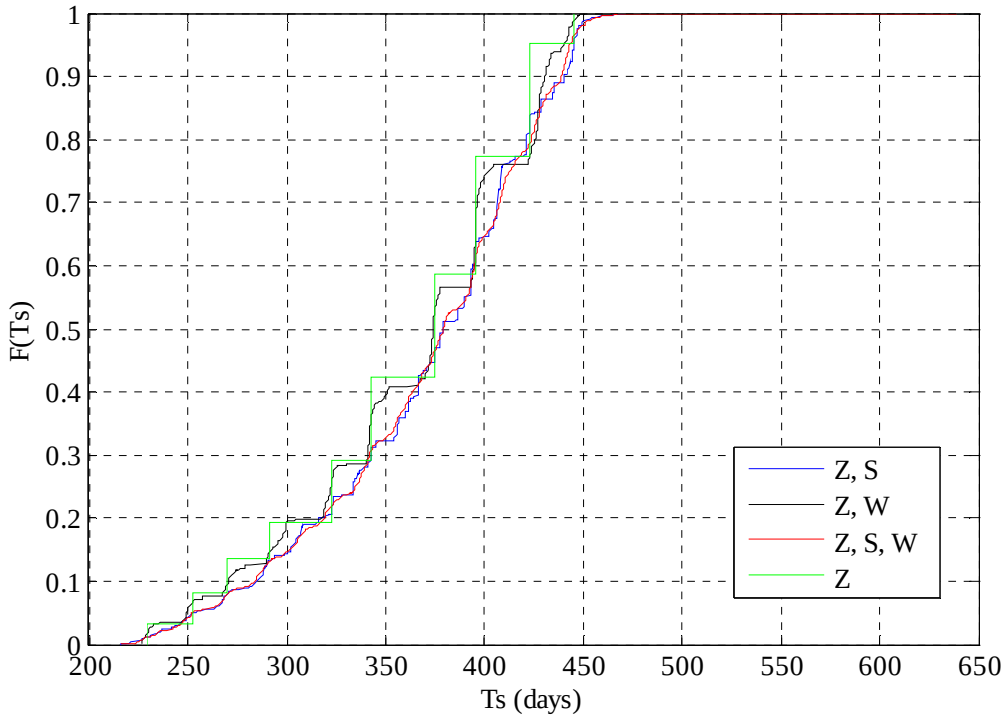

Figure 5.26. CDF plots for Ts when Z varies individually and in pairs for Case II

Figure 5.27 and Figure 5.28 suggest that W has the least effect of Ts followed by S.

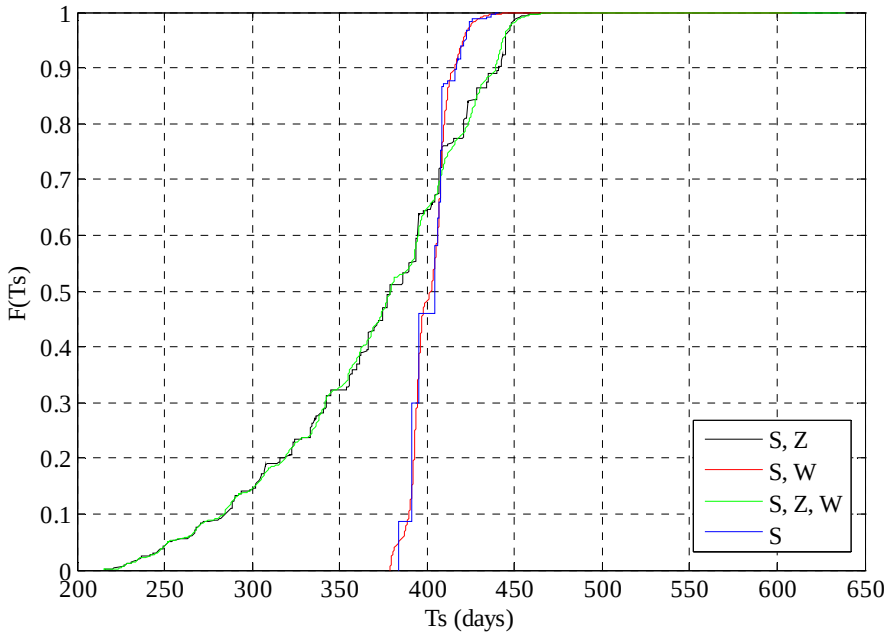

Figure 5.27. CDF plots for Ts when S varies individually and in pairs for Case II

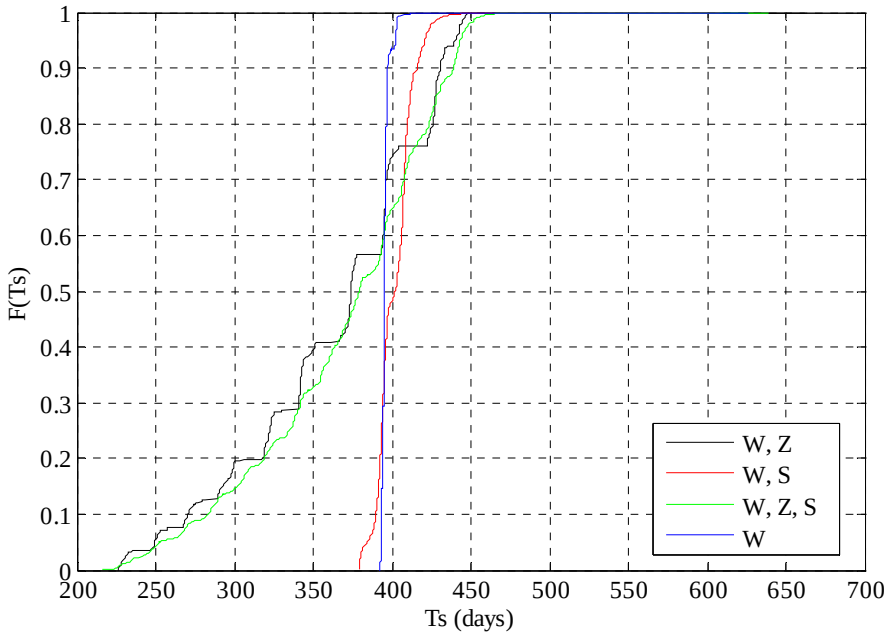

Figure 5.28. CDF plots for Ts when W varies individually and in pairs for Case II

Figure 5.29 confirms that Z has the most influence on Ts followed by S and W.

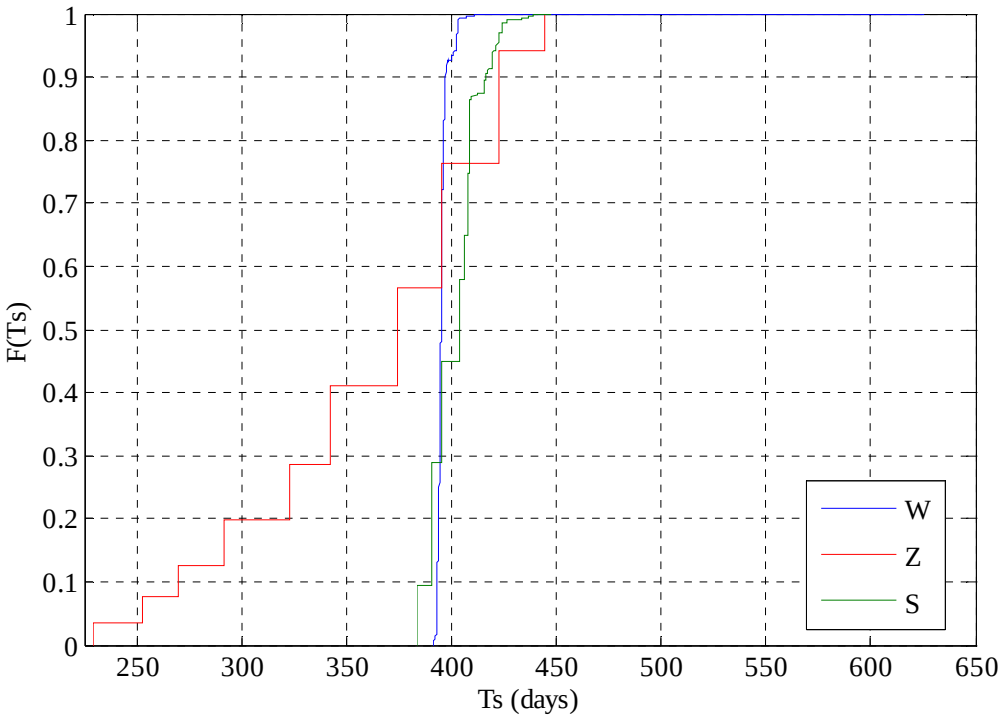

Figure 5.29. CDF plots for Ts when Z, S and W vary individually for Case II

The CDF plots of Q, when W was varied have been plotted separately because W has a huge effect on Q for Case II.

Figure 5.30 shows the CDF plots of Q when Z and S vary individually and in pairs. The order of Q is much higher as compared to Case I. q_m for all the three plots is about 0.41 kg/s.

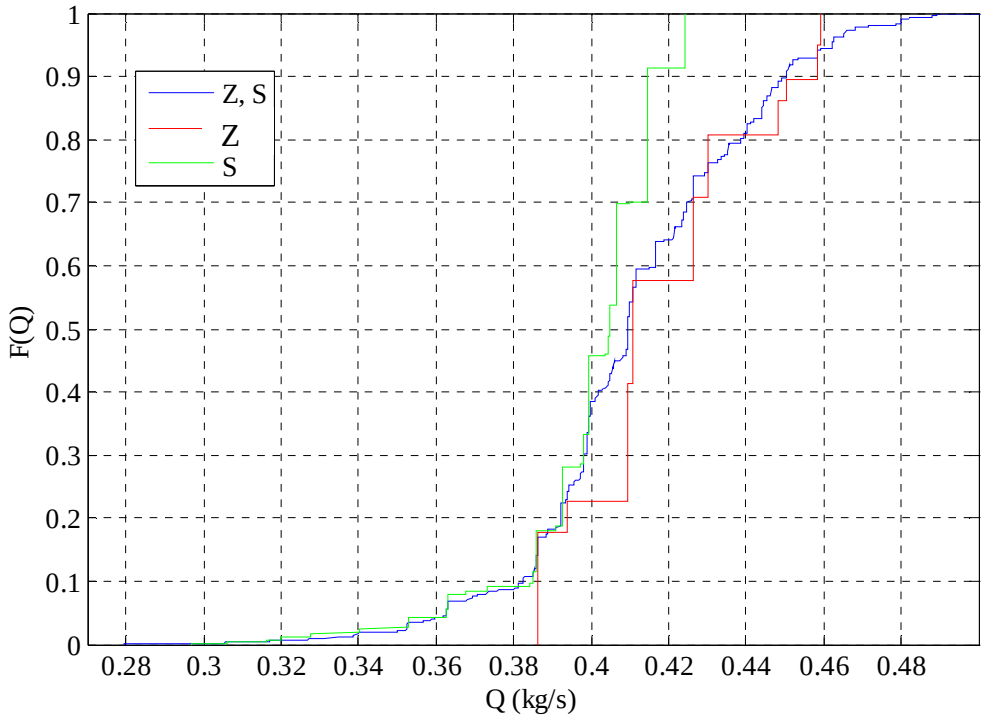

Figure 5.30. CDF plots for Q when Z and S vary individually and in pairs for Case II

Figure 5.31 shows the CDF plots of Q for when W is varying individually and in pairs. The fact that all the CDF plots containing W are superimposed on each other makes it evident that W has the greatest effect on flow rate for Case II. The range of Q is very broad with a maximum value of 90 kg/s.

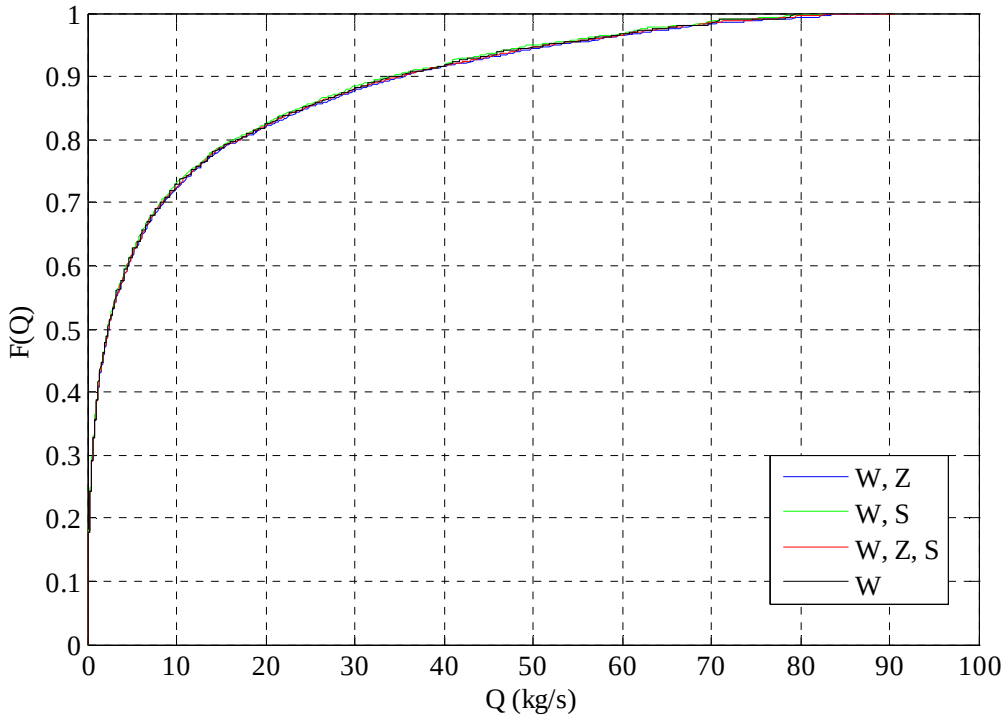

Figure 5.31. CDF plots for Q when W varies individually and in pairs for Case II

5.6 Conclusions

Thus from the probabilistic analysis, it was seen that different crack geometry parameters contribute differently for the two cases. Under the stated conditions and embankment geometry for the case with only vertical cracks (Case I), the depth of the cracks has the greatest impact on the flow rate and time to saturation while spacing between the cracks has intermediate and minimum impact on Ts and Q respectively and aperture of the crack has minimum and intermediate effect on Ts and Q respectively. As for the case with subhorizontal cracks (Case II), Ts was one order of magnitude less than the homogenous while Q was four to five orders of magnitudes higher. The depth of the

crack had maximum and intermediate impact on the Ts and Q respectively. Spacing between the cracks had minimum impact on Ts as well as Q while, crack aperture had maximum and intermediate effect on Ts and Q respectively. Also, there was a stark difference in the way the embankment was saturated in Case II, where the bottom of the core got saturated in the end for the embankment analyzed.

6. CONCLUSIONS AND SCOPE FOR FURTHER WORK

6.1 Summary

The objective of the study was to generate two-dimensional numerical model to analyze the effect of desiccation cracks on seepage of an unsaturated soil embankment. In order to simulate the effect of cracks numerically, joint elements were used. To ascertain their effect on flow rate a simple joint model was developed and it was found that under identical conditions the flow rate was directly proportional to the width of the joint element. In order to validate the model, experimental data from a small scale embankment experiment was used and the model results were found in close agreement with the experimental data. As desiccation cracking is a highly random process, a random model was developed to capture the high degree of variability in the location and the geometry of the cracks. To fulfill this objective, extensive literature review was done in order to generate the required PDFs for depth of the cracks, location of the cracks and spacing between the cracks. The randomly generated crack geometry was the superimposed on the finite element mesh. Finally, the effect of the crack depth, aperture and spacing on Ts and Q were found for the two cases: one with subhorizontal cracks and the other without the subhorizontal cracks. It was observed from the analyses that the waterfronts for the two cases were very different.

6.2 Conclusions

Following conclusions can be drawn from the present research:

1. From modeling the scaled embankment it was seen that a numerical model can be developed using CODE_BRIGHT, which can simulate the transient flow of water through cracks in an unsaturated embankment.
2. From the probabilistic analysis of a full scale synthetic embankment, the steady state conditions were observed. Following conclusions can be drawn from the study:
    - Under the conditions prescribed for the problem, for Case I,
        - The time to saturation (Ts) was lower and flow rate (Q) was higher than Ts and Q respectively for the homogenous case. However, the values of Ts and Q for Case I and the homogenous case were still comparable.
        - The depth of the crack (Z) had the greatest impact on Ts and Q.
        - Spacing between the cracks (S) had intermediate and minimum impact on Ts and Q respectively.
        - Aperture of the crack (W) had minimum and intermediate effect on Ts and Q respectively.
    - Under the conditions prescribed for the problem, for Case II,
        - Ts was one order of magnitude less than the homogenous case while, Q was four to five orders of magnitudes higher than the homogenous case.
        - The depth of the crack had maximum and intermediate impact on the Ts and Q respectively.

- Spacing between the cracks had minimum impact on Ts as well as on Q.
- Crack aperture had intermediate and maximum effect on Ts and Q respectively.

- There was a stark difference in the way the waterfront moved for the two cases. For Case I, the waterfront was regular and very similar to the waterfront of the homogenous case. The water day-lighted at the bottom of the outward slope of the embankment as is usually expected. However, for Case II, the bottom of the core got saturated in the end and the water reached the outward slope of the embankment very quickly with the seepage starting from top of the outward slope of the embankment analyzed.

6.3 Scope for future work

1. The water retention curve for a single crack and crack network has not been studied in detail. There are no simple and reliable models that capture the water retention characteristics of cracks.
2. Fluid flow through a cracked embankment is a hydraulic phenomenon. However, efforts must be made to study the mechanical effect of flow of water through cracks. Some work has been done in this area by Segura and Carol (2004) using zero-width element, but they concentrated on flow through jointed rocks.

3. Cracks in an unsaturated soil embankment open and close according to the moisture content of the soil and the state of stresses in the soil. A finite element approach can be developed that can that can replicate this opening and self-healing behavior of cracks.
4. A three-dimensional analysis should be done to study the 3-D effects of cracks on flow through an unsaturated embankment.

REFERENCES

Abu-Hejleh, A. and Znidarcic, D. (1995) Desiccation theory for soft cohesive soils, *Journal of Geotechnical Engineering*, **121**(6), 493–502.

Aitchison, G. D. (1965) Moisture equilibria and moisture changes in soils beneath covered areas: a symposium in print, Butterworth, Sydney, Australia, p. 15.

Alonso, E.E. and Alcoverro, J. (1998) Catsius Clay Project: Calculation and testing of behaviour of unsaturated clay as barrier in radioactive waste repositories, European Commission, DOC XII/286/98, Brussels.

Alonso, E. E. and Alcoverro, J (2005) DECOVALEX III project: Modelling of FEBEX in-situ test: task 1, Final Report. Statens kärnkraftinspektion, 197 pages.

Ang, A. H. S. and Tang, W. H. (2007) *Probability Concepts in Engineering: Emphasis on applications in civil & environmental engineering*, Wiley, Berkeley.

Aubeny, C. P. and Lytton, R. L. (2004) Shallow slides in compacted high plasticity clay slopes, *Journal of Geotechnical and Geoenvironmental Engineering*, **130**(7), 2004, 717-727.

Bear, J. (1972) *Dynamics of Fluid in Porous Media*. American Elsevier, New York.

Bear, J., and Alexander, H. D. C. (2008) *Modeling Groundwater Flow and Contaminant Transport*, Springer Verlag, Germany.

Bogárdi, I., Máthé, Z. and Tájékoz, V. D. é. (1968). Determination of the degree of protection offered by flood levees and the economic improvement thereof, National Water Authority, Department for Flood Control and River Training.

Brady, B. H. G. and Brown, E. T. (1993). *Rock Mechanics for Underground Mining*, Springer, Dordrecht.

Brooks, R. and Corey, A. T. (1964) Hydraulic properties of porous media, *Hydrology Papers, Colorado State University*(March).

Brown, S. R. (1987) Fluid flow through rock joints: the effect of surface roughness, *Journal of Geophysical Research*, **92**(B2), 1337-1347.

Chandler, R.J., Crilly, M.S. and Montgomery-Smith, G. (1995) A low-cost method of assessing clay desiccation for low-rise buildings, *Proceedings of the Institution of Civil Engineers*, **108**, pp. 135-136

Chertkov, V. and Ravina, I. (1998) Modeling the crack network of swelling clay soils, *Soil Science Society of America Journal*, **62**(5), 1162-1171.

Chertkov, V. and Ravina, I. (1999) Morphology of horizontal cracks in swelling soils1, *Theoretical and Applied Fracture Mechanics*, **31**(1), 19-29.

Christensen, J., Hewitson, B., Busuioc, A., Chen, A., Gao, X., Held, R., Jones, R., Kolli, R., Kwon, W. and Laprise, R. (2007) Regional climate projections, Climate Change, 2007: The Physical Science Basis. Contribution of Working group I to the Fourth Assessment Report of the Intergovernmental Panel on Climate Change.University Press, Cambridge.

Cho, S. E. and Lee, S. R. (2001) Instability of unsaturated soil slopes due to infiltration, *Computers and Geotechnics*, **28**(3), 185-208.

Cooling, L. and Marsland, A. (1953) Soil mechanics studies of failures in the sea defence banks of Essex and Kent, *Proceedings of the ICE Conference on the North Sea Floods of 31 January/1 February 1953*. London.

Corser, P. and Cranston, M. (1991) Geosynthetic design of performance, *Proceeding-Vancouver Geotechnical Society,* Vancouver, BC.

Dahlin, T., Sjödahl, P., Friborg, J. and Johansson, S., (2001) Resistivity and sp surveying and monitoring at the sädva embankment dam, Sweden, *Procs. 5th European ICOLD Symposium*, 25-27 June, Geiranger, Norway, Balkema, Lisse, 107-113.

Dasog, G., Acton, D., Mermut, A. and De Jong, E. (1988) Shrink-swell potential and cracking in clay soils of Saskatchewan, *Can. J. Soil Sci*, **68**, 251-260.

Defra (2008) The Government's Response to Sir Michael Pitt's Review of the Summer 2007 Floods, Department for Environment, Food and Rural Affairs.

DIT-UPC (2011). *CODE_BRIGHT, A 3-D Program for Thermohydromechanical Analysis in Geological Media: User's Guide*, Centro Internacional de Me´todos Nume´ricos en Ingenieri´a (CIMNE), Barcelona

Dyer, M., Utili, S. and Zielinski, M. (2009) Field survey of desiccation fissuring of flood embankments, *Water management*, **162**(3), 221-232.

Edlefsen, N. E. and Anderson, A. B. C. (1943). *Thermodynamics of Soil Moisture*, University of California [Press], Berkeley.

Eigenbrod, K. (2003) Self-healing in fractured fine-grained soils, *Canadian Geotechnical Journal*, **40**(2), 435-449.

Fairbridge, R. W. and Bourgeois, J. (1978) *The Encyclopedia of Sedimentology (vol. 6)*: Dowden, Hutchinson and Ross Inc., Stroudsburg.

Fauchaux, C. and Meriaux, P. (2004) *Geophysical and Geotechnical Methods for Diagnosing Flood Protection Dikes*. Edition QAE. Editions Cemagref, Cirad, Ifremer, Inra.

Fenton, G. A., Griffiths, D. and Center, C. S. o. M. G. R. (1996) Statistics of free surface flow through stochastic earth dam, *Journal of Geotechnical Engineering*, **122**(6), 427-436.

Firoozabadi, A. and Hauge, J. (1990) Capillary pressure in fractured porous media, *JPT*, **289**, 784-791.

Fredlund, D. G. and Rahardjo, H. (1993). *Soil Mechanics for Unsaturated Soils*, Wiley-Interscience, .

Gens, A. and Olivella, S. (2001) THM phenomena in saturated and unsaturated porous media, *Revue française de génie*, **155(**5), 693–717.

Gens A, Sanchez M., Guimarães L., Alonso E., Lloret A., Olivella S., Villar M.V. and Huertas F. (2009). A full-scale in situ heating test for high-level nuclear waste disposal: observations, analysis and interpretation. *Géotechnique* **59(**4): 377-399

GiD (2010) *The Personal Pre and Postprocessor, Version 9.0.4. User's Guide*, Centro Internacional de Me´todos Nume´ricos en Ingenieri´a (CIMNE), Barcelona.

Greco, R. (2002) Preferential flow in macroporous swelling soil with internal catchment: Model development and applications, *Journal of hydrology*, **269**(3-4), 150-168.

Hinsby, K., McKay, L., Jørgensen, P., Lenczewski, M. and Gerba, C. (1996) Fracture aperture measurements and migration of solutes, viruses, and immiscible creosote in a column of clay rich till, *Ground Water*, **34**(6), 1065-1075.

Hopkins, T.C., Allen D.L., Deen R.C. and Grayson, C.G. (1988) Slope Maintenance and slide restoration, FHWA Office of Implementation, Virginia, Report No. FHWA-RT-88-040

Horgan, G. and Young, I. (2000) An empirical stochastic model for the geometry of two-dimensional crack growth in soil (with Discussion)* 1, *Geoderma*, **96**(4), 263-276.

Hornig, T., Sokolov, I. and Blumen, A. (1996) Patterns and scaling in surface fragmentation processes, *Physical Review E*, **54**(4), 4293-4298.

Indraratna, B., Ranjith, P. and Gale, W. (1999) Single phase water flow through rock fractures, *Geotechnical and Geological Engineering*, **17**(3), 211-240.

Jessell, M., Cox, S., Schwarze, P. and Power, W. (1995) The anisotropy of surface roughness measured using a digital photogrammetric technique, *Elsevier*, 67A-68A.

Jimenez-Rodriguez, R., Sitar, N. and Chacon, J. (2006) System reliability approach to rock slope stability, *International Journal of Rock Mechanics and Mining Sciences*, **43**(6), 847-859.

Jinhui, L. (2007) Field Experimental study and numerical simulation of seepage in saturated/Unsaturated cracked soil, PhD thesis, The Hong Kong University of Science and Technology, Hong Kong.

Johansson, S. and Dahlin, T. (1998) Seepage monitoring in Hällby embankment dam by continuous resistivity measurements, *Procs. 8th Congress of the International Ass. of Eng. Geology and the Environment*, Vancouver, 21-25 September 8.

Kim, T. H. and Hwang, C. (2003) Modeling of tensile strength on moist granular earth material at low water content, *Engineering Geology*, **69**(3-4), 233-244.

Kindle, E. (1917) Some factors affecting the development of mud-cracks, *The Journal of Geology*, **25**(2), 135-144.

Kitsunezaki, S. (1999) Fracture patterns induced by desiccation in a thin layer, *Physical Review E*, **60**(6), 6449-6464.

Kleppe, J. H. and Olson, R. E. (1985) *Desiccation Cracking of Soil Barriers*, ASTM International, 263.

Konrad, J. M. and Ayad, R. (1997) A idealized framework for the analysis of cohesive soils undergoing desiccation, *Canadian Geotechnical Journal*, **34**(4), 477-488.

Konrad, J. M. and Ayad, R. (1997) Desiccation of a sensitive clay: field experimental observations, *Canadian Geotechnical Journal*, **34**(6), 929-942.

Kuhn, J. A. and Zornberg, J.G. (2006) Field suction and effect of cracking in highly plastic clay, TxDOT, Austin, Report No. FHWA/TX-07/0-5202-2

Laxmikantha, M. R. (2009) Experimental and theoretical analysis of cracking in drying soils, PhD Thesis, Universitat Politecnica de Catalunya, Barcelona, Spain

Li, A., Merifield, R. and Lyamin, A. (2008) Stability charts for rock slopes based on the Hoek-Brown failure criterion, *International Journal of Rock Mechanics and Mining Sciences*, **45**(5), 689-700.

Liu, C. W., Chen, S. K. and Jang, C. S. (2004) Modelling water infiltration in cracked paddy field soil, *Hydrological Processes*, **18**(13), 2503-2513.

Low, B. (2007) Reliability analysis of rock slopes involving correlated nonnormals, *International Journal of Rock Mechanics and Mining Sciences*, **44**(6), 922-935.

Lytton, R. L., Picornell, M., Garcia, C. and Huang C.C. (1987) Detection and sizing of surface cracks in expansive soil deposits, TTI, College Station, Report No. FHWA/TX-87/187-13

Maerz, N. H., Franklin, J. A. and Bennett, C. P. (1990) Joint roughness measurement using shadow profilometry, *International Journal of Rock Mechanics and Mining Sciences & Geomechanics*, **27**(5), 329-343.

McDonald, A., Beckner, B., Chan, H., Jones, T. and Wooten, S. (1991) Some important considerations in the simulation of naturally fractured reservoirs, *paper presented at SPE meeting*, Denver, Colorado, Apr. 15-17

McKay, L. D., Cherry, J. A. and Gillham, R. W. (1993) Field experiments in a fractured clay till, 1, hydraulic conductivity and fracture aperture, *Water Resources Research*, **29**(4), 1149-1162.

Meakin, P. (1987) A simple model for elastic fracture in thin films, *Thin Solid Films*, **151**(2), 165-190.

Mengel, K., Kirkby, E. A., Kosegarten, H. and Appel, T. (2001). *Principles of plant nutrition*, Kluwer Academic Pub, Dordrecht.

Morris, P. H., Graham, J. and Williams, D. J. (1992) Cracking in drying soils, *Canadian Geotechnical Journal*, **29**(2), 263-277.

Nahlawi, H. and Kodikara, J. (2006) Laboratory experiments on desiccation cracking of thin soil layers, *Geotechnical and Geological Engineering*, **24**(6), 1641-1664.

Nawari, O., Hartmann, R. and Lackner, R. (1997) Stability analysis of rock slopes with the direct sliding blocks method, *International Journal of Rock Mechanics and Mining Sciences*, **34**(3-4), 220.

Ohnishi, Y., Chan, T. and Jing, L. (1996) Constitutive models for rock joints, *Developments in Geotechnical Engineering*, **79**, 57-92.

Olivella, S., Carrera, J., Gens, A. and Alonso, E. (1994) Nonisothermal multiphase flow of brine and gas through saline media, *Transport in porous media*, **15**(3), 271-293.

Olivella, S., Gens, A., Carrera, J. and Alonso, E. (1996) Numerical formulation for a simulator (CODE-BRIGHT) for the coupled analysis of saline media, *Engineering Computations*; **13**(7): 87-112.

Øygarden, L., Kværner, J. and Jenssen, P. (1997) Soil erosion via preferential flow to drainage systems in clay soils, *Geoderma*, **76**(1-2), 65-86.

Plummer, P. and Gostin, V. (1981) Shrinkage cracks: desiccation or synaeresis, *Journal of Sedimentary Petrology*, **51**(4), 1147–1156.

Pruess, K. and Tsang, Y. (1990) On two-phase relative permeability and capillary pressure of rough-walled rock fractures, *Water Resources Research*, **26**(9), 1915-1926.

Pugh, R.S., Parnell, P.G. and Parkes, R.A (1995) A rapid and reliable on-site method of assessing desiccation in clay soils. *Proceedings Institution of Civil Engineers. Geotechnical Engineering*, **113**, 25-30.

Rayhani, M. H., Yanful, E. K. and Fakher, A. (2007) Desiccation-induced cracking and its effect on the hydraulic conductivity of clayey soils from Iran, *Canadian Geotechnical Journal*, **44**(3), 276-283.

Reitsma, S. and Kueper, B. H. (1994) Laboratory measurement of capillary pressure-saturation relationships in a rock fracture, *Water Resources Research*, **30**(4), 865-878.

Rodriguez, R., Sanchez, M., Ledesma, A. and Lloret, A. (2007) Experimental and numerical analysis of desiccation of a mining waste, *Canadian Geotechnical Journal*, **44**(6), 644-658.

Samouëlian, A. C., Richard, I., Tabbagh, G. and Bruand, A. (2003) Electrical resistivity imaging for detecting soil cracking at the centimetric scale, *Soil Sci Soc Am J,* **67**(5):1319–1326

Sanchez, M., Gens, A., Guimarães, L. and Olivella, S. (2005) A double structure generalized plasticity model for expansive materials, *Int. Jnl. Numer. Anal. Meth. Geomech*; **29**:751-787. DOI: 10.1002/nag.434.

Sanchez, M., Gens, A., Guimarães, L. and Olivella, S. (2008) Implementation algorithm of a generalized plasticity model for swelling clays. *Computers and Geotechnics*; **35**: 860–871. doi:10.1016/j.compgeo.2008.08.004

Sanchez, M., Gens, A. and Olivella, S (2010) Effect of thermo-coupled processes on the behavior of a clay barrier submitted to heating and hydration. *Invited lecture at IUTAM (International Union of Theoretical and Applied Mechanics) Symposium (Brazil, 2007).* **82**(1):153-18; Annals of the Braz. Acad. of Sciences. ISSN 0001-3765.

Sanchez M. Gens A., Olivella S. (2011) THM analysis of full scale heating test including clay fabric effects. *Int. Jnl. Numer. Anal. Math. Geomech*;(in press)

Segura, J. and Carol, I. (2004) On zero thickness interface elements for diffusion problems, *International Journal for Numerical and Analytical Methods in Geomechanics*, **28**(9), 947-962.

Sentenac, P. and Zielinski, M. (2009) Clay fine fissuring monitoring using miniature geo-electrical resistivity arrays, *Environmental Earth Sciences*, **59**(1), 205-214.

Shukla, S., Khandelwal, S., Verma, V. and Sivakugan, N. (2009) Effect of Surcharge on the Stability of Anchored Rock Slope with Water Filled Tension Crack under Seismic Loading Condition, *Geotechnical and Geological Engineering*, **27**(4), 529-538.

Snow, D. T. (1969) Anisotropie permeability of fractured media, *Water Resources Research*, **5**(6), 1273-1289.

Valette, G., Prévost, S., Lucas, L. and Léonard, J. (2008) A Dynamic Model of Cracks Development Based on a 3D Discrete Shrinkage Volume Propagation, *Computer Graphics Forum*, **27**(1), 47-62.

Van Genuchten, M. (1980) A closed-form equation for predicting the hydraulic conductivity of unsaturated soils, *Soil Sci. Soc. Am. J*, **44**, 892-898.

Vogel, H. J., Hoffmann, H., Leopold, A., and Roth, K. (2005) Studies of crack dynamics in clay soil:: II. A physically based model for crack formation, *Geoderma*, **125**(3-4), 213-223.

Wan, J. and Wilson, J. L. (1994) Colloid transport in unsaturated porous media, *Water Resources Research*, **30**(4), 857-864.

Wilson, G. W., Fredlund, D. and Barbour, S. (1994) Coupled soil-atmosphere modelling for soil evaporation, *Canadian Geotechnical Journal*, **31**(2), 151-161.

Witherspoon, P., Wang, J., Iwai, K. and Gale, J. (1980) Validity of cubic law for fluid flow in a deformable rock fracture, *Water Resources Research*, **16**(6), 1016-1024.

Yang, X. L., Li, L. and Yin, J. H. (2004) Stability analysis of rock slopes with a modified Hoek–Brown failure criterion, *International Journal for Numerical and Analytical Methods in Geomechanics*, **28**(2), 181-190.

Yang, X. L. and Zou, J. F. (2006) Stability factors for rock slopes subjected to pore water pressure based on the Hoek-Brown failure criterion, *International Journal of Rock Mechanics and Mining Sciences*, **43**(7), 1146-1152.

Yesiller, N., Miller, C., Inci, G. and Yaldo, K. (2000) Desiccation and cracking behavior of three compacted landfill liner soils, *Engineering Geology*, **57**(1-2), 105-121.

Zein el Abedine, A., and Robinson, G. H. (1971) A study on cracking in some vertisols of the Sudan, *Geoderma*, **5**(3), 229-241.

Zielinski, M., Sanchez, M., Romero, E., and Sentenac, P. (2010) Assessment of water retention behaviour in compacted fills, *Proceedings of the ICE-Geotechnical Engineering*, **164**(2), 139-148

APPENDIX A

The MATLAB® code used for the probabilistic analysis is given below:

```
tic
clear all

load s1.txt
load s2.txt

load d111.txt
load l111.txt
load w111.txt

a1=s1';
a2=s2';

[num_files col]=size(d111);

for grand=1:num_files

copyfile('gena.dat','new_gen.dat');
copyfile('grim.dat','new_gri.dat');

depth=d111(grand,1);

width=w111(grand,1);

length=l111(grand,1);


if ((depth/40)==floor(depth/40))
     subh=depth/2;
 else
     subh=ceil(depth/40)*20;
 end
```

```
 fname1='s200.txt';
 fname=strrep(fname1,'200',num2str(subh));

 fid=fopen(fname);
 i=1;
 while ~feof(fid)
     t=fgetl(fid);
     sub(i,:)=str2num(t);
 i=i+1;
 end
 fclose(fid);
k222=((width)^3)/24;
k2=sprintf('%0.2g',k222);


n=(depth/20)+1;
t1=1;
for i=1:128
    if (a1(n,i)~=0)
        p1(:,t1)=a1(1:n,i);
        t1=t1+1;
    end
end

if (n<10)
m=n;
end

if (n>9)
m=n+1;
end

t2=1;

for i=1:25
    if (a2(m,i)~=0)
        p2(:,t2)=a2(1:m,i);
        t2=t2+1;
    end
end

l=length/20;
[m1 n1]=size(p1);
[m2 n2]=size(p2);


u=1;
y=n1;
while (y>0)
    p11(:,u)=p1(:,y);
    u=u+1;
    y=y-l;
```

```
end


u=1;
y=n2;
while (y>0)
    p22(:,u)=p2(:,y);
    u=u+1;
    y=y-l;
end
[m3 n3]=size(p11);

[m4 n4]=size(p22);

for i=1:n3
    q11(1:m3-1,i)=p11(1:m3-1,i);
end

for i=1:n3
    q12(1:m3-1,i)=p11(2:m3,i);
end

q1(:,1)=q11(:);
q1(:,2)=q12(:);


for i=1:n4
    q21(1:m4-1,i)=p22(1:m4-1,i);
end

for i=1:n4
    q22(1:m4-1,i)=p22(2:m4,i);
end

q2(:,1)=q21(:);
q2(:,2)=q22(:);

[m5 n5]=size(q1);
[m6 n6]=size(q2);
[m7 n7]=size(sub);

for i=1:m5
    q(i,:)=q1(i,:);
end


for i=1:m6
    q(m5+i,:)=q2(i,:);
end

 for i=1:m7
```

```
     q(m5+m6+i,:)=sub(i,:);
 end


for i=1:(m5+m6+m7)

        s11(i,:)=[' ',num2str(2000+i)];

%%%%%%%%%%%%%%%%%
    if (q(i,1)<10)
        s21(i,:)=['    ',num2str(q(i,1))];
    end

    if (q(i,1)>=10&&q(i,1)<100)
        s21(i,:)=['   ',num2str(q(i,1))];
    end

    if (q(i,1)>=100&&q(i,1)<1000)
        s21(i,:)=['  ',num2str(q(i,1))];
    end

    if (q(i,1)>=1000)
        s21(i,:)=[' ',num2str(q(i,1))];
    end
%%%%%%%%%%%%%%%%%%%%%%
    if (q(i,2)<10)
        s31(i,:)=['    ',num2str(q(i,2))];
    end

    if (q(i,2)>=10&&q(i,2)<100)
        s31(i,:)=['   ',num2str(q(i,2))];
    end

    if (q(i,2)>=100&&q(i,2)<1000)
        s31(i,:)=['  ',num2str(q(i,2))];
    end

    if (q(i,2)>=1000)
        s31(i,:)=[' ',num2str(q(i,2))];
    end

%%%%%%%%%%%%%%%%%%%%%%%%%%%%%%%%%%%%%%%%%%%%%%
ser(i,:)=sprintf([s11(i,:),'    ',num2str(2),'
',num2str(8),s21(i,:),s31(i,:)]);

end


fid = fopen('new_gri.dat', 'a+');
for i =1:m5+m6+m7
fprintf(fid,'%s\n', ser(i,:));
```

```
end


gr1='    1 -0.5000000E+02';
gr2=' 2128 -0.5000000E+02';
gr3='    1 0.30000000E+00' ;
gr4=' 2000 0.30000000E+00';
gr5=' 2001 0.30000000E+00           0.0           0.0           0.0
0.0100';
gr6=' 2302 0.30000000E+00           0.0           0.0           0.0
0.0100';
gr7='    4    1';
gr8='  922   11  501  864';
gr9='    0    0';
gr10='    2';
gr11='    4    1';
gr12='  910  715  340  115';
gr13='End';
m8=m5+m6+m7+2000;

gr14=strrep(gr5,'0.0100',sprintf('%1.6s',num2str(width)));
gr15=strrep(gr6,'2302',num2str(m8));
gr16=strrep(gr15,'0.0100',sprintf('%1.6s',num2str(width)));


fprintf(fid,'%s\n', gr1);
fprintf(fid,'%s\n', gr2);
fprintf(fid,'%s\n', gr3);
fprintf(fid,'%s\n', gr4);
fprintf(fid,'%s\n', gr14);
fprintf(fid,'%s\n', gr16);
fprintf(fid,'%s\n', gr7);
fprintf(fid,'%s\n', gr8);
fprintf(fid,'%s\n', gr9);
fprintf(fid,'%s\n', gr10);
fprintf(fid,'%s\n', gr11);
fprintf(fid,'%s\n', gr12);
fprintf(fid,'%s\n', gr13);

fclose(fid);

fid = fopen('new_gen.dat','r+');

gen1=' 2128 2302    2    0    2    1    0              !
numnp,numel,ndim,iaxisym,nummat,nhv,igausspoint';
gen2=strrep(gen1,'2302',num2str(m8));
loc = 1;

for i = 1:loc
    temp_line1 = fgetl(fid);
end;
location = ftell(fid);
```

```
fseek(fid,location,'bof');
fprintf(fid,'\n');
fseek(fid,-1,'cof');
fprintf(fid,'%s',gen2);
fclose(fid);


fid = fopen('new_gen.dat','r+');
gen3='Kxx int. perm.         1.0e-06
! FALSE';
gen4=strrep(gen3,'1.0e-06',k2);
loc = 48;

for i = 1:loc
    temp_line1 = fgetl(fid);
end;
location = ftell(fid);
fseek(fid,location,'bof');
fprintf(fid,'\n');
fseek(fid,-1,'cof');
fprintf(fid,'%s',gen4);
fclose(fid);

fid = fopen('new_gen.dat','r+');
gen5='Kyy int. perm.         1.0e-06
! k(m2)=K(m/s)*1e-7';
gen6=strrep(gen5,'1.0e-06',k2);
loc = 49;
for i = 1:loc
    temp_line1 = fgetl(fid);
end;
location = ftell(fid);
fseek(fid,location,'bof');
fprintf(fid,'\n');
fseek(fid,-1,'cof');
fprintf(fid,'%s',gen6);
fclose(fid);

fid = fopen('new_gen.dat','r+');
gen7='Kzz int. perm.         1.0e-06';
gen8=strrep(gen7,'1.0e-06',k2);
loc = 50;
for i = 1:loc
    temp_line1 = fgetl(fid);
end;
location = ftell(fid);
fseek(fid,location,'bof');
fprintf(fid,'\n');
fseek(fid,-1,'cof');
fprintf(fid,'%s',gen8);
fclose(fid);

system('/home/Siddharth/folder2/cb.exe');
```

```
fid = fopen('fort.80');
n10 = 0;
while ~feof(fid)
    line = fgetl(fid);
    n10 = n10 + 1;
end
fclose(fid);

fid = fopen('fort.80');

trashline1=fgetl(fid);
trashline2=fgetl(fid);
trashline3=fgetl(fid);
trashline4=fgetl(fid);
trashline5=fgetl(fid);
trashline6=fgetl(fid);
trashline7=fgetl(fid);
trashline8=fgetl(fid);
trashline9=fgetl(fid);
trashline10=fgetl(fid);
trashline11=fgetl(fid);

n0=n10-11;

for j=1:n0
tline(j,:)= fgetl(fid);
end

fclose(fid);
t0=str2num(tline);

tm=max(t0(:,2));

for j=1:n0
if(t0(j,2)==tm)
t_sat(grand,1)=t0(j,1);
break
end
end


    fid = fopen('fort.70');
n1 = 0;
while ~feof(fid)
    line = fgetl(fid);
    n1 = n1 + 1;
end
fclose(fid);
n=n1+1;
fid = fopen('fort.70');
```

```
for i=1:n-164
    fgetl(fid);
end

    for i=1:163
    pline(i,:)= fgetl(fid);
    end
qline=str2num(pline);
t_sat(grand,2)=sum(qline(1:72,2));
t_sat(grand,3)=sum(qline(73:96,2));
t_sat(grand,4)=sum(qline(96:163,2));
t_sat(grand,5)=d111(grand,1);
t_sat(grand,6)=l111(grand,1);
t_sat(grand,7)=w111(grand,1);

fclose(fid);

clear p1 p2 p11 p22 q11 q22 q1  q12 q2 q21 q s11 s21 s31 ser tline
pline qline tm
delete('fort.*','*.dat','new_out.out','newflavia.*','newflavia.res');

end

save ('t_sat')
toc
exit
```

APPENDIX B

Flow rate, Q (Case I)

The cumulative mean and the standard deviation of flow rate, Q is shown in Figure B1 and Figure B2 respectively. Q for the homogenous case is 1.30×10^{-5} kg/s. As it can be seen from the Figure B1, amongst the plots showing variation of a single parameter, S (fuchsia) has the least impact on the flow rate, followed by W (yellow line) and again Z (Cyan) has globally the greatest impact on Q. From Figure B2 it can be inferred that standard deviation of flow rate, Q is least when only W (yellow line) is varying, while the standard deviation is maximum when Z alone (red line) is varying. For parameters varying in pairs it can be seen that the combination where both Z, W vary have the largest impact on flow rate, while for S, W it is the least and Z, S show intermediate response. Again cumulative mean of flow rate, ‘ μ(Q) ’ after 4000 simulations of Z, S, W all varying simultaneously (black line) can be viewed as the average response of the embankment when there is no knowledge about the cracking.

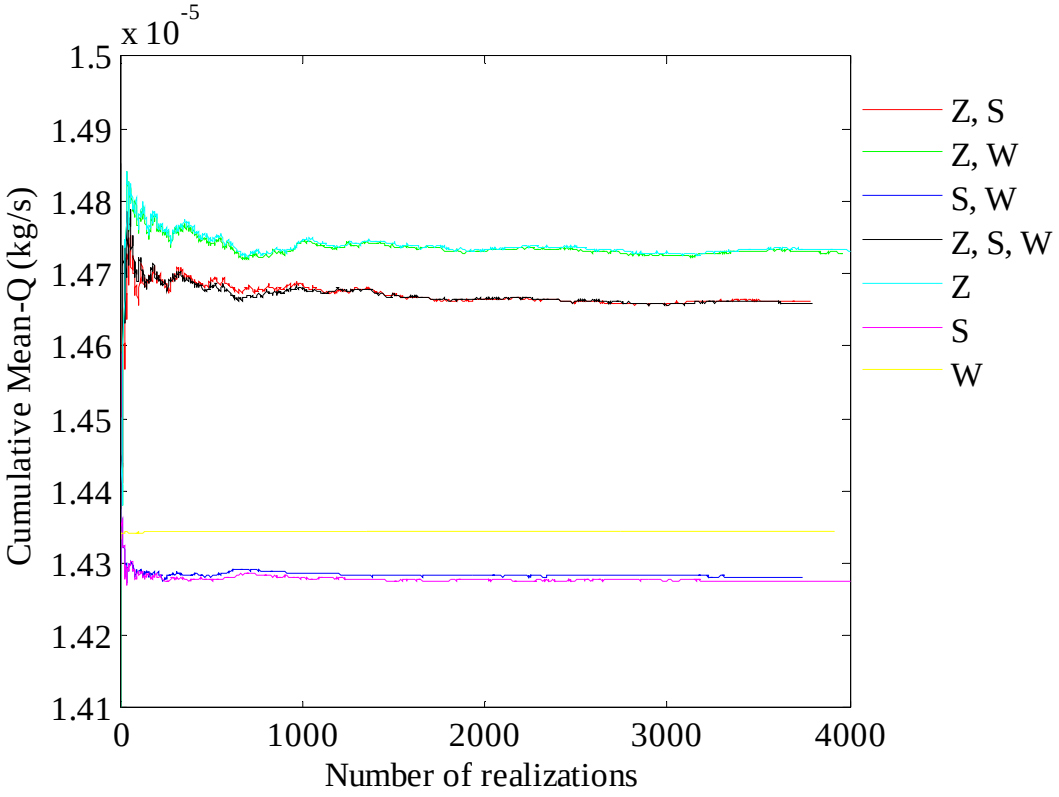

Figure B1. Cumulative mean plots of Q for Case I

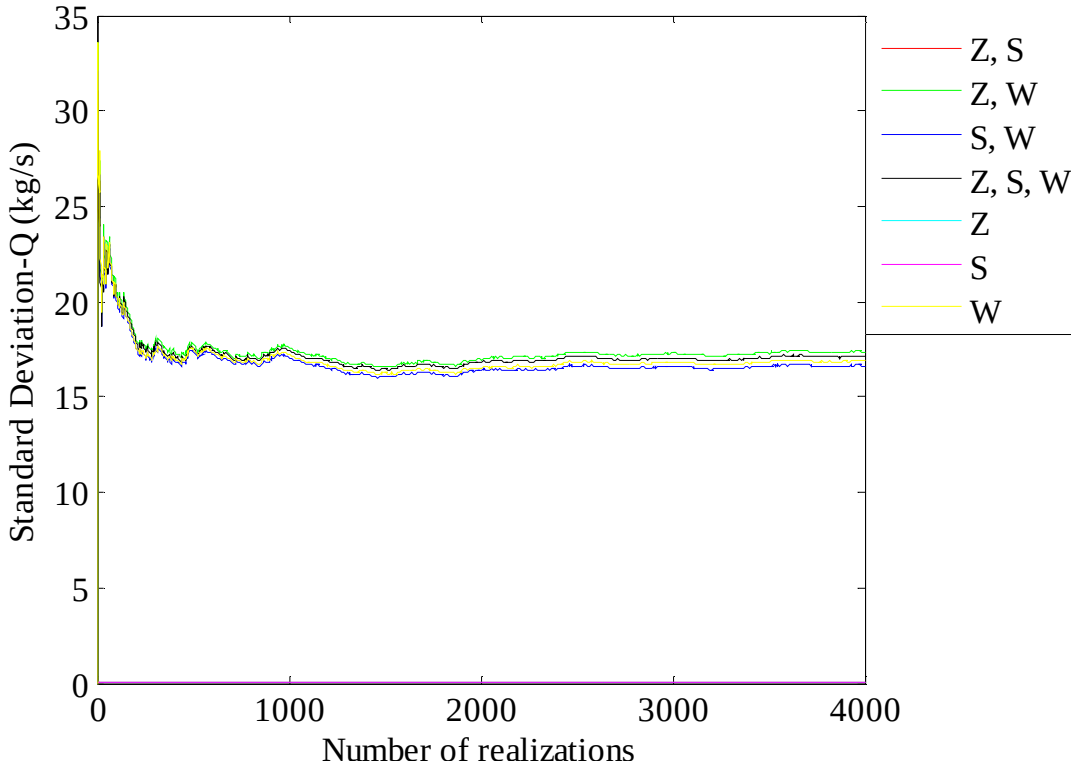

Figure B2. Standard deviation plots of Q for Case I

Time to saturation, Ts (Case II)

Figure B3 and Figure B4 show cumulative mean, 'μ(Ts)' and standard deviation, 'σ(Ts)' of time to saturation, respectively for different cases. It can be seen that Ts for Case II is about one order of magnitudes less than Case I or the homogenous case. In the cases where only individual parameters were varied, Z (cyan line) has the highest impact on Ts followed by crack aperture, W (yellow line) and crack spacing S (fuchsia line). Again the response given by black line (Z, S and W) varying can be seen as average response of the embankment when there is no information about the crack geometry.

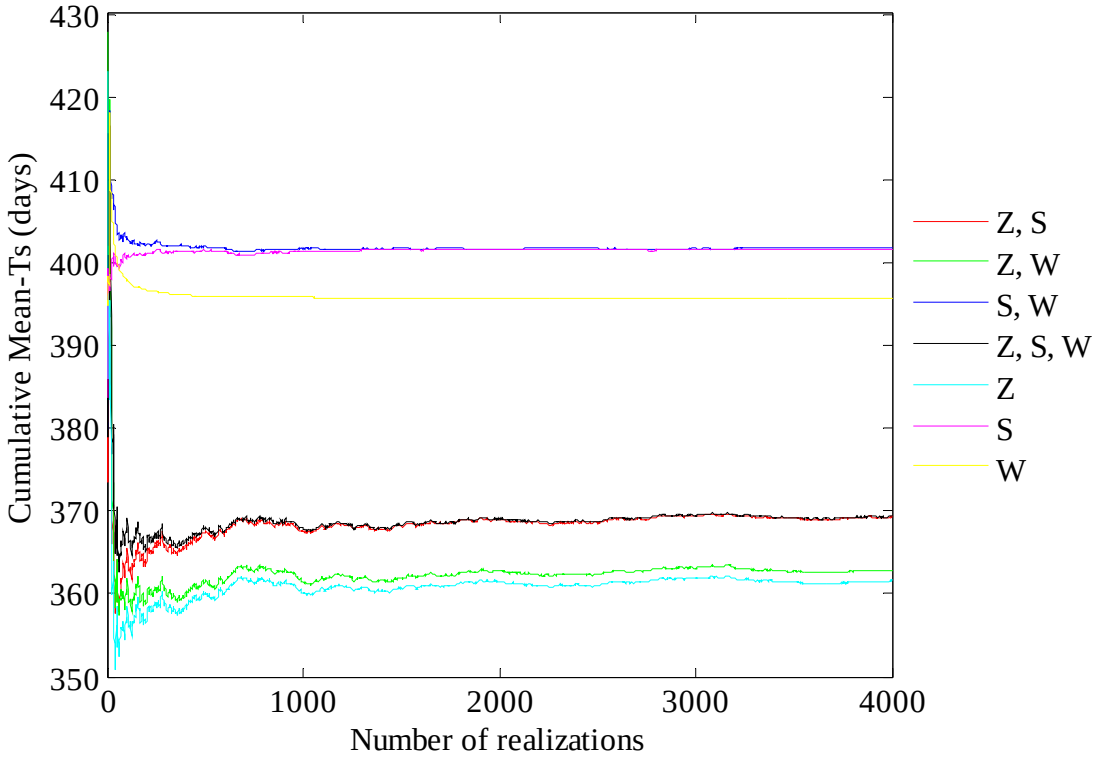

Figure B3. Cumulative mean plots of Ts for Case II

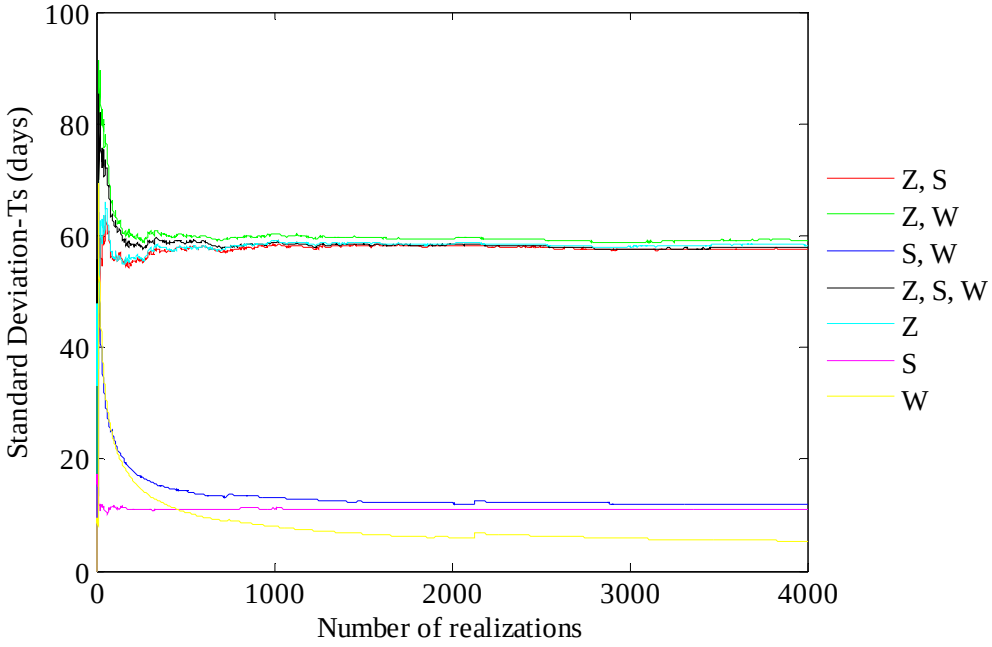

Figure B4. Standard deviation plots of Ts for Case II

Flow rate, Q (Case II)

Figure B5 and Figure B6 show $\mu(Q)$ and $\sigma(Q)$, respectively for different cases. It can be seen that the W has the most influence on Q. All the cases containing W show little difference their response. This can be explained by the fact that the subhorizontal cracks take the flow directly to the other side of the embankment. As established in section 3, flow rate is directly proportional to the aperture of the cracks ($Q \propto W$). Also the cases in which W was kept constant show relatively much smaller flow rates.

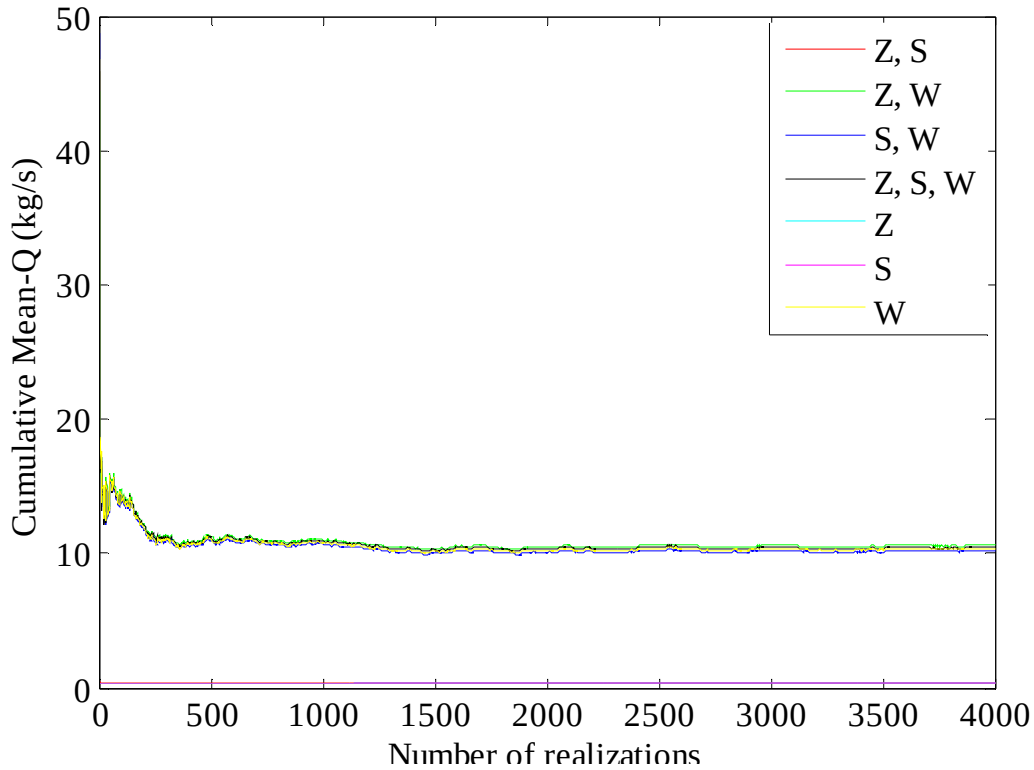

Figure B5. Cumulative mean plots of Q for Case II

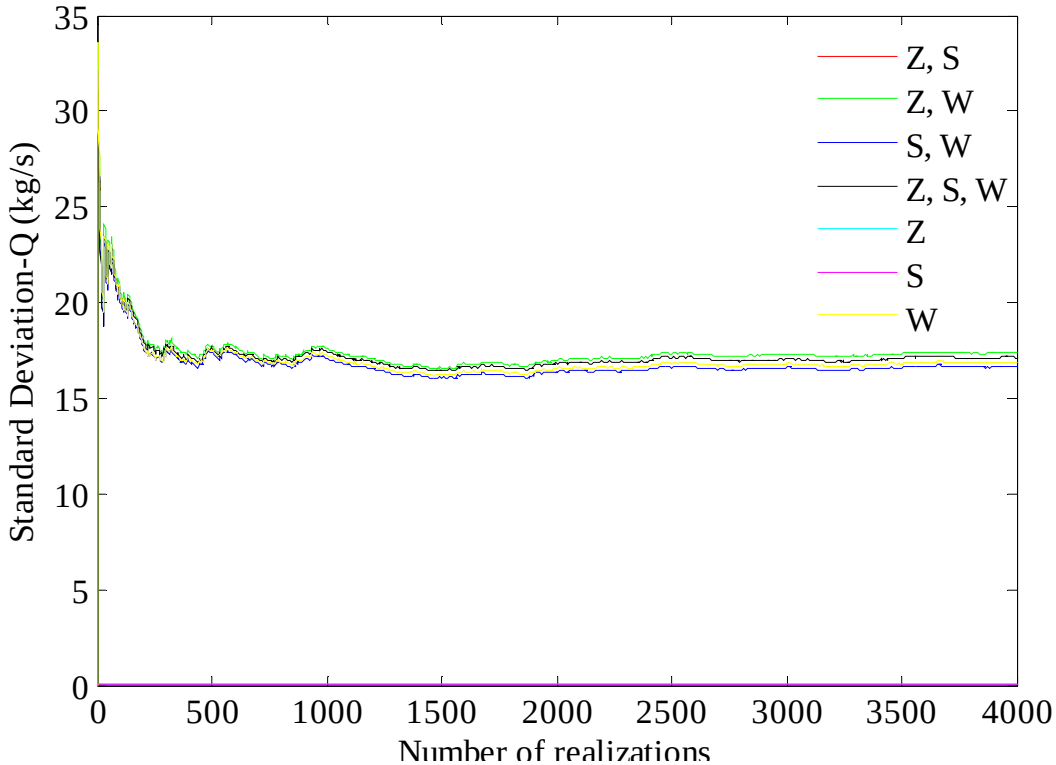

Figure B6. Standard deviation plots of Q for Case II

VITA

Siddharth Khandelwal received his Bachelor of Technology degree in Mining Engineering from Banaras Hindu University in 2009. He entered the Civil Engineering program at Texas A&M University in September 2009 and received his Master of Science degree in May 2011. His research interests include unsaturated soil mechanics, numerical modeling and random field analysis. He plans to publish peer reviewed journal papers on these topics, focusing on the phenomena of desiccation cracking.

Mr. Khandelwal may be reached at Department of Civil Engineering, Texas A&M University, 3136 TAMU, College Station, Texas 77843-3136, USA. His email is siddharth.khandelwal2011@gmail.com.